DNA Damage Induced by Low-Energy Electrons: A Theoretical Approach

Renjith B.

Roll No. 09612210

Department of Chemistry

Indian Institute of Technology Guwahati

This dissertation is submitted for the degree of

Doctor of Philosophy

May 2015

Dedicated to my parents ...

Certificate

This is to certify that the thesis entitled **DNA Damage Induced by Low-Energy Electrons: A Theoretical Approach** submitted by **Mr. Renjith B. (Roll No. 09612210)** to the Indian Institute of Technology Guwahati, in partial fulfillment for the award of the degree of Doctor of Philosophy is a bona fide record of research work carried out by him under my supervision. The contents of this thesis, in full or in parts, have not been submitted to any other Institution or University for the award of any degree or diploma.

_____

Thesis Supervisor, Dr. Manabendra Sarma

Declaration

I hereby declare that except where specific reference is made to the work of others, the contents of this dissertation are original and have not been submitted in whole or in part for consideration for any other degree or qualification in this, or any other university. This dissertation is my own work and contains nothing which is the outcome of work done in collaboration with others, except as specified in the text and Acknowledgements.

Renjith B.

May 2015

Acknowledgements

First and foremost, I would like to thank my supervisor, Dr. Manabendra Sarma, for his constant help and support during my career as a graduate student and researcher. Had he not been there to help me with my small and not-so-small problems in every wake of my research none of the work presented here would have taken shape. I appreciate all his contributions of time, ideas, and funding to make my Ph.D. experience productive and stimulating. The joy and enthusiasm he has for his research was contagious and motivational for me, even during tough times in the Ph.D. pursuit.

I am also grateful to Professor Arun Chattopadhyay (Chairman), Dr. Ashish Kumar Gupta, and Dr. Biplab Bose for serving as my doctoral committee members. Their comments, valuable suggestions and advice often helped me to solve new problems and come up with a totally different point of view for the old ones. Their knowledge, wisdom and experience have always been a source of inspiration for me.

I also extend my sincere gratitude to Dr. Lal Mohan Kundu of our Department for being my "acting supervisor" for a period of one year from 2011 to 2012.

I gratefully acknowledge the funding sources that made my Ph.D. work possible. I was funded by the Ministry of Human Resources and Development (MHRD) GATE fellowship for my 5 years and was honored to be for a Department of Science and Technology (DST) Travel grant for attending an International workshop. My work was also supported by DST project fellowship. I am also grateful to Department of Chemistry, and Indian Institute of Technology Guwahati for providing the infrastructure facilities.

I would like to express my sincere and humble gratitude to Prof. Susan Varugheese Prof. Rachael Mathew, Prof. Jacob George and Prof. Tomy Paul, teachers in Physical and

Theoretical Chemistry of my Master's Degree education at C.M.S college, Kottayam. They are the ones who inspired me to look at everything with a scientist's eye.

I would also like to thank my parents for their unconditional love and care and for being there for me at every stage of my life. They have always been a constant source of love, support and motivation.

Last but not the least, I would like to thank my relatives, friends, and colleagues for being at my side always and motivating me all the way along.

Abstract

Recent experimental and theoretical investigations on resonant electron scattering off DNA and DNA fragments using low energy electrons (LEEs), to propose the mechanism for single strand breaks (SSBs) and double strand breaks (DSBs), have received considerable attention. We have investigated theoretically the comprehensive route to SSB in a selected DNA fragment, viz., 2′–deoxycytidine–3′–monophosphate (3′–dCMPH), induced by LEE (0–3 eV) scattering using local complex potential based time dependent wave packet (LCP-TDWP) approach. To the best of our knowledge, we have provided the time dependent quantum mechanical dynamics insight for this DNA fragment for the first time. Initial results obtained from our calculation in the gas phase provide a good agreement with experimental observation and show the plausibility of SSB at 0.75 eV, which is very close to the highest SSB yield reported from the experimental measurement (0.8 eV) on plasmid DNA in condensed phase.

Further, the effect of quantum mechanical tunneling on SSBs induced by LEE has been investigated in gas phase 3′–dCMPH molecule. The potential energy curves for the sugar-phosphate C–O (3′ C–O) bond cleavage have been generated using second order Møller Plesset perturbation theory (MP2) at the 6-31+G(d) accuracy level. Results from the electronic structure theory calculations in conjunction with our time dependent calculations for the 3′ C–O bond rupture in 3′–dCMPH using LCP-TDWP approach show significant quantum tunneling of the 3′ C–O bond from the bound vibrational states above 1 eV of the anionic potential energy curve. A comparison of the fragmentation profile with that of our gas phase investigations based on Hartree–Fock (HF) and density functional theory (DFT) – Becke, 3-parameter, Lee-Yang-Parr (B3LYP) methods with 6-31+G(d) basis set is also provided. In addition, inspection of the singly occupied molecular orbitals (SOMOs)

generated at different 3′ C–O bond lengths clearly indicate the electron transfer from the low lying base–π^* shape resonance state to the phosphate P=O π^* orbital of the DNA backbone during the strand breaks. The decisive step during LEE induced strand breaks follows via "charge induced dissociation" (CID) for the metastable anion formed below 1 eV, whereas quantum mechanical tunneling is out-weighted the CID mechanism for the LEE above 1 eV.

We have also carried out LEE induced cytosine base release in gas phase 3′–dCMPH molecule using ab initio electronic structure methods and time dependent quantum mechanical calculations. It has been noted that the cytosine base scission is comparatively difficult process than the 3′ C–O bond cleavage from the lowest π^* shape resonance in energy region <1 eV. This is mainly due to the high activation energy barrier associated with the electron transfer from the π^* orbital of the base to the σ^* orbital of the glycosidic N–C bond. Moreover, the metastable state formed after impinging LEE (0–1 eV) has very short lifetime (10 fs) which may decay in either of the two competing auto-detachment or dissociation process simultaneously. On the other hand, the selected N–C mode may cleave to form the cytosine base anion at higher energy regions (>2 eV) via tunneling of the glycosidic bond. Resonance states generated within this energy regime will exist for a duration of $\sim$ 35–55 fs. Comparison of salient features of the two dissociation events, i.e., 3′ C–O single strand break and glycosidic N–C bond cleavage in 3′–dCMPH molecule are also provided.

Moreover, we have studied the LEE induced single strand break in gas phase cytidine nucleotide known as 2′–deoxycytidine–5′-monophosphate (5′–dCMPH) molecule by means of ab-initio electronic structure methods and local complex potential based time-dependent wavepacket quantum mechanical calculations. We have found that the LEE attachment to this cytidine nucleotide takes place at the cytosine nucleobase center, results in the formation of a transient metastable anion. The quantum dynamical calculations show that the electron transfer from π^* orbital of cytosine to the σ^* orbital of the sugar-phosphate 5′ C–O bond occur within 18–20 fs. The characteristic electron attachment fragmentation profile is peaked $\sim$ 1 eV, which is in good agreement with the available experimental observations. Quantum mechanical tunneling of the 5′ C–O bound vibrational energy levels may contribute to SSB only above 1.5 eV energy regimes.

Finally, we have carried out the LEE attachment in a modeled sugar-phosphate-sugar (SPS) moiety to investigate the likely electron attachment other than the nucleobase center and the subsequent single strand break ($3'$ C–O and $5'$ C–O) in DNA fragments. We have treated these two competing dissociation channels separately. We have found that the LEE attachment (0.6 eV) takes place at the phosphate center. To our surprise, we have also noted that the metastable state possess longer lifetime ($\sim$ 40–55 fs) compared to the resonance state formed at the cytosine center. This indicates the probability of dissociation is more if the resonance is formed at the phosphate center. Moreover, $5'$ C–O bond rupture is favored in comparison with $3'$ C–O bond dissociation due to it's low activation energy barrier. In addition, the quantum tunneling of the sugar-phosphate bond is seen only above $>$ 1.5 eV.

Table of contents

List of figures

List of tables

Chapter 1

Introduction

1.1 Ionizing radiations and it's role in DNA damage

The lethal effect of primary ionizing radiations [e.g., β, γ (>100 keV), UV, X (0.1–100 keV), and cosmic rays] are potentially characterized by their ability to generate free radicals, disrupt or form chemical bonds, damage bio-molecules such as DNA, RNA, proteins which are involved in regulating vital cell processes, alterations of the genome and so forth [1–4]. Exposure to these radiations often results in various forms of (major/minor) damages to living tissues, for example, many ageing related diseases, radiation sickness, burns, cancer induction or long-term genetic diseases may lead to death [1]. The Hiroshima, Nagasaki, Chernobyl, and Fukushima Daiichi disasters have reminded us of the hazardous effect of radioactive radiations on living organisms. Secondary electrons (1–20 eV) are generated in large amount when primary ionizing radiation comes into contact with living organisms [5–10]. These electrons have a very short period of life time (normally less than 1 ps before it gets solvated) and can induce irreversible cell damages such as DNA strand breaks, alteration to nucleobases, sugar destruction, cross-link and dimer formation and so forth [11]. Findings of experimental investigations indicate that the chemical modifications to the cellular metabolism caused by high-energy radiation can be ascribed to a series of low-energy events [7, 8, 11, 12].

Before discussing various instances of the significant physical, chemical, and biological levels of low energy electron (LEE) induced DNA damages, let us briefly look into the anatomy of a cell with respect to the interaction of the high energy quanta. This will enable us to differentiate between the direct and indirect effect of ionizing radiations in living organisms. The most sensitive part of a cell is considered as the typical dimensions of DNA, and therefore, any chemical modifications taking place in DNA might lead to the loss of genetic information. DNA is a highly viscous biopolymer gel comprising four nucleobases such that adenine pairs with thymine (A–T) and guanine with cytosine (G–C) resulting in the well-known right-handed double-helix form [13]. DNA is surrounded by proteins, packed within the cell nucleus forming a high density molecular region. This combination of DNA and proteins, also known as nucleosome, are further packed into a loops of 30-nm fiber resulting in the formation of chromatin [14]. Chromosomes are the condensation products of chromatin. It is this chromatin which plays a major role to tightly bound DNA into a smaller volume of the cell. However, DNA comprises only 1% of the total volume of a cell [15]. Hence, the probability for direct energy deposition (direct effect) on DNA is very low. Consequently, most (about 2/3 rd) of the damages to DNA occurs via indirect effects due to the secondary particles [16]. These secondary species, generated along the track of ionizing radiations, are acting as the precursors of DNA damage to induce further chemical transformations. Biomolecules, specifically DNA, are more likely to be victims of indirect effect of radiation induced damages [16–18].

The mechanism of radiation damage on a molecular level is only partially understood. The major bottleneck to discover the glimpses of complex reaction events is the lifetime of the species involved during these series of processes [17]. Various instances of radiation induced DNA damage processes are shown in Fig. 1.1. It is clear from the Fig. 1.1 that a majority of the low energy events take place in an ultrashort timescale. In particular, ionization and excitation of biomolecules take place within femtoseconds after the deposition of the high energy quanta [16, 17]. The net effect is the distribution of high energy into a large number of low energy particles ($\approx 10^5$/MeV) [16]. A recent work published by Pimblott et al. reported the most probable energy possessed by secondary electrons is about

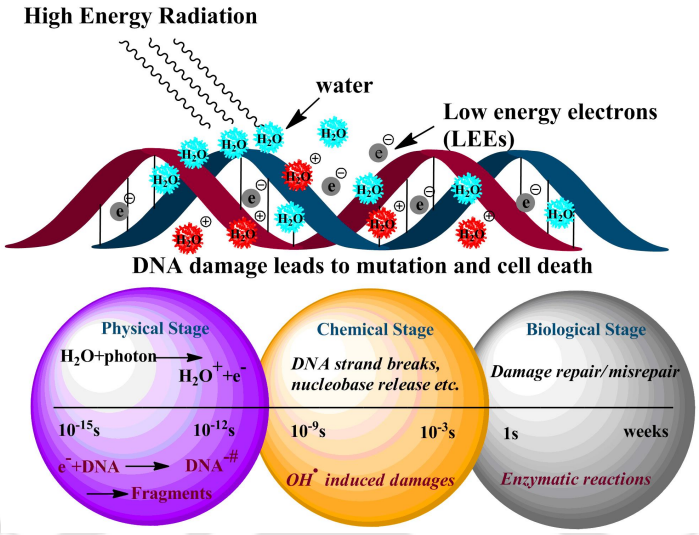

Fig. 1.1 Schematic representation of various stages of DNA damage induced by ionizing radiations. Initial events like ionization and excitation processes takes place at the physical stage followed by the chemical stage. Long term effects are seen only at the biological stage. Dissociative electron attachment (DEA) process, our interest, takes place at very early stages in the timescale shown [19].

9 eV [9]. A small fraction of (almost 1/3 rd) electrons possess an energy below 1 eV [5]. The secondary electrons, once generated inside the cell, gradually loose energy through inelastic collisions with other biomolecules and eventually become solvated within 1 ps [11]. During the course of electron formation to solvation, they are active to ionize biomolecules like DNA and create potentially lethal lesions to such systems [6, 12]. A more detailed description of the process by which the molecules such as DNA undergo LEE induced damage, known as dissociative electron attachment (DEA), is provided later in this chapter. Another highly reactive secondary species involved during the biomolecular damage process is the hydroxyl radical ($OH^{\bullet}$) [10]. They are generated *in vivo* through the ionization and subsequent dissociation of water at the physical stage. The hydroxyl radical ($OH^{\bullet}$) is a potential candidate to induce lethal lesions such as DNA strand breaks, nucleobase release and cross links within a duration of nanoseconds to milliseconds [10]. The events due to secondary species take place in physical stage and chemical stage are collectively referred to as indirect damage [10, 16]. DNA strand breaks are of different types in which single strand breaks (SSBs) can be repaired by enzymatic reactions. However, clustered DNA

damages like double strand breaks (DSBs), multiple double strand breaks (MDSBs) are mostly irreparable, mutagenic in nature, and eventually lead to the pathogenesis of cancer, apoptosis, and many other aging-related diseases [1, 6]. The biological stage of radiation damage normally occurs after some seconds of the chemical stage. Apparently the events that take place at the physical and chemical stages greatly influence the final biological effects developed after the deposition of primary quanta. All these discussions lead us to understand the role of ionizing radiations and also the importance of secondary species (e.g., LEEs and $OH^{\bullet}$) in inducing DNA damage since more than 80% of the energy of primary quanta is carried by LEEs after the primary ionization events.

1.2 An insight into electron-driven processes in general

Before going to the detailed description of the action of LEEs in DNA, let us briefly analyze the electron induced processes in general. The energetic species formed after the collisions of electrons with molecules and atoms can produce physical and chemical changes of matter in environments that range from plasmas to living tissues [17]. For example, in the present context, attachment of secondary electrons to the fragment molecules of DNA cause damage to the metabolic activities of vital living systems [3, 8]. The fundamental processes that may take place during an electron-molecule collision event can be categorized as given below.

$$
\begin{aligned}
e^- + M \rightarrow \quad & e^- + M \Longrightarrow && \text{(elastic scattering)} \\
e^- + M(v) \rightarrow \quad & e^- + M(v') \Longrightarrow && \text{(vibrational excitation)} \\
e^- + M \rightarrow \quad & A + B + e^- \Longrightarrow && \text{(electron impact dissociation)} \\
e^- + M \rightarrow \quad & A^- + B \Longrightarrow && \text{(dissociative attachment)} \\
e^- + M \rightarrow \quad & M^+ + 2e^- \Longrightarrow && \text{(electron impact ionization)}
\end{aligned}
$$

where "e^-" represents the electron, "M" being the target molecule, and "A" and "B" are the fragmented products. The list given above are not final. Any of the above mentioned processes [20–22] can occur during an electron-molecule collision as a single event or a combination of

them. In particular, the collision event which follows the molecular dissociation process has received considerable attention[12, 16–18] where dissociative attachment is a special case in which the electron attaches to one of the fragmented species after the dissociation. The mechanism for the LEE induced chemical bond rupture has not been fully understood. Even, it is difficult to characterize the transient nature of the intermediates or the products, and information about the states of the neutral fragments and so forth [17]. All these difficulties make both the experimental and theoretical investigations of molecular dissociation extremely challenging [17].

In general, all of the above mentioned processes can happen both in gas and condensed phases [22]. A complete understanding of any of these process is not yet achieved in gas phase and condensed phases. In particular, the key application areas of radiation damage to living tissue happen almost exclusively in the aqueous phases or *in vivo*. Thus a progressive step can be made in this field through the investigations of simple systems in the gas phase and gradually explore the clusters in condensed media or what is referred as the "bottom-up" approach analysis [8].

1.3 Dissociative electron attachment

Electrons whose energy lie below the threshold for ionization can also induce malignant damage in molecules. For example the principal mechanism behind DNA damage processes is found to proceed via the formation of a transient negative ion (TNI) followed by the dissociation of a covalent bond within the system [11]. This electron impact dissociation of a target molecule resulting in a negative fragment ion and one or more neutral radicals is popularly known as dissociative electron attachment (DEA), which by itself is a resonant process [20–23]. This means that it occurs significantly only in a particular energy region [20]. It is also to be noted here that the DEA reactions are enormously sensitive to the lifetime of the TNIs ($M^{-\#}$) formed [21]. Here, the compound state of the target and the projectile, i.e., $M^{-\#}$ is known as a quasi-bound state, or the so called "resonance" state lying in the $e^- + M$ continuum [23]. Further, the attachment cross section for the electron-molecule interaction is

greatly influenced by the energy of the incoming electron [20]. This implies that the DEA cross sections and the resonant attachment energies are different for different molecules. Therefore, DEA can be considered as an effective process in the gas phase or condensed phase ubiquitous for particular molecules. In addition, DEA process is significantly affected in those molecules where the metastable state formed redistributes the excess energy by means of a process known as intramolecular vibrational energy redistribution (IVR) [24].

The after effect of DEA reaction is dangerous since it produces free neutral radicals and anions both of which can further initiate the molecular bond-breaking chain propagator mechanism [10]. In some cases, DEA occurs under complex environments. For example depletion of ozone layer in polar stratospheric clouds in which the DEA takes place via interaction of electron with the molecules at the surface [25]. It is a significant challenge to theory for modeling these reactions and its properties. So far, modeling of DEA process has been done only for diatomic molecules and/or polyatomic compounds modeled by diatomics [17, 18]. Some of these investigations include electron induced chemical modification takes place at surfaces and in thin films on substrates, chemical reactions take place in solution where the electron comes from the substrate molecule and transfers to a target molecule and so forth [12, 17, 18]. What is most interesting in resonance mediated DEA reactions is the gradual decrease of attachment cross sections with increasing electron energies.

It has recently been known that DEA plays a pivotal role during LEE induced DNA damage [12]. In addition, experimental findings were reported in the literature where the high probability of generating LEEs surrounding the living tissues through interatomic Coulombic decay (ICD) [26] were discussed. A combined effect of both ICD and DEA will substantially enhance the rate of damage to DNA as the former occurs in water surrounding the tissue, while the latter happens within the close proximity of water [27]. Thus, exposure to ionizing radiation for longer duration makes the life at risk and may produce "bystander" effects [27, 28].

Understanding of LEE induced unimolecular dissociation of complex biomolecules is at it's preliminary stage. Many low lying TNI states were identified both experimentally [29, 30] and theoretically [16] for DNA bases and it's fragments. Recent gas phase studies of

DEA phenomenon using theoretical principles focus on the mechanistic pathway by which the process takes place and also on calculating the cross sections and rate constants of these ultrafast processes [16–18]. In a way, we can visualize DEA process as an electron-molecule scattering phenomenon popularly studied using advanced quantum mechanical principles. As discussed earlier, implementing quantum approach to examine the characteristics of resonant electron attachment process in simple diatomic molecules is quite accomplished. However, as the complexity of the target molecules increases it may possess several TNI states and in such cases, it is very difficult to employ the quantum approach to deduce the features of resonant electron molecule scattering effectively. It is also to be noted here that if a given "resonance" is associated with different decay channels, it is even more difficult to calculate the DEA cross sections using ab initio electronic structure methods and quantum dynamical calculations. A more detailed description of DEA process or the *resonant electron molecule scattering* process in quantum viewpoint is given in the next section.

1.4 Electron molecule scattering theory: A quantum approach

Electron-molecule scattering phenomenon is widely used to identify the metastable continuum states associated with physical and chemical processes like energy exchange between electronic and nuclear motions, electron transport, and so forth. In electron-molecule scattering theory, "resonance" is referred as an electron-impact scattering phenomenon which involves the formation of a TNI [20]. During resonance, the projectile becomes temporarily trapped in the vicinity of the target molecule and the energy at which resonance occurs is commonly referred to as the "resonance energy" [21]. Resonance take place when the incoming electron gets attached by a virtual molecular orbital. The captured electron may re-emit (autoionize) after a time, typically within 10^{-15} s to 10^{-12} s which is substantially longer than the transit time for unhindered propagation across the molecule [20]. In short, we can consider this electron-scattering phenomenon as the formation of a short-lived negative ion, since the molecule acquires an extra electron during this process and the compound state

posses a finite lifetime. Theoretical considerations manifest the formation of the short lived negative ion as a "*characteristic peak*" or "*resonance*" in the scattering cross section. Thus, this phenomenon is also termed as "*resonance electron scattering*" [20, 21]. It should be noted here that the terms like *resonance, temporary negative ion, and compound state* used throughout in this dissertation is referring to the same physical entity.

1.4.1 Feshbach and Shape resonance

Molecular negative-ion resonances are traditionally divided into two categories, *Shape* and *Feshbach* resonances [20, 21, 23]. Let us briefly consider, on account of the electronic configuration of a generic TNI, what these entities are. If a *resonant state* is produced without causing any variation in the electronic configuration of the target molecule, then a "one" particle resonance is formed. This can be treated simply as the addition of an electron into the virtual molecular orbital of the target involved during the collision. Whereas, in some cases the extra electron does perturb the electronic configuration of the target molecule during resonance formation popularly known as the so-called "two-particle" resonance, or "core-excited" resonance. In a two-particle resonance, the energy of TNI (M^{*-} in the Fig. 1.2) can be either above or below the energy of the corresponding electronically excited target molecule (M^*). If the energy of M^{*-} is greater than that of M^*, then the TNI corresponds to an open-channel resonance. The other category falls into the closed-channel core-excited resonance, also known as *electronic Feshbach* resonance. Feshbach resonances are characterized by their inability to decay directly into the ground electronic state (M). From Fig. 1.2, it is clear that such a transition requires long lifetime since it needs more time to rearrange the electronic configuration. Let us now consider both the one-particle resonance and open channel core-excited resonance. In either of the two cases, the incoming electron gets trapped in to the effective potential formed via the interaction between the incident particle and the target molecule. The shape of the potential allows the particle to remain inside the barrier. The TNIs formed this way are termed as *shape* resonances. From the Fig. 1.3, it is clear that the projectile will experience an attractive potential in those spatial regions where the molecular mass is centered. This region is surrounded by a region of repulsive

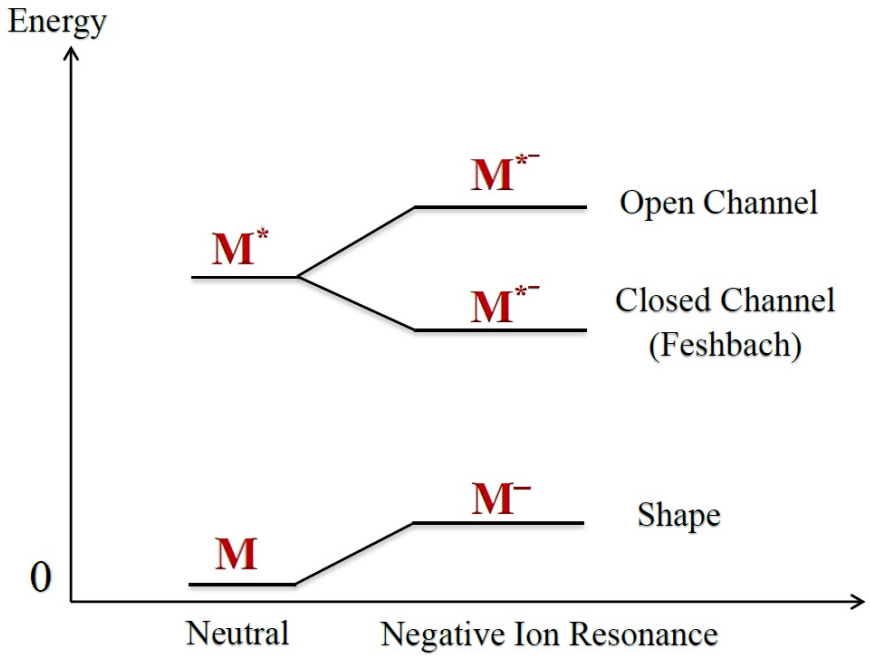

Fig. 1.2 M, M^* are the neutral species at their ground and excited state respectively. M^- and M^{*-} are displayed schematically to illustrate the formation of resonances such as Shape, Feshbach, and core-excited open channel resonances [20, 21, 23].

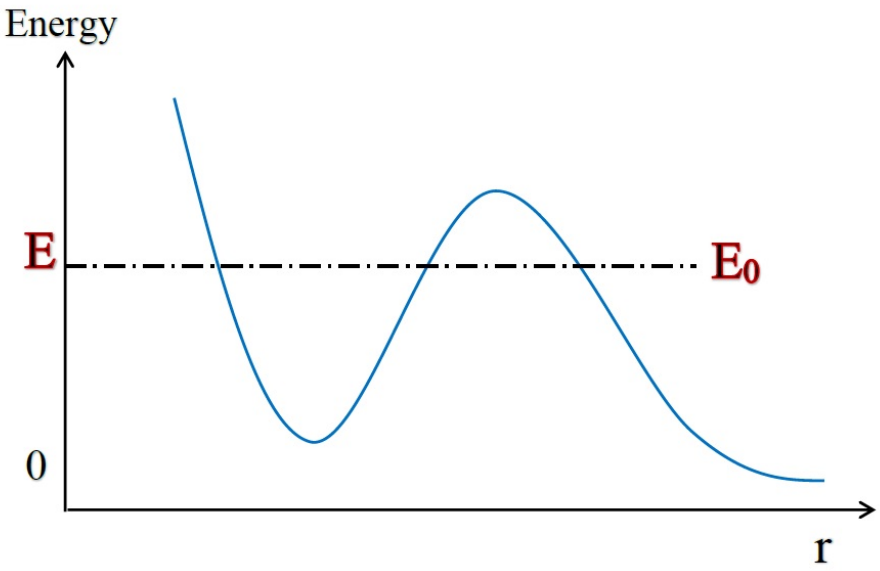

Fig. 1.3 Potential energy curve representing the dynamical trapping of an incoming particle. E_0 is the kinetic energy of the projectile. 'r' is the internuclear distance. Since the shape of the potential is responsible for the formation of a resonance state, this type of resonance is known as Shape resonance [23].

potential. The particle initially trapped inside the barrier may tunnel through depending upon it's kinetic energy. There comes a situation when a combined action of both the attractive and repulsive regions prevent the particle's re-emission (also called autodetachment) at least for the time necessary for the TNI to be experimentally detected.

1.4.2 Overview of the resonance scattering process

In summary, the physics of the "*resonant electron-molecule scattering*" process [23] can be collectively classified into the sequence of the following stages:
(i) *Capture*:- The processes responsible for the formation of the negative ion state. It consists the mechanism by which the projectile gets trapped into the target molecule.
(ii) *Dynamics*:- The distortion take place within the target molecule after the attachment of the incident particle. This stage comprises events like excess energy transfer or redistribution within the host molecule, or some rearrangement within the compound system. All these processes take place within the lifetime of the resonance.
(iii) *Detachment*:- This stage attributes all those processes responsible for the decay of the metastable state formed in stage 1.

1.5 Recent findings in LEE induced DNA damage

Recent experimental and theoretical investigations have received considerable interest in the role of DEA in biomolecules [17, 18]. In particular, remarkable observations on DNA damage as single and double strand breaks, and its mechanistic pathway were made initially by Sanche and co-workers in the early years of the last decade [12]. It was also found that these effects are directly linked to the carcinogenicity and more broadly to radiation chemistry and radiation damage [7]. Excellent review articles were published discussing the electron-induced DNA damage reactions [17, 18]. It is found that LEEs can efficiently induce strand breaks in plasmid DNA at energies above 5 eV [12]. Soon after, theoretical calculations predicts the formation of SSBs even below 1 eV with basically no threshold energy [31]. A striking feature observed in the yield curves of both SSB and DSB caused

in plasmid DNA by LEEs is a resonant behavior. In particular, the maxima at 10 eV for DSB and 0.8 eV for SSB [12]. A DNA strand break occurs when one or more chemical bonds at the DNA backbone would rupture, the most common lesion found at the C–O or P–O bond framework. The characteristic resonant features of these strand breaks were attributed due to the DEA phenomenon [32]. Several mechanisms were proposed to explain the observed LEE induced strand break phenomenon [17]. The mechanism follows an excess charge transfer process in which the nucleobases act as the LEE receiver. Once the electron gets localized on the nucleobase moiety, a bond cleavage occurs within the DNA backbone resulting in a strand break via the transfer of LEE from the base to the phosphate group [16, 18]. In addition, electron attachment at the backbone phosphate group was predicted in some of the remarkable investigations [33]. However, this possibility has been suggested only at higher energies, around 2 eV [34]. An alternative mechanism was suggested by Dabkowska et al. for LEE induced strand breaks in DNA [35]. They have considered intramolecular proton transfer from the sugar moiety to the cytidine base which eventually leads to the dissociation of the C–O bond residing at the backbone. Further, investigations on self-assembled monolayers of DNA using high resolution electron energy loss spectroscopy (HREELS) and X-ray photoelectron spectroscopy (XPS) studies suggest that LEEs can mainly interact with the DNA backbone [36]. Also, the nucleotide components exhibit a number of shape resonance states, a majority of which are found between 0 to 3 eV [37–49].

A number of DEA studies in smaller units like DNA and RNA nucleobases have been carried out in the gas phase. It was found that all of these nucleobases (NBs) can capture LEEs (preferably below 10 eV) [30, 50]. The main dissociative pathway after the electron attachment is the loss of a neutral hydrogen atom forming the closed shell anion $[NB–H]^*$. Moreover, decomposition of the pyrimidine or purine ring systems is also observed. What is most interesting in the H abstraction is the site and energy selectivity during the dissociation process. N_1H bond dissociation at 1.0 eV was demonstrated in thymine and uracil bases (this bond is connected to the sugar in nucleosides known as the glycosidic bond). However, an electron energy of 1.8 eV is required to break the N_3H bond in these pyrimidine bases [50]. Investigations on electron-induced reactions in isotope-labeled nucleobases also revealed

that the bond rupture is highly energetic and site selective. In short, for instance, it is the energy of the incoming electron which determines the specific atom (either N_1 or N_3) from which the hydrogen abstraction to occur [30, 38].

1.5.1 Factors affecting the DEA in DNA fragments

Investigations of DNA damage in various DNA fragments both in gas phase and aqueous phase suggest that the solvation has a profound influence on the DNA damage regulated by LEEs. In some cases, studies have reported an enhancement factor of 1.6 for DEA yield [17, 51]. Therefore, it is very essential to include water molecules for modeling the LEE induced unimolecular reactions in biomolecular systems. Other factors which may have serious role in bond dissociation are hydrogen bonding, DNA π-stacking interaction, etc. [16] which are directly or indirectly linked to the lifetime of the metastable species formed. Another important factor to address during the investigation of DEA reaction in DNA fragments is the role of DNA binding proteins in electron-induced DNA damages [52]. A recent experiment addressed this issue using self-assembled monolayers [52]. However, further investigations are required. Functional groups also plays a major role to determine the characteristic electron energies for the formation of the negative ion state [53].

1.6 Our objective

A number of investigations have been carried out over the past decade to understand the molecular mechanisms of electron-induced DNA damages [17, 18]. However, there exist controversial results which may directly be related to the complexity of the system considered. For instance, it was proposed that DNA strand breaks are mainly caused due to the initial localization of LEEs at the nucleobases or at the backbone [31, 39, 47]. Experimental investigations find limitation to characterize the role of TNIs during the DEA reactions. This is because the compound state of LEE and the target has only a fleeting existence, thereby it is difficult to characterize this state in an electron molecule scattering experiment [11]. Therefore, a well formulated theoretical modeling is an essential requirement for

understanding the role of metastable states during DEA processes in conjunction with the experimental findings. Moreover, to gain knowledge on how these physical or chemical changes take place, we should have an idea about the fundamental processes that underlie them. A more careful investigation on the rates and products of molecular dissociation may help in understanding the genotoxic effects of ionizing radiation with complex bio-molecules. One will always be curious to know about the possible fragmentation products during an electron-molecule collision event. This makes a great challenge to the existing experimental and theoretical capabilities and demands development of new techniques. Energy can be effectively transferred to and from the electronic degrees of freedom of the target molecule during electronic collisions. One more point should be noted here, the incident electron has the same mass as those that bind with the target molecule together, and is physically indistinguishable from them. This implies that LEEs are strongly coupled to the molecule's internal degrees of freedom. Such a difficult situation arises in every electron collision with matter in which they occur, irrespective of the medium where it takes place. With this perspective, our present work explores the state of the art in theory of electron induced unimolecular dissociation processes.

Recently, our group has developed a new implementation of the local complex potential based time dependent wave packet (LCP-TDWP) approach for the calculation of vibrational excitation cross-sections in electron-molecule scattering [54, 55]. The method has been applied to systems like resonant e-N_2, e-H_2, e-CO scattering and the results obtained are quite reasonable. A single calculation can provide the cross-section profile for a wide range of energy values. The necessary ingredients in our method are the target potential energy (PE) curve, the anionic PE curve, and the anionic decay function resulting from electron attachment. With the basic foundation from those works, we would like to extend this new approach to larger molecular networks, i.e., DNA fragments in the present context, to investigate the characteristics of various DNA damages via DEA in the low energy regime (0–3 eV). It is important for any electron-molecule collision investigation to understand the electron attachment energies to the target molecule in the gas phase. It will provide information about the ease with which a compound can be reduced in the absence of any

surrounding medium, thereby, allowing one to make a reference point from which one can measure the effects of solvation. These energies are determined at the ground-state geometries of the isolated neutral and anionic molecules. Information about these energies will be very helpful to develop suitable theoretical models for discussing electron transfer taking place in DNA. They also serve in understanding the role of molecular distortions associated with LEE localization on the nucleobase. Therefore, it is our purpose in this dissertation to understand how LEE induces various DNA damages in gas phase using time dependent quantum mechanical perspectives and to provide a rigorous quantitative formalism rather than qualitative ones proposed by other groups [16–18].

Once the LCP-TDWP approach is implemented to deduce the molecular mechanism of various DNA damages, our goal is to find out the role of LEEs in chemically modified DNA fragments which may act as potential radiosensitizers used in the treatment of cancer. For instance, LEE induced yield of SSBs and DSBs in DNA are found to be enhanced by a factor of 1 to 5 (depending upon the energy used) when cisplatin is used as the drug, with a maximum in the yield observed at 10 eV. Therefore, modeling the underlying DEA processes to understand the mechanism of various forms of DNA damages may find suitable implications for the design of new radiosensitizers, which will eventually open a new avenue for the development of more efficient protocols in cancer therapy [56, 57].

1.7 Challenges of theoretical modeling

Finding absolute cross sections for mass analyzed ion fragments are difficult to determine accurately using the existing experimental techniques. Experimental measurements are presently restricted to those compounds which cannot undergo thermal decomposition when introduced into the gas phase, a severely limiting constraint. Similarly, modeling DEA processes also finds great difficulty to meet the requirements for an accurate description of the underlying mechanism. In principle, DEA process is a multidimensional process and one has to consider these multidimensional effects in nuclear dynamics. Inclusion of these effects will dramatically increase the computational cost due to the large scale of calculations

which will be more complicated than simple dissociation calculations. At present, a number of calculations have been done for diatomic and a few polyatomic molecules, considering the multidimensional effects. Moreover, a well sophisticated theoretical approach is an essential requirement to address the issues associated with the electron driven chemistry processes. The obvious concerns are not only limited to the issues of timeliness, but also to come up with the accuracy of the calculated results. The necessary ingredients required for the calculation involves the generation of potential energy surfaces and the simulations of the system using scattering techniques. In short, one has to utilize both the *ab initio* electronic structure and electron-molecule scattering principles to successfully produce results on a relevant time scale.

Finally, it has also become another concern about the computer resources needed for the bound electronic state calculations of very large biomolecules. The extension of these *ab initio* electronic structure calculations in the aqueous medium is a daunting computational task. An optimum performance without any compromise in accuracy of the results can be achieved via an active usage of high performance massively parallel computing resources with the latest graphical processing unit (GPU) which can extend to tens of thousands of processors.

1.8 Applications of electron induced processes

It is now well understood that interaction of electron with molecules often results in the formation of energetic species which plays a key role in driving the chemistry of a number of processes. There are a wide range of applications one can find for these electron-initiated processes in gas phase, at surfaces and interfaces, and in condensed matter. However, we are discussing one of it's several applications, in the context of *chemotherapy* [56–58]. As discussed above, the secondary electrons (0–20 eV) have a major impact in inducing damage to DNA and initiate further chemistries within the cell metabolism. This principle is responsible for the technique of radiotherapy, which is the most common treatment for cancer. Indeed, most of the cancer patients are subjected to ionizing radiation (IR) at some

point as their treatment. The aim of this process is to attain cell death via irradiating with high energy radiation for which DNA molecule is the most important target. We should also keep in mind that DNA is present inside the nucleus in eukaryotic cells and therefore, IR should reach inside the nucleus for having an effective clustered DNA damage. Otherwise, the damage will be limited to the membrane or cytoplasm only. At the same time, since IR deposits its energy in a random fashion, it can damage the normal tissues surrounding the cancer cells and may further mutate. Therefore, it is necessary to minimize the radiation dose given to the cancer patient. One way of achieving this is by the use of chemotherapeutic drugs. These drug molecules once injected to the affected area will enhance the radiation induced damage, and thereby minimizing the radiation dose given to the patient. At this level, suitable molecules which may lead to maximum efficiency are very few and this is one of the prime fields where electron-molecule scattering studies can find immense applications to suggest suitable candidate molecules for the treatment of cancer.

References

[1] O. Yamamoto, in *Aging, Carcinogenesis and Radiation Biology;* edited by K. Smith (Plennum: New York, 1976), p 165.

[2] C. von Sonntag *The Chemical Basis for Radiation Biology;* (Taylor and Francis, London, 1987).

[3] A. F. Fuciarelli, J. D. Zimbrick, *Radiation Damage in DNA: Structure/Function Relationships at Early Times*, (Battelle: Columbus, Ohio, 1995).

[4] *Radiation Research 1895-1995 Congress Proceedings, Vol. 2: Congress Lectures, 10th ICRR;* edited by U. Hagen, D. Harder, H. Jung, C. Streffer (Universitätsdruckerei H. Stürtz AG, Würzburg, 1995).

[5] J. A. LaVerne, S. M. Pimblott, Radiat. Res. **141**, 208 (1995).

[6] B. D. Michael and P. O'. Neil, Science **287**, 1603 (2000).

[7] L. Sanche, Eur. Phys. J. D **35**, 367 (2005).

[8] P. Swiderek, Angew. Chem. Int. Ed. **45**, 4056 (2006).

[9] S. M. Pimblott and J. A. LaVerne, Radiat. Phys. Chem. **76**, 1244 (2007).

[10] E. Alizadeh and L. Sanche, Chem. Rev. **112**, 5578 (2012) and references therein.

[11] G. Hanel, B. Gstir, S. Denfil, P. Scheier, M. Probst, B. Farizon, M. Farizon, E. Illenberger, and T. D. Mark, Phys. Rev. Lett. **90**, 188104 (2003).

[12] B. Boudaïffa, P. Cloutier, D. Hunting, M. A. Huels, and L. Sanche, Science **287**, 1658 (2000).

[13] P. Ball, Nature **421**, 421 (2003) and references therein.

[14] K. Luger, A. W. Mader, R. K. Richmond, D. F. Sargent, and T. J. Richmond, Nature **389**, 251 (1997).

[15] G. Felsenfeld and M. Groudine, Nature **421**, 448 (2003).

[16] J. Simons, Acc. Chem. Res. **39**, 772 (2006) and references therein.

[17] I. Baccarelli, I. Bald, F. A. Gianturco, E. Illenberger, and J. Kopyra, Phys. Rep. **508**, 1 (2011) and references therein.

[18] J. Gu, J. Leszczynski, and H. F. Schaefer III, Chem. Rev. **112**, 5603 (2012).

[19] I. Bald, in *Ideas in Chemistry and Molecular Sciences;* edited by Bruno Pignataro (Wiley-VCH, 2010), p 144.

[20] J. N. Bardsley and F. Mandl, Rep. Prog. Phys. **31**, 471 (1968).

[21] G. J. Schultz, Rev. Mod. Phys. **45**, 379 (1970).

[22] A. Chutjian, A. Garscadden, and J. M. Wadehra, Phys. Rep. **264**, 393 (1996).

[23] R. E. Palmer and P. J. Rous, Rev. Mod. Phys. **64**, 383 (1992).

[24] T. Uzer and W. H. Miller, Phys. Rep. **199**, 73 (1991).

[25] Q. B. Lu, Int. J. Mod. Phys. B **27**, 1350073 (2013).

[26] L. S. Cederbaum, J. Zobeley, and F. Tarantelli, Phys. Rev. Lett. **79**, 4778 (1997).

[27] H. Kim, J. Titze, M. Schoffler, F. Trinter, M. Waitz, J. Voigtsberger, H. Sann, M. Meckel, C. Stuck, U. Lenz, M. Odenweller, N. Neumann, S. schossler, K. Ullmann-Pfleger, B. Ulrich, R. C. Fraga, N. Petridis, D. Metz, A. Jung, R. Grisenti, A. Czasch, O. Jagutzki, L.

Schmidt, T. Jahnke, H. Schmidt-Bocking, and R. Dorner, Proc. Natl. Acad. Sci. U.S.A **108**, 11821 (2011).

[28] J. B. Little, Carcinogenesis **21**, 397 (2000).

[29] K. Aflatooni, G. A. Gallup, and P. D. Burrow, J. Phys. Chem. A **102**, 6205 (1998).

[30] S. Ptasinska, S. Denifl, P. Scheier, and T. D. Mark, J. Chem. Phys. **120**, 8505 (2004).

[31] R. Barrios, P. Skurski, and J. Simons, J. Phys. Chem. B **106**, 7991 (2002).

[32] M. A. Huels, B. Boudaïffa, P. Cloutier, D. Hunting, and L. Sanche, J. Am. Chem. Soc. **125**, 4467 (2003).

[33] X. Li, M. D. Sevilla, and L. Sanche, J. Am. Chem. Soc. **125**, 13668 (2003).

[34] J. Berdys, I. Anusiewicz, P. Skurski, and J. Simons, J. Phys. Chem. A **108**, 2999 (2004).

[35] I. Dabkowska, J. Rak, and M. Gutowski, Eur. Phys. J. D **35**, 429 (2005).

[36] M. R. Vilar, A. M. B. do Rego, A. M. Ferraria, Y. Jugnet, C. Nogues, D. Peled, and R. Naaman, J. Phys. Chem. B **112**, 6957 (2008).

[37] X. Pan, P. Cloutier, D. Hunting, and L. Sanche, Phys. Rev. Lett. **90**, 208102 (2003).

[38] H. Abdoul-Carime, S. Gohlke, E. Fischbach, J. Scheinke, and E. Illenberger, Chem. Phys. Lett. **387**, 267 (2004).

[39] F. Martin, P. D. Burrow, Z. Cai, P. Cloutier, D. Hunting, and L. Sanche, Phys. Rev. Lett. **93**, 068101 (2004).

[40] J. Berdys, I. Anusiewicz, P. Skurski, and J. Simons, J. Am. Chem. Soc. **126**, 6441 (2004).

[41] A. M. Scheer, K. Aflatooni, G. A. Gallup, and P. D. Burrow, Phys. Rev. Lett. **92**, 068102 (2004).

[42] S. Ptasińska, S. Denfl, P. Scheier, E. Illenberger, and T. D. Märk, Angew. Chem. Int. Ed. **44**, 6941 (2005).

[43] Y. Zheng, P. Cloutier, D. J. Hunting, L. Sanche, and J. R. Wagner, J. Am. Chem. Soc. **127**, 16592 (2005).

[44] J. Gu, Y. Xie, and H. F. Schaefer III, J. Am. Chem. Soc. **127**, 1053 (2005).

[45] S. Tonzani and C. H. Greene, J. Chem. Phys. **124**, 054312 (2006).

[46] J. Gu, Y. Xie, and H. F. Schaefer III, J. Am. Chem. Soc. **128**, 1250 (2006).

[47] J. Gu, J. Wang, and J. Lesczynski, J. Am. Chem. Soc. **128**, 9322 (2006).

[48] X. Bao, J. Wang, J. Gu, and J. Leszczynski, Proc. Natl. Acad. Sci. U.S.A. **103**, 5658 (2006).

[49] J. Simons, Adv. Quantum Chem. **52**, 171 (2007).

[50] S. Denifl, P. Sulzer, D. Huber, F. Zappa, M. Probst, T. D. Mark, P. Scheier, N. Injan, J. Limtrakul, R. Abouaf, and H. Dunet, Angew. Chem. Int. Ed. **46**, 5238 (2007).

[51] S. Ptasinska and L. Sanche, Phys. Rev. E **75**, 031915 (2007).

[52] T. Solomun and T. Skalicky, Chem. Phys. Lett. **453**, 101 (2008).

[53] V. S. Prabhudesai, D. Nandi, A. H. Kelkar, and E. Krishnakumar, J. Chem. Phys. **128**, 154309 (2008).

[54] R. K. Singh, M. Sarma, and M. K. Mishra, Indian J. Phys. **81**, 983 (2007).

[55] M. Sarma, S. Adhikari, and M. K. Mishra, J. Chem. Phys. **126**, 044309 (2007).

[56] Y. Zheng, D. J. Hunting, P. Ayotte, and L. Sanche, Phys. Rev. Lett. **100**, 198101 (2008).

[57] L. Sanche, Chem. Phys. Lett. **474**, 1 (2009).

[58] J. Kopyra, Phys. Chem. Chem. Phys. **14**, 8287 (2012).

Chapter 2

Single strand breaks in 2′-deoxycytidine-3′-monophosphate

2.1 Introduction

Single strand breaks (SSBs) are one of the most studied form of DNA damage induced by low energy electrons (LEEs). Discontinuities which occur in one strand of the DNA double helix are known as SSB [1]. These damages are usually accompanied by loss of a single nucleotide resulting in the formation of a 5′- and/or 3′-termini at the site of the break. Cells have evolved with a rapid and efficient mechanisms to repair these discontinuities. However, if these chromosomal SSBs are not repaired appropriately, they pose a serious threat to genetic stability and cell survival [2]. The mechanism by which these SSBs are formed inside the cell is not characterized fully yet. As discussed in chapter 1, LEEs play a prominent role in inducing strand breaks to DNA molecule. In this chapter, we address the mechanistic pathway of SSBs induced by LEEs that may have a major role in cell death. To be specific, we are interested in the reactions taking place at the physical stage of radiation induced DNA damage. Moreover, out of the three sites reported for DNA damage induced by LEEs, [3] the DNA backbone, i.e., sugar-phosphate C–O bond is more susceptible to scission than the base N–H and glycosidic (N–C) bonds due to the lowest activation energy barrier for the electron for the C–O bond cleavage. In addition, large electron affinity of the

phosphate radical ($\sim$ 5 eV) [3, 4] enforces electron migration to that site; such a phenomenon favors cleavage of the C–O bond [3–5]. Moreover, the most favorable position where the attachment of LEE was assumed to be either base-π^* or phosphate P=O π^* orbital, the former is preferred for LEE attachment in the 0–3 eV range [3, 4]. Further, the electron attachment to these DNA components is found to be resonant in nature. Many possible mechanisms were proposed, for DNA damage, by various experimental [6–10] and theoretical groups [3, 5, 11–17]. However, the principal mechanism behind such adverse processes proceeds via the formation of a transient negative ion (TNI) followed by the dissociation of a covalent bond within the system [8].

2.2 Theoretical Method

2.2.1 An outline of wavepacket approach

As discussed in our objectives, our aim is to implement the local complex potential based time dependent wave packet (LCP-TDWP) approach [18, 19] for the calculation of DEA cross-sections in selected DNA fragments. A well formulated theoretical modeling is an essential requirement for understanding this damage process in conjunction with the experimental findings. Before going to the details of our theoretical modeling, let us see some of the basic features of wavepacket analysis in general. At this moment, we would like to mention that we have considered only the modeling of "half-collision" experiment, i.e., we have focused on the theoretical descriptions of the *"dynamics"* and *"detachment"* stages of the *resonant electron-molecule scattering* process [20]. In general, the initial wavepacket corresponds to the nuclear wavefunction of the neutral system in a particular vibrational state. Upon electron attachment, this initial wavepacket will drift to the anionic potential energy curve following the Franck-Condon transition. Since the wavepacket is initially localized in space, it contains a range of energies as a result of Heisenberg's uncertainty principle. Each energy component within the wavepacket propagates independently since energy is a conserved quantity according to the energy conservation principle. Thus, we can compute the observable quantities such as cross section or fragmentation profile for all energies contained within the

initial wavepacket. Therefore, a single calculation of the wavepacket dynamics can provide cross section yield over a wide range of energies. This factor enables wavepacket analysis as a most powerful technique in the field of reactive scattering. We have employed this approach in conjunction with local complex potential formalism for describing the uni-molecular dissociation process in selected DNA fragments. To add further, we have tested our method on a "bottom-up" approach (in terms of molecular modeling and theoretical approach) basis in the polyatomic systems where the quantum reaction dynamics is carried out for one dimensional potential energy curves only.

2.2.2 LCP-TDWP approach

The interaction of LEEs with DNA components is, in principle, a multidimensional problem. However, for our "bottom-up" approach analysis we have not considered more than single dissociation channels due to the problems associated in dealing with the multidimensional potential energy surfaces for the time-dependent quantum mechanical calculations. Intra molecular vibrational energy redistribution (IVR) [21] may take a leading role in “vibrational state specificity” during the nuclear dynamics. If IVR process distributes energy into a large number of vibrations in a short time compared to the bond dissociation process, then one has to consider the multi-dimensional decay channel during the dynamics. In general, the IVR takes place in a much longer time scales (usually within picosecond timescale) than the shape resonance lifetime (within 10–100 fs) for the selected DNA fragments. Therefore, we can reasonably treat the coupled dissociation channels separately. Alternatively, one can consider the “heavy atom effect” in which the heavy atoms can block the IVR from one mode of vibration to other modes in gas phase. In either way, we can qualitatively treat the multidimensional problem into single channel dissociation.

The electron attachment to the neutral molecule (A) leads to the formation of a metastable compound molecular anion (A^-) and the nuclear motion now evolves under the influence of the anionic Hamiltonian (H_{A^-}). The nuclear motion of A^- (for quantum dynamical calculations, A^- represents only the chemical bond which is undergoing dissociation) in the

time dependent formalism can be written as [18, 19]

$$\psi_i(R,t) \simeq e^{-iH_{A^-}(R)t/\hbar}\phi_i(R) \quad \text{with} \tag{2.1}$$

$$H_{A^-}(R) = -\frac{\hbar^2}{2\mu_{A^-}}\nabla^2 + W_{A^-}(R); \quad \text{and} \tag{2.2}$$

$$W_{A^-}(R) = E_{A^-}(R) - \frac{i}{2}\Gamma_{A^-}(R) \tag{2.3}$$

where $\psi_i(R,t)$ corresponds to the time evolution of the i-th initial vibrational wave function $\phi_i(R)$ of the neutral target. μ_{A^-} and $W_{A^-}(R)$ are the reduced mass and local complex potential (LCP) of the metastable A^- respectively. The vibrational eigen functions $\phi_i(R)$ and $\chi_i(R)$ are obtained by employing Fourier grid Hamiltonian (FGH) method [22] to $E_A(R)$ and $E_{A^-}(R)$ respectively. FGH method has proved to be a versatile and efficient method for obtaining bound state eigen values and eigen vectors.

In local complex potential (LCP) formulation, the time evolution of the metastable anion is controlled by a complex energy i.e., $\psi_n \propto exp(-iW_nt/\hbar)$ with $W_n = E_n - \frac{i}{2}\Gamma_n$, where W_n is called LCP as stated above. It follows that $|\psi_n|^2 \propto exp(-\Gamma_n t/\hbar)$ and the real part of W_n, i.e., E_n serves as the PE of the anion in the time evolution of nuclear dynamics and imaginary part Γ_n is related to the life time (τ) as $\tau = \frac{\hbar}{\Gamma}$ and controls the decay pattern of the metastable anionic state. The nuclear motion of the metastable compound anion A^- therefore takes place in a complex potential, [18, 19, 23, 24] $W_{A^-}(R)$, whereby availability of these complex potentials becomes the critical input to any investigation of the dynamical features underlying the formation and decay of these metastable resonances.

The width function for the metastable anion $\Gamma_{A^-}(R)$ is calculated as a decaying exponential as [18, 19],

$$\Gamma_{A^-}(R) = \delta_1 \times exp(-\alpha R) \tag{2.4}$$

where α is chosen such that $\Gamma_{A^-}(R)$ goes to zero at the crossing point R = R_x between $E_A(R)$ and $E_{A^-}(R)$ and δ_1 has been chosen such that the wave function for nuclear motion exist only within the lifetime for a shape resonance phenomenon. This is due to the fact that at the Franck Condon region (the region where the propagation starts) the density of states

coupled to the continuum is higher (hence, the decay) than that at the larger internuclear distances. In other words, we can say that the interference effects become more pronounced at the Franck Condon region and it reduces as we move from the equilibrium internuclear distance to the larger internuclear distances. This gradual decrease can be approximated to an exponential decay which can also understand from the energy-time uncertainty relationship. We have used this model resonance width function from our earlier investigations on e-N_2, e-H_2, and e-CO scattering [18, 19] due to the non availability of the resonance width for the DNA fragment (Fig. 2.1). As we can see from Eq. (2.4), one can control the decay pattern and consequently the nuclear motion of the wave function by controlling α and δ_1.

The time propagation is carried out by solving time dependent Schrödinger equation

$$i\hbar\frac{\partial\psi_i}{\partial t} = \hat{H}_{A^-}\psi_i \tag{2.5}$$

The effect of kinetic energy operator in $(\hat{H}_{A^-}\psi_i)$ of the anionic Hamiltonian on the initial vibrational wave function $\psi_i(R,t=0)$=$\phi_i(R)$ is computed by fast Fourier transform technique [25] and Lanczos scheme (see Appendix C) [26] is used for time propagation of the initial wave function in our implementation.

Finally, we have utilized the Fourier transform of the auto correlation function $\langle\chi_i(R)|\psi_i(R,t)\rangle$ which is the projection of anionic eigen functions obtained using anionic PE curve with time dependent wave function to calculate the fragmentation profile σ(E) as [27]

$$\sigma(E) = \int_{-\infty}^{\infty} exp(iEt/\hbar)\langle\chi_i(R)|\psi_i(R,t)\rangle dt \tag{2.6}$$

2.2.3 Modeling of 3′–dCMPH molecule

It is difficult to consider *in vivo* DNA as a computational model for our study because of the presence of large number of atoms, thereby, making the system computationally expensive. Therefore, we have selected a portion of the full DNA molecule which contains the region where the LEE attachment takes place and also the region where the strand breaks occur. In case of a real DNA, substantial amount of water is also present besides counter ions like Na^+,

K^+, etc. for neutralizing the negative charge on phosphate group. So, besides solvation, it is necessary to neutralize the negative charge on the phosphate group so that a reliable *in vivo* system can be approximated computationally. On the other hand, a gas phase system, although not being identical to the solvated state, can be a suitable choice for exploring the mechanistic pathway of DNA damage. One such system that we have considered in this investigation is 2′-deoxycytidine-3′-monophosphate [5, 12], in short 3′-dCMPH, (A) [Fig. 2.1]. The generated radical centers at DNA backbone are neutralized by adding hydrogen

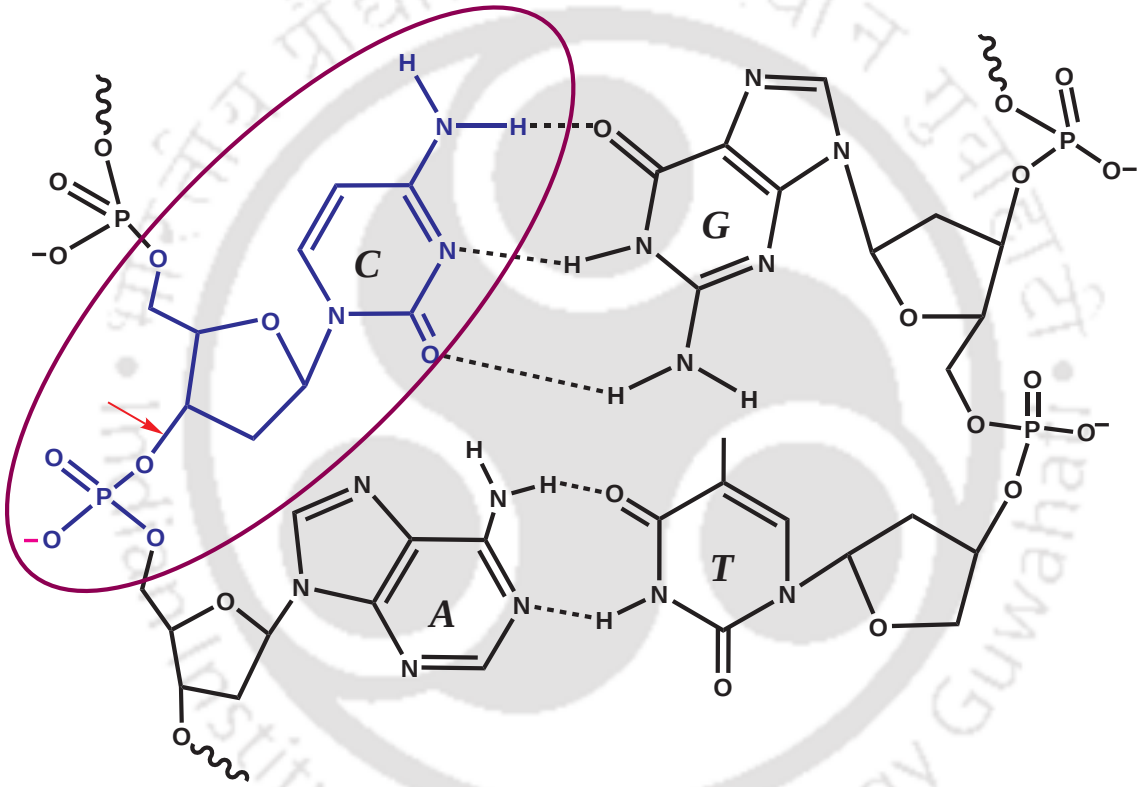

Fig. 2.1 Fragment excised from DNA molecule representing base-sugar-phosphate group (taken from Ref. 5) known as 2′-deoxycytidine-3′-monophosphate (3′-dCMPH) in blue color inside the circle while the bond susceptible to cleave (single strand breaks) is labeled with a red arrow mark.

while the negative charge on phosphate group ($-OPO_3^-$) is neutralized by adding a proton to ensure the smooth attachment of the incoming electron. If such centers were not so terminated, it would provide an artificial electron attachment sites during our modeling. The modeled nucleotide system contains cytosine pyrimidine nucleobase whose observed

vertical attachment energy is 0.32 eV [28] for the lowest π^* delocalized orbital system. Further, a deoxy ribose sugar, characteristic of all such fragments of DNA, is connected to the cytosine base via N–C glycosidic bond. A phosphate group is attached to this sugar via the sugar-phosphate C–O bond which is going to be ruptured (known as SSBs in the present case) after the electron attachment.

2.2.4 Electronic structure calculation

The PE curves of neutral and anionic systems in the gas phase have been computed using Gaussian 03W program suite [29]. In this initial attempt, we have chosen Hartree Fock (HF) method and 6-31+G(d) as the basis set for calculating these PE curves. The neutral PE curve [E_A(R)] has been generated from the optimized geometry stretching the labeled sugar-phosphate C–O bond at 256 equally discretized points in the interval of 1–10 a_0 with a step size of 0.04 a_0 using the rigid option. To calculate the anionic PE curve [E_{A^-}(R)], we have added an electron to the LUMO, π^*– orbital of the base, and have utilized the unrestricted HF theory with the same basis set and options that we have used for the neutral molecule.

2.3 Results and Discussions

As mentioned earlier, E_A(R) and E_{A^-}(R), where A = 3′–dCMPH have been calculated by stretching the labeled C–O bond through 256 equally discretized points within the range of 1–10 a_0 using HF level of accuracy with 6-31+G(d) as basis set and are plotted together in Fig. 2.2(a). From the PE curves [Fig. 2.2(a)], it is seen that electron attachment is endothermic by $\sim$ 0.65 eV whereas the electron affinity for the C–O group calculated is $\sim$ 2.37 eV. The crossing point between neutral and anionic curves is at 5.04 a_0 (2.66 Å). The width function, another ingredient, has been calculated using Eq. (2.4) at each grid points, as a decaying function where the parameter δ_1 is chosen as 65 to sustain the metastability of the system and is shown in Fig. 2.2(b). The highest value of Γ_{A^-}(R) = 103.8 eV, is at the lowest C–O bond length may be due to the larger internuclear repulsion experienced by the two nuclei

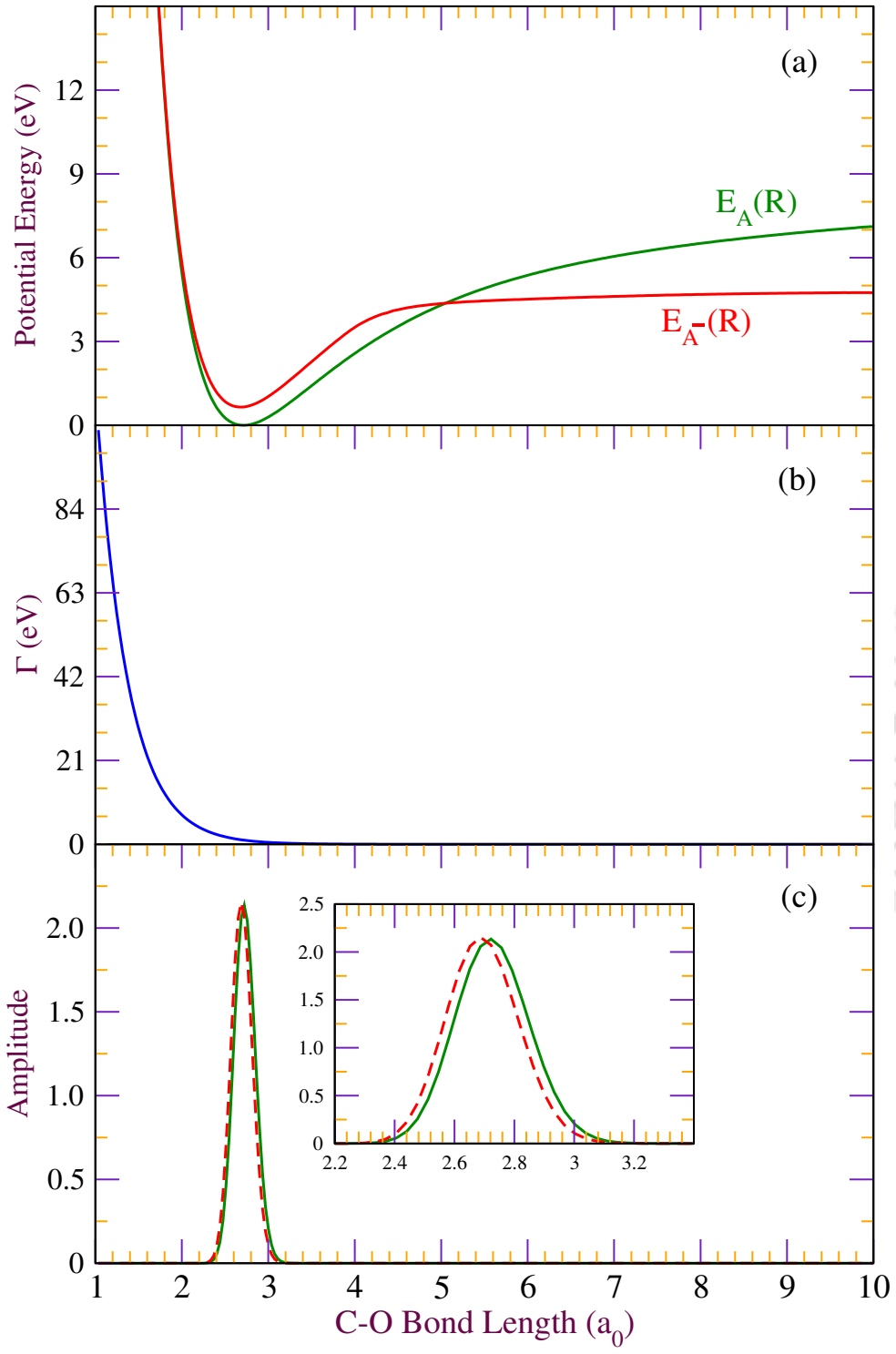

Fig. 2.2 (a) Potential energy curves for neutral [E_A(R)] and the real part [E_{A^-}(R)] of the local complex potential [W_{A^-}(R)] for A=3′–dCMPH, (b) the width function [Γ_{A^-}(R)], and (c) ground state vibrational eigenfunctions for neutral [ϕ_0(R)] (solid line) and anionic [χ_0(R)] (dashed line) systems.

whereas at equilibrium bond length Γ_{A^-}(R) has the value of 0.92 eV. Its value goes to zero at the crossing point and assists as a decaying function for wave function in the nuclear dynamics. The vibrational eigenfunctions of neutral [ϕ_i(R)] and anionic [χ_i(R)] systems have been calculated using FGH method [22]. In Fig. 2.2(c), we have plotted the ground state vibrational wave functions of neutral and anionic systems. As we can see, both the wave functions have similar spatial profiles with neutral one being slightly shifted towards the right turning point of the PE curve than the anionic wave function.

Time evolution of the ground state wave function of the neutral molecule under the effect of metastable anionic Hamiltonian initiated at time t = 0 and propagated in time steps of Δt = 1 au of time ($\sim$ 0.02 fs) for a total of 8192 time steps ($\sim$198 fs). Some snapshots of the time evolution at t = 0, 2, 4, 6, 8, 10, 12, 14, 16, 18, 20, and 22 fs are presented in Fig. 2.3. A careful analysis of the time evolution plots lead to the following remarks: (a) the amplitude of the wave function significantly diminishes with time, (b) the wave function is moving slowly towards the right turning point of classical region, (c) there is no reflection of the wave function from the right turning point, and (d) near 18 fs, the probability amplitude spreads over to the classical region. These observations from our nuclear dynamics calculation enable us to suggest that during the decay of metastable anion, the C–O bond does not get enough time to execute at least one vibration, since as mentioned by Barrios et al., [5] the vibrational period of a C–O bond is around 33 fs. Notably, our calculation shows that the C–O bond gets ruptured within 18 fs which falls under the expected shape resonance life time for this metastable species.

The above discussions lead us to support the mechanism provided by Gu et al. [12] where they discussed the possibility of electron migration from cytosine to sugar-phosphate bond, operates directly through the spatial overlap between atomic orbitals of C_6 of pyrimidine and C_3' of sugar, resembles like S_N2 type mechanistic pathway. Therefore, the underlying phenomena during LEE induced SSB may be outlined in following two steps.

Step 1: LEE attachment to the LUMO of cytosine resulting in the formation of a metastable species,

Step 2: The atomic orbital overlaps between C_6 center of the non-planar cytosine and the C_3'

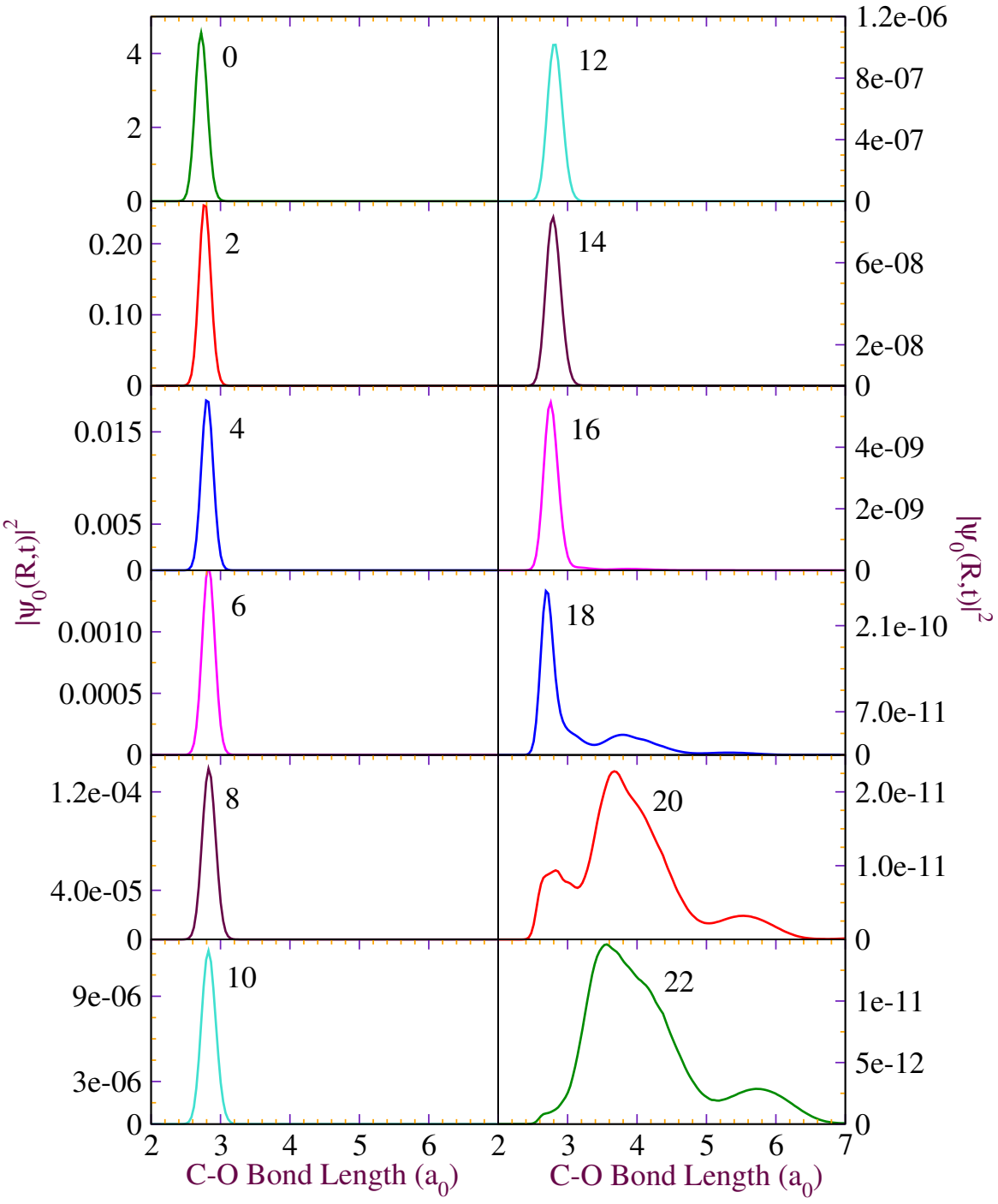

Fig. 2.3 Time evolution plots of ground state wave function ϕ_0(R) [Fig. 2.2(c)] under the effect of anionic Hamiltonian at time t = 0, 2, 4, 6, 8, 10, 12, 14, 16, 18, 20, and 22 fs.

center of the sugar where the excess charge induces dissociation of the C–O bond, tagged as "charge induced dissociation", while migrates to the DNA backbone [12]. Large electron affinity of the phosphate radical ($\sim$ 5 eV) [3, 4] may favor the atomic orbitals overlap and fission of the bond and thus generates comparatively stable nucleoside radical as well as phosphate anion.

As suggested earlier, the time requires for LEE induced SSB from our calculation thus reinforces the above mentioned steps since S_N2 reactions are typically fast processes. Singly occupied molecular orbitals (SOMOs) of the anionic species (Fig. 2.4) show the electron migration from cytosine to phosphate radical is evident as it resides in the π^* orbital of the cytosine base at equilibrium bond length (1.45 Å) [Fig. 2.4(a)] while at larger C–O bond length (3 Å) [Fig. 2.4(b)] the electron locates on the phosphate group.

In Fig. 2.5(a), we have plotted the auto correlation function ($\langle\chi_0(R)|\psi_0(R,t)\rangle$) which shows the maximum overlap when propagation starts and decreases exponentially to negligibly small values at t = 10 fs. Fourier transformation of this auto correlation function yields the fragmentation profile and is compared with that of experimental investigation on plasmid DNA in condensed phase [9], shown in Fig. 2.5(b). As we can see from our fragmentation profile, the maximum peak position is found to be around 0.75 eV which is in very good agreement with experimental maximum peak position (0.8 eV) and assures the involvement of shape resonance phenomena during SSB. The structureless feature in the fragmentation profile may be linked as *impulse model* [24] classification [Impulse model arises if the vibrational period ($\frac{1}{\omega}$) of the resonance potential is greater than the resonance life time ($\frac{\hbar}{\Gamma}$), i.e., $\Gamma \gg \hbar\omega$.] and this can be confirmed from time evolution plots of Fig. 2.3, where only simple diminution of the probability amplitude with no typical movement of the amplitude between right and left turning points of the PE curve is seen. Therefore, our approach may provide a new insight to the area of electron induced scattering in DNA and its related fragments.

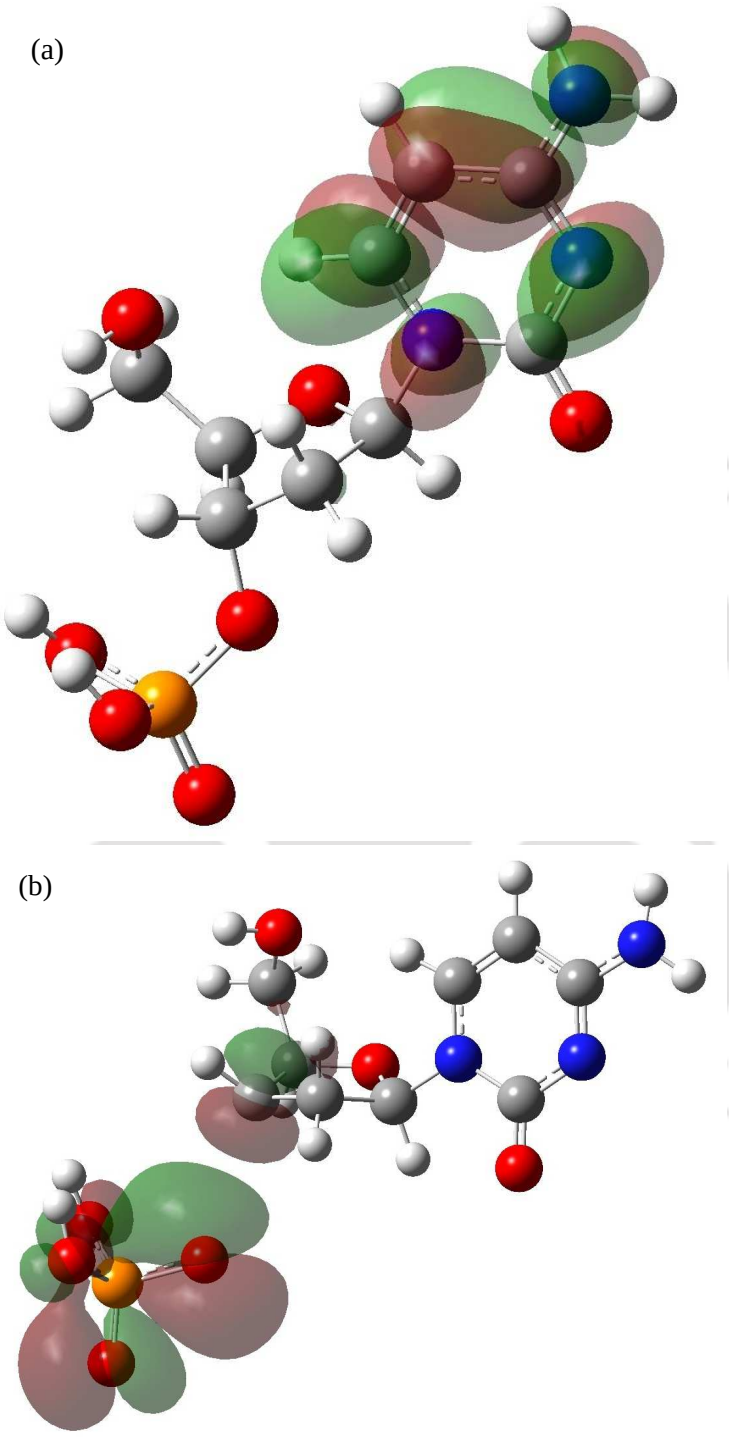

Fig. 2.4 Singly occupied molecular orbitals for anionic 3′–dCMPH molecule at equilibrium C–O bond length 2.75 a_0 (1.45 Å) (a) where extra electron is situated at base π^* orbital, and at 5.67 a_0 (3 Å) where excess charge locates on phosphate group shown in (b).

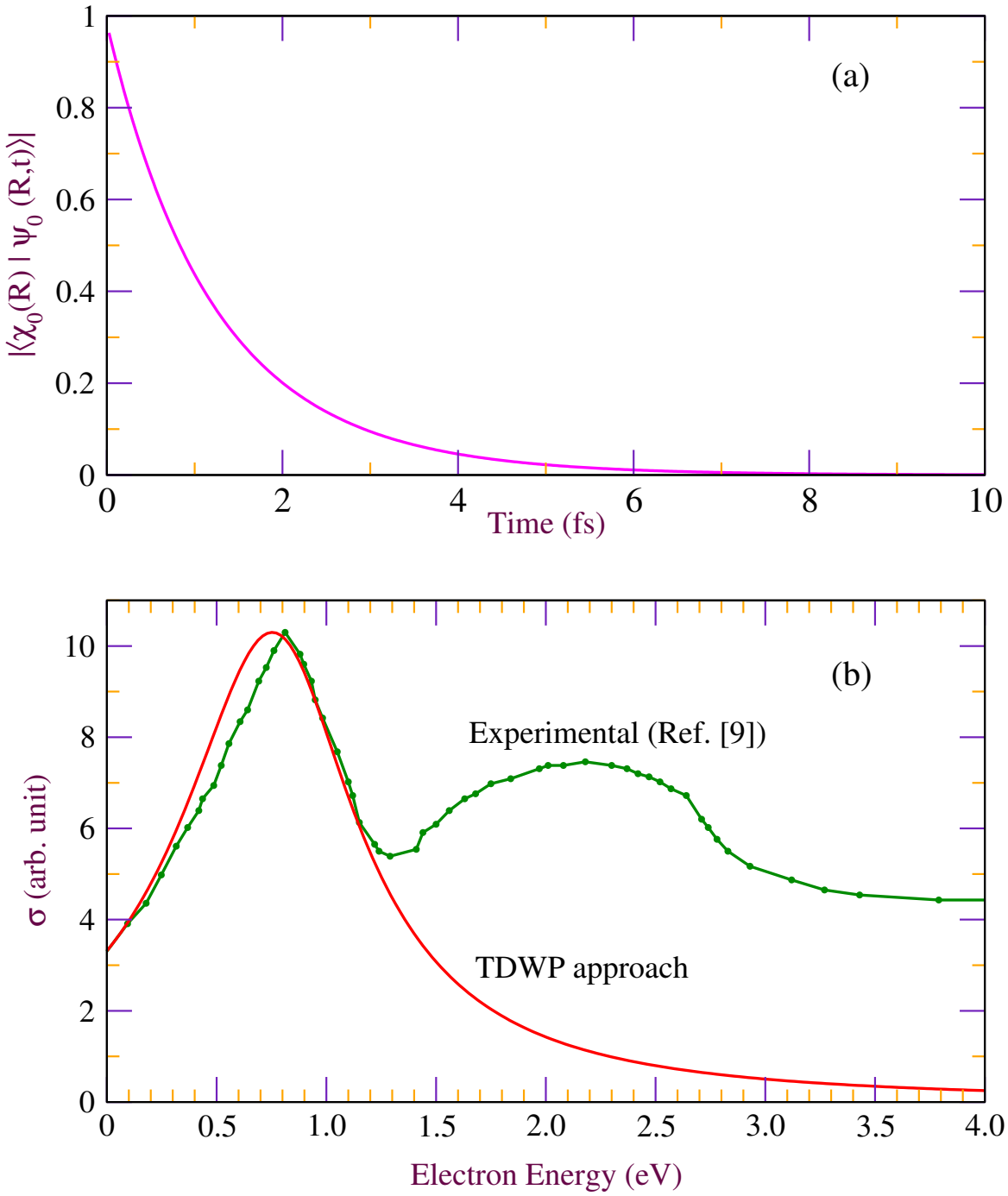

Fig. 2.5 (a) Calculated auto correlation function $|\langle\chi_0(R)|\psi_0(R,t)\rangle|$ exhibiting the shape resonance phenomenon, and (b) comparison of corresponding fragmentation profile, σ(E), of (a), with the experimental result [9].

2.4 Concluding Remarks

Our objective in this work is to offer a quantitative profile for low energy electron induced SSB in 3′–dCMPH using local complex potential based time dependent wave packet approach. Preliminary results from our calculations are in agreement with earlier investigation [12] highlighting the involvement of shape resonance phenomena through which SSB can occur in the gas phase for this fragment. Most of the earlier theoretical findings [3–5] suggested that SSB can be activated only for a solvated system using LEEs. However, Gu et al. have shown the presence of a low activation energy (6.2 kcal/mol) barrier during C–O bond cleavage and proposed the possibility of SSB in gas phase for the same moiety from their time independent study [12]. To the best of our knowledge, no theoretical cross section is available in the literature for this DNA fragment using time dependent quantum mechanical treatment till date. Thus, our time dependent study has provided a direct comparison between theoretical and experimental results for the first time.

We hope our findings from LCP-TDWP calculations offer a starting point for further investigations on LEE induced scattering in DNA and DNA fragments. We also would like to emphasize that, the findings of this initial calculations are by no means definitive. Therefore, we have generated the PE curves for this system using correlated methods like second order Møller–Plesset perturbation theory (MP2) so that a comparative analysis can be made for the mechanistic pathway to SSB induced by LEEs and also can deduce the electron correlation effects during the damage process. The details of these calculations are provided in the next chapter.

References

[1] K. W. Caldecott, Nature Rev. Genet. **9**, 619 (2008).

[2] B. D. Michael and P. O'. Neil, Science **287**, 1603 (2000).

[3] J. Simons, Acc. Chem. Res. **39**, 772 (2006) and references therein.

[4] J. Simons, Adv. Quantum Chem. **52**, 171 (2007).

[5] R. Barrios, P. Skurski, and J. Simons, J. Phys. Chem. B **106**, 7991 (2002).

[6] B. Boudaïffa, P. Cloutier, D. Hunting, M. A. Huels, and L. Sanche, Science **287**, 1658 (2000).

[7] G. Hanel, B. Gstir, S. Denfil, P. Scheier, M. Probst, B. Farizon, M. Farizon, E. Illenberger, and T. D. Mark, Phys. Rev. Lett. **90**, 188104 (2003).

[8] M. A. Huels, B. Boudaïffa, P. Cloutier, D. Hunting, and L. Sanche, J. Am. Chem. Soc. **125**, 4467 (2003).

[9] F. Martin, P. D. Burrow, Z. Cai, P. Cloutier, D. Hunting, and L. Sanche, Phys. Rev. Lett. **93**, 068101 (2004).

[10] L. Sanche, Eur. Phys. J. D **35**, 367 (2005).

[11] J. Gu, Y. Xie, and H. F. Schaefer III, J. Am. Chem. Soc. **128**, 1250 (2006).

[12] J. Gu, J. Wang, and J. Leszczynski, J. Am. Chem. Soc. **128**, 9322 (2006).

[13] X. Bao, J. Wang, J. Gu and J. Leszczynski, Proc. Natl. Acad. Sci. U.S.A. **103**, 5658 (2006).

[14] P. F. Loos, E. Dumont, A. D. Laurent, X. Assfeld, Chem. Phys. Lett. **475**, 120 (2009).

[15] C. R. Wang, J. Nguyen, and Q. B. Lu, J. Am. Chem. Soc. **131**, 11320 (2009).

[16] E. Brun, P. Cloutier, C. S. Roselli, M. Fromm, and L. Sanche, J. Phys. Chem. B **113**, 10008 (2009).

[17] J. Gu, J. Wang, and J. Lesczynski, Nucl. Acids Res. **38**, 5280 (2010).

[18] R. K. Singh, M. Sarma, and M. K. Mishra, Indian J. Phys. **81**, 983 (2007).

[19] M. Sarma, S. Adhikari, and M. K. Mishra, J. Chem. Phys. **126**, 044309 (2007).

[20] R. E. Palmer and P. J. Rous, Rev. Mod. Phys. **64**, 383 (1992).

[21] T. Uzer and W. H. Miller, Phys. Rep. **199**, 73 (1991).

[22] C. C. Marston and G. G. Balint-Kurti, J. Chem. Phys. **91**, 3571 (1989).

[23] L. Dubé and A. Herzenberg, Phys. Rev. A **20**, 194 (1979).

[24] J. N. Bardsley and J. M. Wadehra, Phys. Rev. A **20**, 1398 (1979).

[25] D. Kosloff and R. Kosloff, J. Comput. Phys. **52**, 35 (1983).

[26] C. Leforestier, R. H. Bisseling, C. Cerjan, M. D. Feit, R. Friesner, A. Guldberg, A. Hammerich, G. Jolicard, W. Karrlein, H.-D. Meyer, N. Lipkin, O. Roncero, and R. Kosloff, J. Comput. Phys. **94**, 59 (1991).

[27] J. Zhang, D. G. Imre, and J. H. Frederick, J. Phys. Chem. **93**, 1840 (1989).

[28] K. Aflatooni, G. A. Gallup, and P. D. Burrow, J. Phys. Chem. A **102**, 6205 (1998).

[29] M. J. Frisch, G. W. Trucks, H. B. Schlegel, et al., *GAUSSIAN 03*, Revision E.01, Gaussian,Inc., Wallingford, CT, 2004.

Chapter 3

Effect of quantum tunneling on single strand breaks in 3′-dCMPH molecule

3.1 Introduction

It is well known that quantum tunneling plays a pivotal role during the decay of a metastable state formed after impinging electrons on the system [1]. Moreover, it has also been shown that the decay of such a quasistationary system can be to a good approximation modeled using an exponential law [2]. In certain cases, nonexponential nature of decay by tunneling is also observed wherein the depth of the potential energy curve become significant to determine the duration for which the resonant state becomes alive [3]. It was Heller and Brown [4] who have discussed the need for multidimensional tunneling calculations in the decay of metastable states.

In chapter 2, we have demonstrated single strand breaks (SSBs) in a modeled DNA fragment 2′-deoxycytidine-3′-monophosphate (3′-dCMPH) in gas phase from the ab-initio Hartree Fock (HF) [5] method and local complex potential based time dependent wave packet (LCP-TDWP) approach. The starting point for our quantum dynamical calculations (QDCs) were the neutral and anionic PE curves of the 3′-dCMPH moiety and the decay function resulting from the electron attachment to the target (3′-dCMPH) molecule. Low energy electron (LEE) captures by the nucleobase (cytosine in 3′-dCMPH) plays a prominent

role during the cleavage of the sugar-phosphate C–O (3′ C–O) bond and the fragmentation profile calculated clearly manifest the shape resonance phenomena during the process [5]. However, since the cross section peak is highly method dependent and therefore, to verify the same, here in this chapter, we present the results obtained from the computationally more demanding second order Møller–Plesset perturbation theory (MP2) at the 6-31+G(d) accuracy level in conjunction with LCP-TDWP approach.

Furthermore, in our DFT-B3LYP based investigation on 3′-dCMPH moiety, a hyperbolic cosine barrier was seen in the anionic PE curve [6]. We argued the presence of the PE barrier may be a result of coupling between π^* and σ^* resonance states of the 3′-dCMPH moiety owing to electron correlation. The barrier in the anionic PE curve give us indication towards a non negligible quantum tunneling probability of the 3′ C–O bond from the highest vibrational level of the anionic PE curve during single strand breaks. We summarized in the DFT-B3LYP based investigation that the signature of quantum tunneling might have a considerable role during SSBs [6]. Therefore, to explore the electron correlation effect and to examine what extent the quantum tunneling is effective during SSB, it is our aim in this chapter to revisit the problem at the MP2/6-31+G(d) theoretical accuracy. Finally, we provide a comparative assessment between results from various ab initio calculations for describing the electron-molecule scattering phenomenon in LEE induced DNA damage.

A brief description of the state-of-the-art computational method is discussed in the following section. The prominent results along with discussion are presented thereafter. A salient summary of the investigation concludes this chapter.

3.2 Computational Method

3.2.1 Electronic structure calculations

Details of the modeling of 3′-dCMPH system can be found in method section 2.2.3 of chapter 2. Potential energy (PE) curves of the target [E_A(R)] and anionic [E_{A^-}(R)] systems (A = 3′-dCMPH) have been generated using G03W program suite [7] at the MP2/6-31+G(d)

accuracy level. The labeled R = 3′ C–O bond has been computed for 256 equally spaced grid points within the interval of 1–10 a_0.

3.2.2 Quantum dynamical calculations

LEE (0–3 eV) attachment to the neutral 3′-dCMPH (A) molecule results in the formation of a transient negative ion (TNI) [A^-] which is also known as *resonance* state has a typical lifetime of around 10–100 fs [8]. Time dependent characteristics of the metastable or resonance state is calculated using the successfully implemented LCP-TDWP approach [5]. Adequate descriptions of this method can be found in chapter 2.

3.2.3 Tunneling

As mentioned in the introduction, electron correlation effect might result in an a hyperbolic cosine barrier in the anionic PE curve obtained from DFT-B3LYP [6] based investigation. In our current investigation since we have used a more correlated method [MP2/6-31+G(d)], there is a possibility of interaction between π^* and σ^* states which in turn may result in a barrier in the anionic PE curve similar to that obtained in our DFT-B3LYP results [6]. Thus, to calculate the transmission coefficient, T, we will seek any one of the following functional form [9, 10]

$$T = \frac{\sinh^2(\pi k/a)}{\sinh^2(\pi k/a) + cos^2[\frac{1}{2}\pi\sqrt{1-8mU_0/\hbar^2a^2}]}, \text{ for } 8mU_0/\hbar^2a^2 < 1 \quad (3.1)$$

or,

$$T = \frac{\sinh^2(\pi k/a)}{\sinh^2(\pi k/a) + cosh^2[\frac{1}{2}\pi\sqrt{8mU_0/\hbar^2a^2-1}]}, \text{ for } 8mU_0/\hbar^2a^2 > 1 \quad (3.2)$$

where, U_0 is the height of the potential barrier, a is the width parameter, and $k = \frac{(2mE_i)^{\frac{1}{2}}}{\hbar}$. In this study, m is the reduced mass of the C–O bond and E_i is the energy of the bound vibrational state (i) of the anionic PE curve [E_{A^-}(R)].

3.3 Results and Discussions

The neutral [E_A(R)] and anionic [E_{A^-}(R)] PE curves of the 3′-dCMPH moiety have been calculated from the corresponding optimized geometries using G03W codes [7] at the ab-initio MP2/6-31+G(d) accuracy level in adiabatic approximation and are shown in Fig. 3.1(a). The kink seen in the anionic PE curve may be treated as an avoided crossing between two anionic states viz. π^* state arising from the electron attachment to the base and the sugar–phosphate C–O σ^* state, but not a diabatic representation of the PE curve. Qualitatively, the smaller 3′ C–O bond length region up to the kink [R_{C-O}: 1.0 a_0 (0.53 Å) to 3.46 a_0 (1.83 Å)] represents π^* state of the base while the region after the kink (barrier) i.e., larger 3′ C-O bond length region [$> R_{C-O}$: 3.46 a_0 (1.83 Å)] shows the repulsive C–O σ^* character. The two (π^* and σ^*) anionic states mentioned above preferably follow an avoided crossing rather than make a sudden jump from one anionic curve to the other curve due to the slow moving carbon and oxygen nuclei; a result of the adiabatic approximation considered in the present investigation. These two states may intersect to form a conical intersection which, however, has not been investigated in the present calculation. In order to study the features and the quantum dynamical aspects of diabaticity and conical intersection, use of the multi-reference methods like multi configurational self consistent field (MCSCF), multi-reference configuration interaction (MRCI) etc. are very much desirable. At present, due to our limited infrastructure facilities, it does not permit us to calculate the same.

Further, the relative height of the neutral and anionic PE curves do strongly depend on the solvent medium. In fact, previous work by Simons and co-workers [8] found that the solvent medium relatively enhances the stability of the anion formed. i.e., the π^* anion formed lies below the neutral PE curve. In such an ambiance, the rate of SSBs need not compete with autodetachment process [8]. In order to understand the damage process under realistic conditions, one can represent the physiological environment as that of *in vivo* DNA by including counter ions like Na^+ and K^+ ions, though computation of PE curves using these ions will be demanding. Such calculations will provide a modified picture of DNA damage to some extent closer to what a real biological situation is supposed to behave towards low energy electrons. One such investigation [11] using a molecular dynamics (MD) simulation

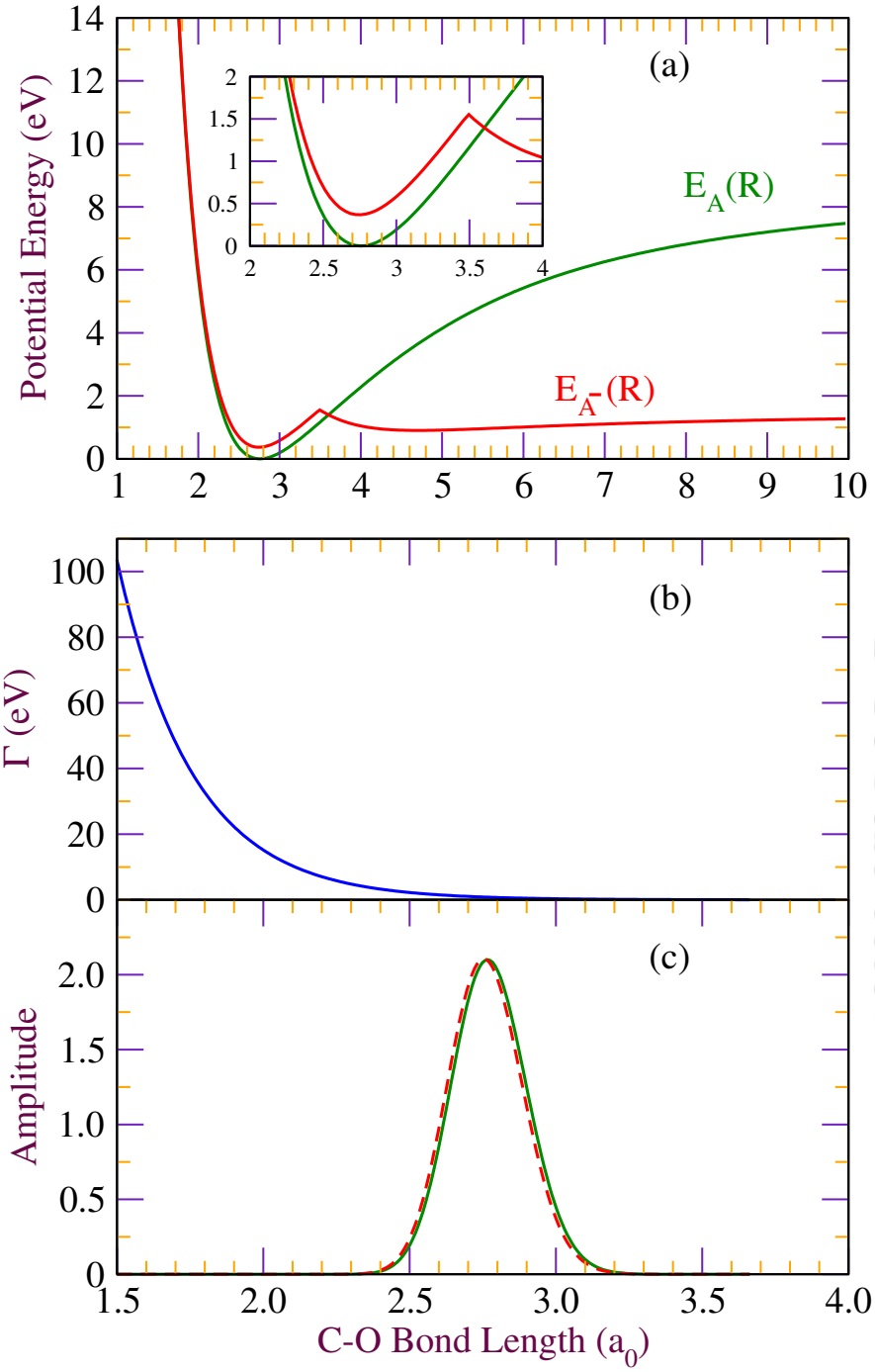

Fig. 3.1 (a) MP2/6-31+G(d) calculations based potential energy curves for the neutral [$E_A(R)$] (green solid line) and the anionic [$E_{A^-}(R)$] (red solid line) 3′-dCMPH molecules. The curtailed PE curves taken into consideration for dynamical calculation are provided in inset; (b) The imaginary part [$\Gamma_{A^-}(R)$] of the local complex potential [$W_{A^-}(R)$] for A=3′-dCMPH; (c) neutral [$\phi_0(R)$] (green solid line) and anionic [$\chi_0(R)$] (red dashed line) ground vibrational state eigenfunctions for 3′-dCMPH system.

with fully solvated thermal fluctuations of the DNA fragments like dCMP, dTMP, dAMP, dGMP (where C=Cytosine, T=Thymine, A=Adenine, G=Guanine and MP=Monophosphate) shows that the free energy barrier for the C–O bond cleavage is around 5–10 kcal/mol indicating that LEE can induce SSB in solvent medium.

The equilibrium 3′ C–O bond distance of the neutral molecule is 2.759 a_0 (1.459 Å) whereas that of the anionic molecule is 2.744 a_0 (1.452 Å) and are tabulated in Table 3.1. It can be seen from the Table 3.1 that in all three methods (HF, DFT-B3LYP, and MP2), the neutral 3′ C–O bond is more stretched than that of it's anionic counterpart. In comparison to HF method [5], DFT-B3LYP and MP2 [6, 12] 3′ C–O bond length values of respective neutrals and anions are closer to each other. The vertical attachment energy (VAE) calculated at the neutral equilibrium geometry is endothermic by 0.37 eV, which is an intermediate value between earlier HF (0.65 eV) and DFT-B3LYP (0.10 eV) results (Table 3.1). Further, the crossing point (R_x) between $E_A(R)$ and $E_{A^-}(R)$ is at 3.60 a_0 (1.90 Å). We have tested various combinations of α and δ_1 for current investigation and finally chosen the value of α = 3.84 and δ_1 = 1200 to sustain the metastability of the resonance intermediate state. A plot of width function [$\Gamma_{A^-}(R)$] with respect to the 3′ C–O bond distance (R_{C-O}) is shown in Fig. 3.1(b). As we can see from Fig. 3.1(b), the width function goes nearly to zero at R = 3.60 a_0 which is the intersection point between $E_A(R)$ and $E_{A^-}(R)$, as mentioned above. Since the crossing point (R_x) between $E_A(R)$ and $E_{A^-}(R)$ in HF, DFT-B3LYP, and MP2 methods are different, therefore we have accordingly adjusted the values of α and δ_1 (Table 3.1) for the calculation of $\Gamma_{A^-}(R)$ in each method so that the width vanishes at the respective crossing point (R_x)s. A summary of all these properties/parameters used in our present and previous calculations are collected in the Table 3.1 for comparison.

Quantum dynamical calculations (QDCs) have been done on a curtailed slice of $E_A(R)$ and $E_{A^-}(R)$ ranging from R_{C-O} = 1.42 – 3.66 a_0 with 256 equally discretized points. The reason for curtailing the R_{C-O} range for QDCs is due to the limitation of our method at present. The vibrational eigenfunctions of neutral [$\phi_i(R)$] and anionic [$\chi_i(R)$] systems have been calculated employing the well known FGH method [13] on the respective PE curve. We have found a total of 10 bound vibrational states [$\chi_{i=0-9}(R)$] for the anionic 3′-dCMPH

Table 3.1 Comparison of various properties/parameters for 3′-dCMPH molecule.

Properties	HF [5]	DFT–B3LYP [6]	MP2 [12]
[a]R_{C-O} (Å)	1.435 [b]	1.459 [b]	1.459 [b]
	1.418 [c]	1.454 [c]	1.452 [c]
VAE (eV)	0.65	0.10	0.37
R_x(Å)	2.66	1.77	1.90
δ_1	65	2500	1200
α	2.74	4.12	3.84
Barrier Height (eV)	–[d]	0.75	1.18
Barrier Width (Å)	–[d]	0.33	0.17[e]
$\sigma^{max}_{0\leftarrow 0}$(E) [eV]	0.75	0.15	0.48

[a] Equilibrium C–O bond length.
[b] Neutral 3′-dCMPH moiety.
[c] Anionic 3′-dCMPH moiety.
[d] No barrier was seen in the HF/6-31+G(d) calculation.
[e] Taken from the fitted curve of Eq. (3.3).

moiety. The spatial profiles of ϕ_i(R) and χ_i(R) are similar in nature and in accordance to our earlier studies [5, 6]. As these bound wave functions are well behaved within and including the extreme turning points of the respective PE curves, the QDCs on the shortened R_{C-O} range may not further influence quantum dynamical results.

Results obtained from our electronic structure calculations and QDCs are analyzed considering two vibrational energy regimes viz. (a) LEE and $\chi_{i=0-5}$(R) vibrational states with energy < 1 eV and (b) LEE and $\chi_{i=6-9}$(R) vibrational states with energy > 1 eV. The reason for opting for these two energy regimes is the likely involvement of two different mechanisms which may significantly contribute towards SSB in the 3′-dCMPH moiety.

3.3.1 LEE and $\chi_{i=0-5}$(R) vibrational states with energy below 1 eV [S_N2 type mechanistic pathway]

To begin with, singly occupied molecular orbital (SOMO)s for the anionic 3′-dCMPH at various distances of potential bond breaking pathway are provided in Fig. 3.2. As we can see in Fig. 3.2(a), at R_{C-O} = 2.75 a_0 (1.45 Å), SOMO shows pure π^* character on the base and

changes to π^*–σ^* coupling/overlap just before the barrier height [R_{C-O} = 3.42 a_0 (1.81 Å)] in Fig. 3.2(b). At the barrier height [R_{C-O} = 3.46 a_0 (1.83 Å)] in Fig. 3.2(c), the electron is still residing in the overlapping orbital showing the similarity with the Fig. 3.2(b). After the barrier height [R_{C-O} = 3.50 a_0 (1.85 Å)], the excess charge is seen in the 3′ C–O σ^* orbital [Fig. 3.2(d)]. The fragmented products at R_{C-O} = 5.67 a_0 (3.00 Å) of Fig. 3.2(e) are seen as the highly stable phosphate anion and the nucleoside radical with the extra electron is located on the phosphate group in analogy to that we found in our HF investigation [5] but differ from that of our DFT-B3LYP based investigation [6] where the extra electron was seen over the deoxyribose ring. The electron transfer originates from the base π^* to the 3′ C–O σ^* orbital as proposed in our earlier HF [5] and DFT-B3LYP [6] based studies once again show comforting confirmation from the present investigation. The atomic orbital overlap between C_6 center of the cytosine base and C_3' center of the sugar moiety can be visualized from Fig. 3.2(b) and can be understood as an S_N2 type process [14]. Further, large electron affinity (∼ 5 eV) of the phosphate radical [15] may play a crucial role in "charge induced dissociation" [14] of the sugar phosphate C-O bond.

For QDC, we have used the ground state wave function (ϕ_0) at t = 0 of the neutral 3′-dCMPH and then carried out time propagation under the effect of metastable anionic Hamiltonian [H_{A^-}(R)] to a total time of ∼198 fs. A few images of the time evolved wave packet from t = 0–30 fs at the interval of 2 fs are provided in Fig. 3.3. As we can see from Fig. 3.3, the amplitude of the wave function significantly diminishes with time, being reduced to 2.5x10^{-7} at t = 20 fs. It is also seen that the wave function is moving slowly towards the right turning point of the anionic PE curve. Though, we have used different width function [Γ_{A^-}(R)] in the present and previous studies, the life time of the metastable anion still lies within 18–20 fs range which falls under the expected shape resonance life time (10–100 fs) for the anionic 3′–dCMPH molecule. The amplitude of the vibrational wave-function moves towards the right turning point of the E_{A^-}(R) right from the beginning in the time evolution plots, thereby justifying an *impulse model* [16] resonance process and support our similar findings in earlier investigations [5, 6] for this system.

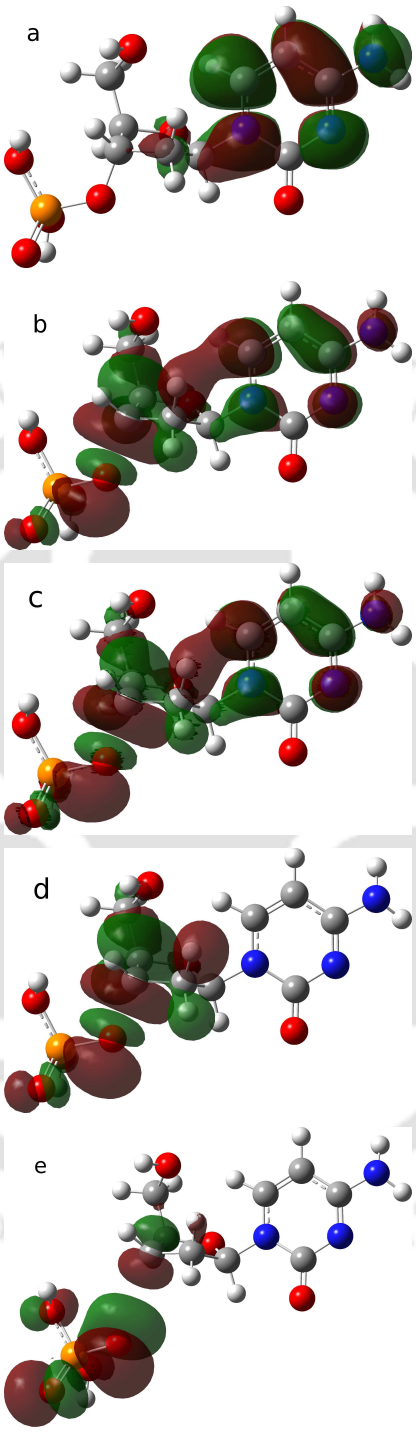

Fig. 3.2 Singly occupied molecular orbital (SOMO)s generated for anionic 3′-dCMPH moiety for the 3′ C–O bond lengths of (a) 2.75 a_0 (1.45 Å), (b) 3.42 a_0 (1.81 Å), (c) 3.46 a_0 (1.83 Å), (d) 3.50 a_0 (1.85 Å), and (e) 5.67 a_0 (3.00 Å).

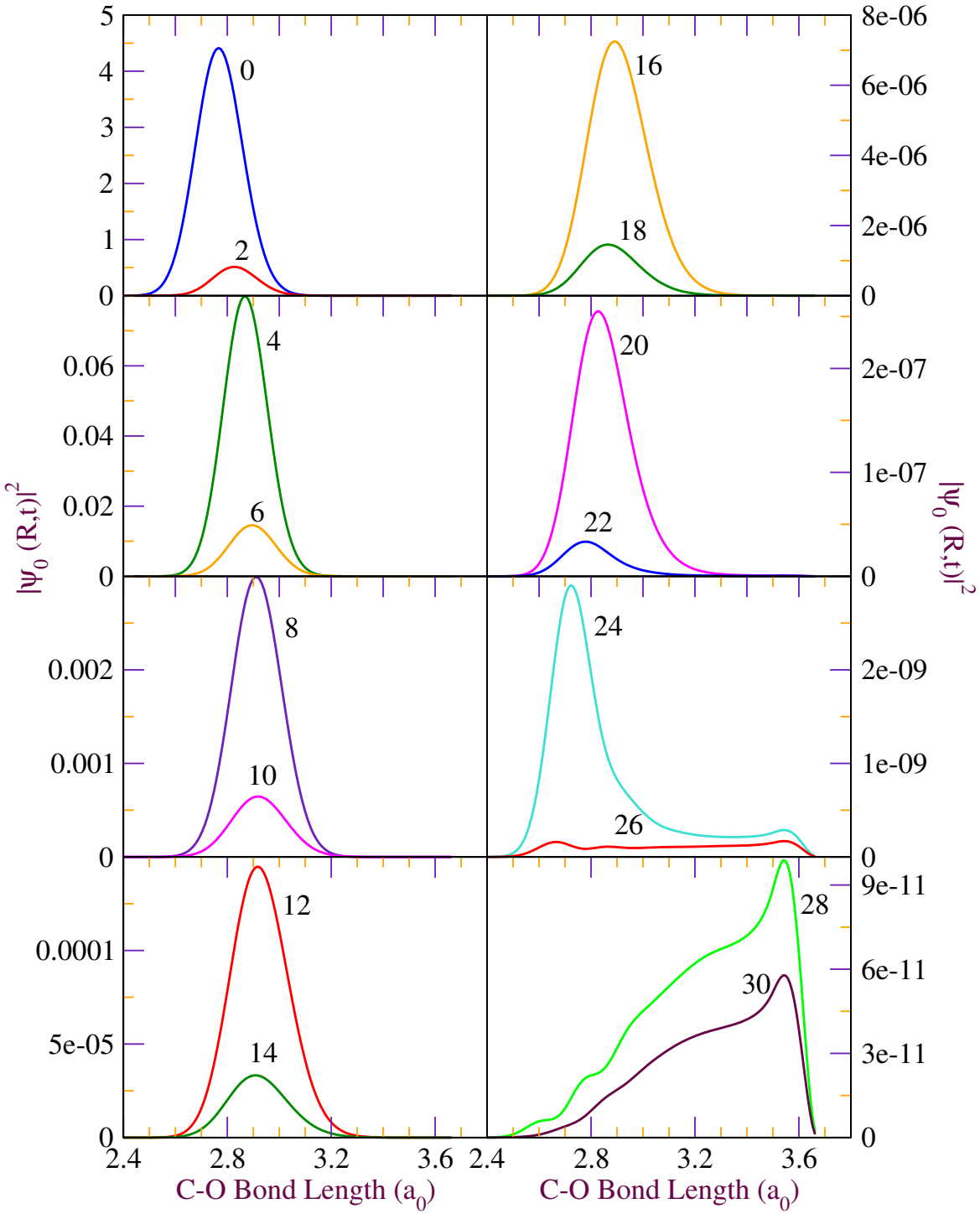

Fig. 3.3 Time evolution plots of the ground state wave function [ϕ_0(R)]of the target 3′-dCMPH under the effect of anionic Hamiltonian at time t=0–30 fs.

In Fig. 3.4(a), we have plotted the auto correlation function $\langle\chi_0(R)|\psi_0(R,t)\rangle$ obtained from present and previous [5, 6] quantum dynamical calculations. The auto correlation function shows the maximum overlap when the propagation starts and decreases to negligibly small values at t = 18 fs. Fourier transformation of this auto correlation function yields the fragmentation profile, $[\sigma_{0\leftarrow 0}(\mathrm{E})]$, and is plotted in Fig. 3.4(b) along with those calculated from HF [5], DFT-B3LYP [6] methods and experimental result [17].

The calculated $\sigma_{0\leftarrow 0}(\mathrm{E})$ fragmentation profile of Fig. 3.4(b) are similar to HF and DFT-B3LYP profiles with differences in energy peak positions. The maximum in the fragmentation profile $[\sigma^{max}_{0\leftarrow 0}(\mathrm{E})]$ of HF, DFT-B3LYP, and MP2 methods are seen centered at 0.75 eV, 0.15 eV, and 0.48 eV respectively and also tabulated in Table 3.1. The structure-less feature of all three fragmentation profiles presumably show the *impulse* [16] behavior of the resonance process which is already justified from the time evolution plots of Fig. 3.3. Though, the C–O bond rupture spectrum obtained using HF method is found to be in good agreement with the experimental observation (0.83 eV) [17] over those obtained by other two methods (DFT-B3LYP and MP2). Overall the three methods now shown the evidence of shape resonance phenomena during SSB. However, the reason for this discrepancy between HF, DFT-B3LYP, and MP2 results may be owing to the difference in the PE curves electron correlation plays a significant role in DFT-B3LYP and MP2 results.

It is noteworthy to mention that there is a barrier in the anionic PE curve with a barrier height of $\sim$1.18 eV with the barrier minimum and maximum are seen as 0.37 eV and 1.55 eV respectively. This barrier is higher than what we found in our previous DFT-B3LYP method ($\sim$0.75 eV) [6]. This may signify an effective coupling between π^* and σ^* resonance states than that in DFT-B3LYP method. The steeper barrier seen in Fig. 3.1(a) may also be a signature of stronger electron correlation effect than DFT-B3LYP and HF methods. The presence of this potential barrier may influence a $3'$ C–O bond break at higher vibrational energies of the $\mathrm{E}_{A^-}(\mathrm{R})$ through quantum mechanical tunneling and is being discussed in the following section.

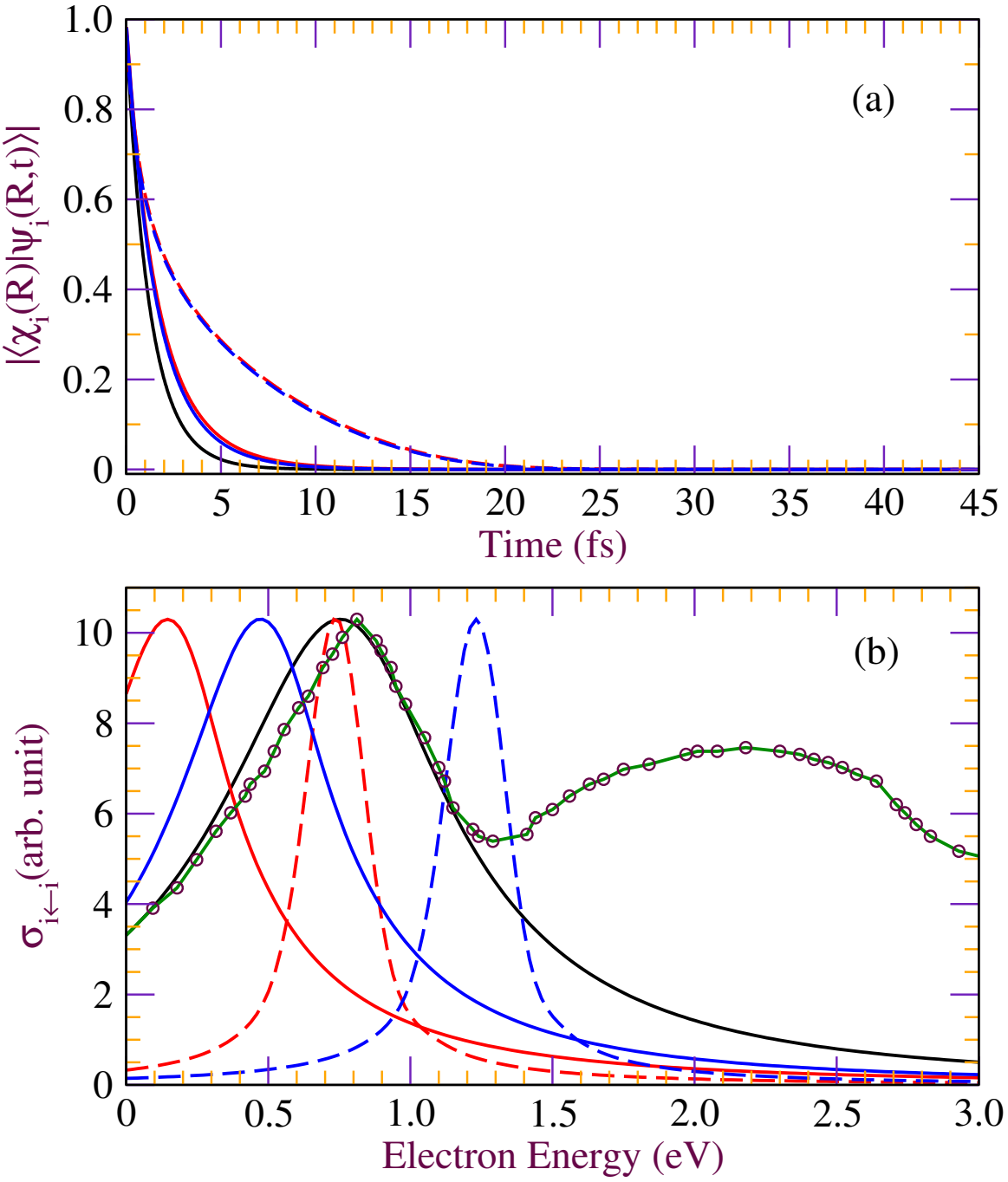

Fig. 3.4 (a) Auto correlation functions $|\langle\chi_i(R)|\psi_i(R,t)\rangle|$ from our HF (i=0, black solid line), DFT-B3LYP [(i=0, red solid line) and (i=5, red dashed line)], MP2 [(i=0, blue solid line) and (i=6, blue dashed line)], (b) comparison of corresponding fragmentation profiles $\sigma_{i\leftarrow i}$(E) from our HF (i=0, black solid line), DFT-B3LYP [(i=0, red solid line) and (i=5, red dashed line)], MP2 [(i=0, blue solid line) and (i=6, blue dashed line)] theoretical results [5, 6] with experimental measurement [17].

3.3.2 LEE and $\chi_{i=6-9}$(R) vibrational states with energy above 1 eV [SSB through the C–O bond tunneling]

As mentioned above, the anionic PE curve [E_{A^-}(R)] of Fig. 3.1(a) comprises of two potential wells with a barrier around 3.0 – 5.0 a_0 of the C–O bond length, we have therefore investigated the probable dissociative channel through 3′ C–O bond tunneling. We have divided E_{A^-}(R) [Fig. 3.1(a)] into three regions viz., Region 1 ($R_{C-O} \sim$ 2.2–3.5 a_0), Region 2 ($R_{C-O} \sim$ 3.0–4.0 a_0), and Region 3 ($R_{C-O} >$ 3.5 a_0, asymptotic region of the C–O bond) and are shown in Fig. 3.5 along with the earlier studied DFT-B3LYP anionic PE curve [6].

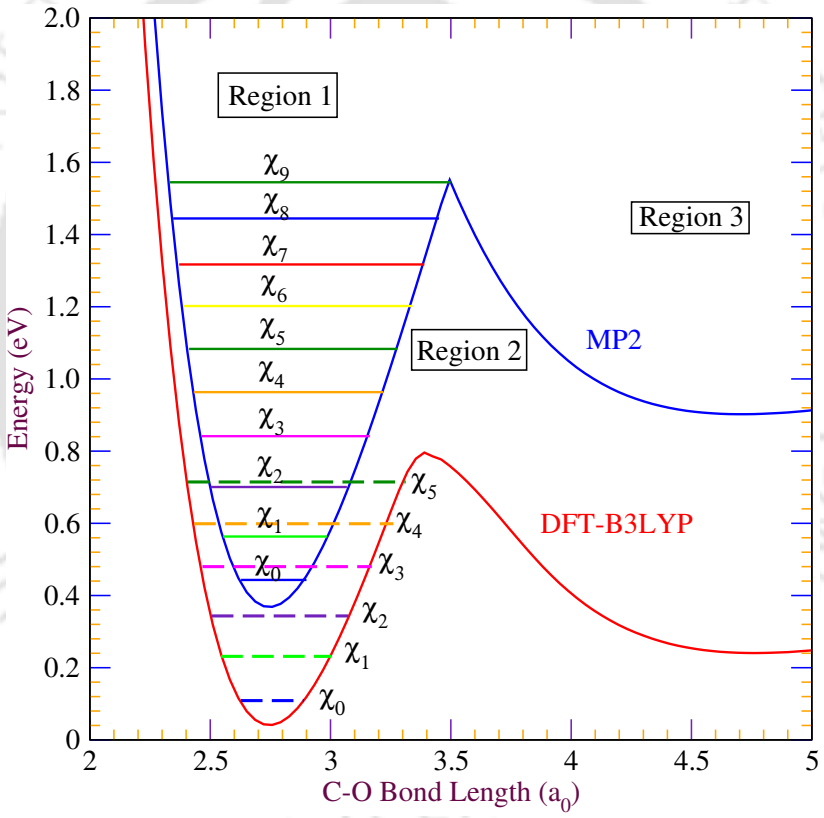

Fig. 3.5 The energies of different anionic vibrational states of anionic PE curves of Fig. 3.1(a) and DFT-B3LYP method [6] after the formation of metastable compound anion are shown in Region 1. Region 2 indicates the hyperbolic cosine barriers and Region 3 is the dissociative regions of the C–O bond.

The bound vibrational states in Region 1 of the MP2 anionic PE curve are marked as $\chi_{i=0-9}$ respectively from the lower to the higher energy levels. In comparison to the six

bound vibrational states ($\chi_{i=0-5}$) in DFT-B3LYP anionic PE curve, there are ten bound states ($\chi_{i=0-9}$) are seen in the MP2 curve. The Region 2 of Fig. 3.5 can be assumed as a hyperbolic cosine barrier and therefore the transmission probability, T, can be calculated using either of Eq. (3.1) or Eq. (3.2) given in the section 3.2.3 of the method section. In our present investigation, as it is difficult to find out the value of barrier width (a) from the anionic MP2 curve of Fig. 3.5, we have decided to use a model potential barrier [U(R)] of the following form [10] for finding out the same

$$U(R) = \frac{U_0}{\cosh^2(aR)} \tag{3.3}$$

Where, in the present context, R is the C–O bond length of the anion. We have used different combinations of U_0 and a and the best choice (U_0 = 1.18 eV and a = 3.04 a_0^{-1}) is compared with the anionic MP2 PE curve (Fig. 3.5) in Fig. 3.6. As we can see from Fig. 3.6, the fitted

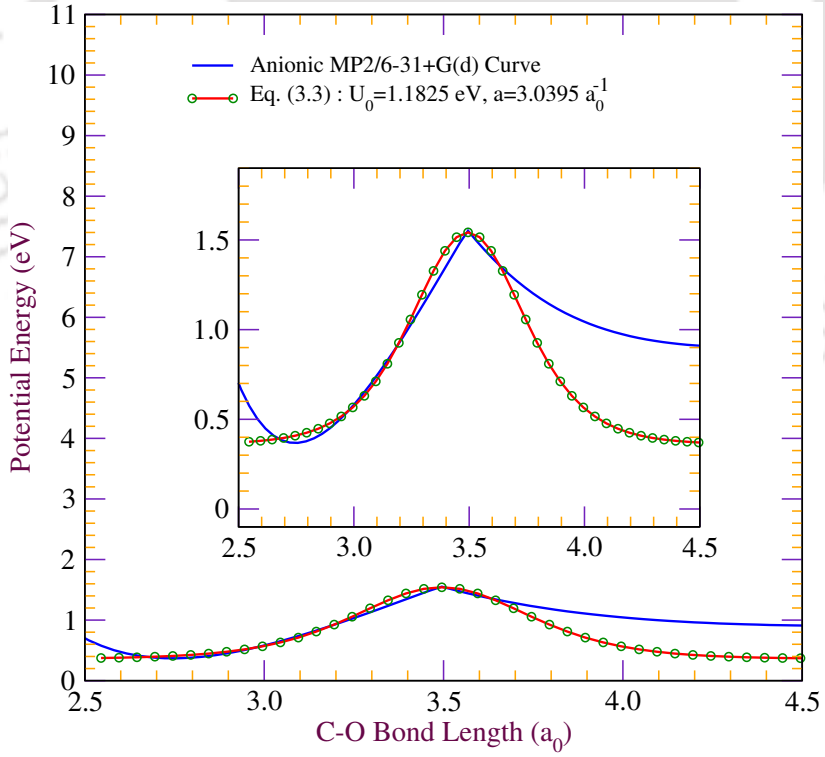

Fig. 3.6 Comparison of analytical hyperbolic cosine curve fitted using Eq. (3.3) with the anionic PE curve of Fig. 3.1(a).

potential barrier [U(R)] compares well with the calculated MP2 curve.

These optimal values of U_0 and a permit us to calculate the transmission coefficient (T) of the C–O bond using Eq. (3.2) for all ten bound vibrational states those are thermally accessible for the formation of the metastable compound anion. The calculated T values for the ten eigen states ($\chi_{i=0-9}$) of the Region 1 are provided in Table 3.2 and also compared with those obtained from our DFT-B3LYP investigation [6]. A plot of tunneling probability, T, vs. vibrational energy covering all bound states of the anion are offered in Fig. 3.7. As

Table 3.2 Transmission coefficient (T) calculated using Eq. (3.2)

Vibrational State (χ_i)	Vibrational Energy χ_i(E) [eV]		Transmission Coefficient (T)	
	B3LYP [6]	MP2 [12]	B3LYP [6]	MP2 [12]
0	0.11	0.44	1.41×10^{-28}	2.52×10^{-12}
1	0.23	0.57	1.77×10^{-20}	9.36×10^{-10}
2	0.36	0.70	1.54×10^{-14}	1.66×10^{-7}
3	0.48	0.83	1.15×10^{-9}	1.73×10^{-5}
4	0.60	0.96	1.85×10^{-5}	1.19×10^{-3}
5	0.72	1.08	9.27×10^{-2}	5.56×10^{-2}
6	–	1.21	–	0.69
7	–	1.33	–	0.98
8	–	1.45	–	0.99
9	–	1.55	–	0.99

can be seen from the Table 3.2 and Fig. 3.7, the T values are: (a) negligibly small for $\chi_{i=0-4}$ states, (b) non-negligible for χ_5 state, and (c) for $\chi_{i=6-9}$ states, the T values are significant. This seems reasonable due to the larger reduced mass of the C–O bond thereby not allowing or allowing only small amount of the probability density from $\chi_{i=0-5}$ states to flow towards the dissociative region of the E_{A^-}(R). The sudden jump in the tunneling probability values ranging from 69-99% for the higher vibrational states ($\chi_{i=6-9}$) may be attributed to the corresponding high vibrational energies and the low barrier width from the respective states to the other side of the PE curve makes the effect of reduced mass of the C–O bond less effective. Additionally, the very small tunneling probabilities of the first six vibrational states ($\chi_{i=0-5}$) are comparable to that of our earlier DFT-B3LYP investigation

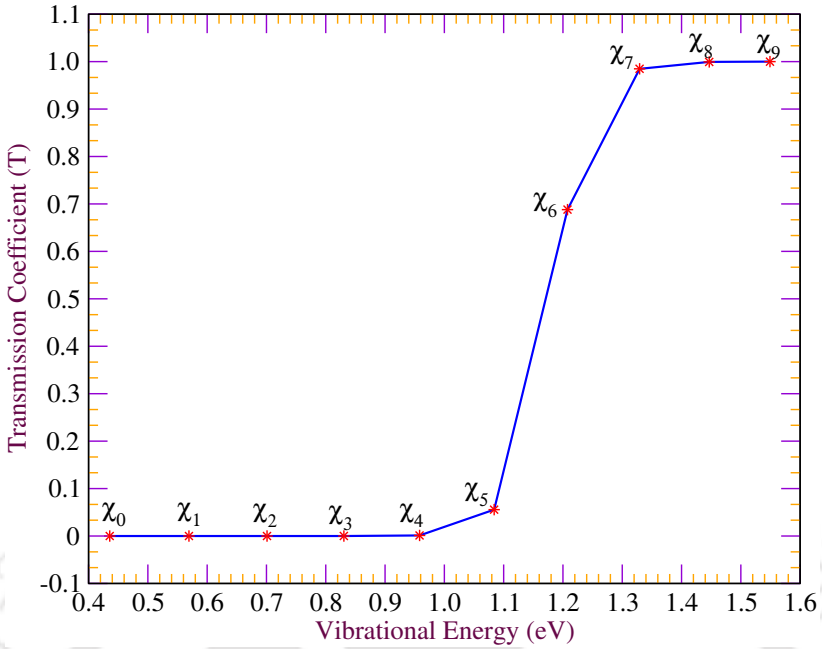

Fig. 3.7 Transmission coefficient (T) for tunneling from the C-O bond using vibrational states, $\chi_{i=0-9}$, of the curtailed anionic PE curve of Fig. 3.1(a).

pointing towards the S_N2 type resemblance of the decay channel for the TNI formed below 1 eV as mentioned in the earlier section. On the other hand, the effect of quantum mechanical tunneling is much more significant in upper lying bound vibrational states ($\chi_{i=6-9}$) owing to the larger tunneling probability of the same. Effect of quantum mechanical tunneling may be seen experimentally, if higher vibrational states of *in vivo* DNA can be populated using sub-excitation electrons. Therefore, using a proper recipe for populating higher vibrational states, the effect of quantum tunneling can be maximized experimentally. It is also worthwhile to mention here that the "S-shaped" curve of Fig. 3.7 is similar to that of the hydrogen atom tunneling in the photo-excited methylamine [10].

As the four upper lying states $\chi_{i=6-9}$ gives rise to large T values, therefore, to see the effect of quantum tunneling during SSB in 3′-dCMPH moiety, we have considered the χ_6 state (which is the lowest among four states) for further analysis with the use of time evolution, auto correlation, and cross-section profiles.

The time evolution of the ϕ_6 state as the initial state [ψ_6(R, t=0) = ϕ_6 (R)] has been computed using Eq. (2.1) and a few snapshots (t = 0–42 fs) from this time evolution are

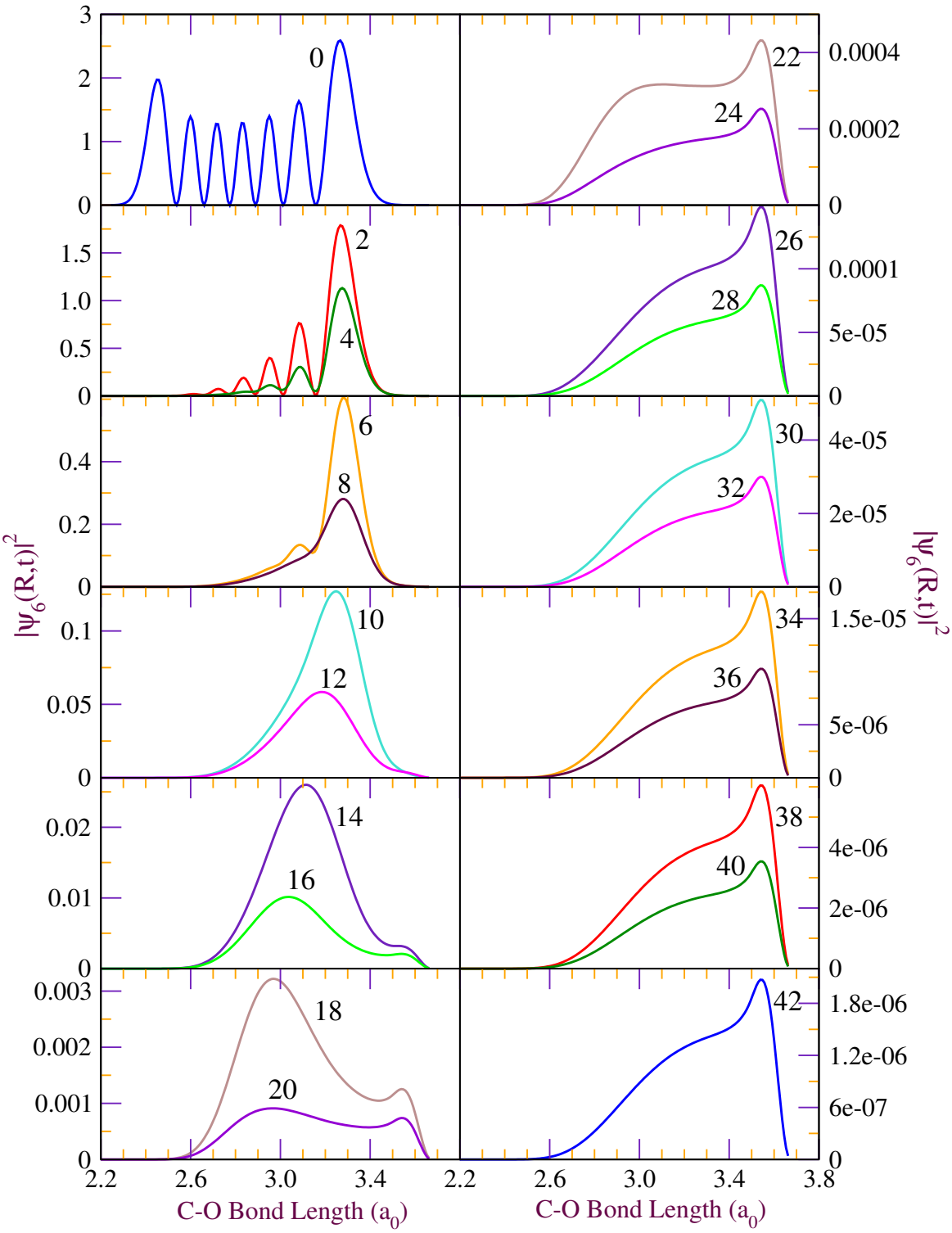

Fig. 3.8 Time evolution plots of initial wave function of the target 3′-dCMPH [ϕ_i(R)] under the effect of anionic Hamiltonian at time t=0–42 fs for the sixth excited vibrational state [ϕ_6(R)].

provided in Fig. 3.8. As we can see from Fig. 3.8, the six nodes of the initial wave function (t = 0 fs) disappearing to four at t = 2 fs followed by two at t = 4 fs and by t = 8 fs, all the nodes have completely vanished. As the Region 2 of the Fig. 3.1(a) falls under $R_{C-O} \sim$ 1.9–5.0 a_0 and on comparing this range with the time evolution plots of t = 16–42 fs, there is a signature of shoulder and subsequent exponential decay of the wave function (around $R_{C-O} \sim$ 3.5–3.7 a_0 of t = 18 and 20 fs plots), which we believe is due to the tunneling of the C–O bond from the χ_6 state. Further, the life time of the compound anion seen from Fig. 3.8 is $\sim$ 42 fs, longer than that seen in Fig. 3.4 (18–20 fs). The reason for this increased life-time of the compound anion at χ_6 state may be due to the fact that the higher vibrational states eigen functions have larger spatial spread [18], leading to a longer life-time of the metastable anion. The effect of increased life time of the metastable anion can also be seen from the auto-correlation function, $\langle \chi_6(R)|\psi_6(R,t)\rangle$ [upper panel of Fig. 3.4(a)] which has a longer decay time than that of $\langle \chi_0(R)|\psi_0(R,t)\rangle$ in the same plot.

The corresponding cross-section profile [$\sigma_{6\leftarrow 6}$(E)] [blue dashed line, Fig. 3.4(b)] is broad and structure less, which once again justifies the *impulse model* [16] classification for this moiety. The maximum in the cross section is observed at an energy of 1.3 eV and is higher than that of the experimental maximum (0.83 eV) [17] and to all other theoretical results [5, 6], signifies the pronounced C–O bond tunneling in the 3′-dCMPH SSB for an electron of energy above 1 eV. Therefore, our new results may shed an insight in the field of resonant electron capture followed by SSB in DNA and DNA fragments. To conclude, we do not attempt to ascertain the best choice among the three ab-initio methods (HF, DFT-B3LYP, and MP2) employed but comment that all the methods are reliable for the description of LEE induced single strand breaks in this system.

3.4 Concluding Remarks

In this investigation, we have offered a quantitative description for the low energy electron (LEE) induced single strand breaks (SSBs) in a modeled DNA fragment 2′-deoxycytidine-3′-monophosphate (3′-dCMPH) from the electronic structure theory and quantum dynamical

calculations. Fragmentation profile obtained here in conjunction with our earlier investigations highlight the involvement of shape resonance phenomena during LEE induced SSBs. In particular, the results obtained from our present calculations are interesting and agree with earlier studies. An outline of the major remarks of our analysis are:

(a) The pyrimidine nucleobase, cytosine in 3′-dCMPH, acts as an effective electron (LEE) receiver.

(b) If the LEE attaches to the base below 1 eV, the favorable pathway for transferring the excess charge in the gas phase is exclusively via "charge induced dissociation" which resembles an S_N2 type process [5, 6, 14] and the time taken for such a process is found to be within 18–20 fs. This implies that the first six anionic bound states are smoothly connected to S_N2 type decay channel.

(c) If the LEE attaches to the base above 1 eV i.e., at higher vibrational levels, the prominent decay channel changed from S_N2 type to quantum mechanical tunneling which may have a substantial role during DNA damage. However, to observe the effect of quantum tunneling experimentally, one has to achieve populating higher vibrational states (like χ_6 state), which is still a difficult task.

(d) The LEE – 3′-dCMPH interaction is found to follow an *impulse model* [16] resonance process irrespective of the above mentioned [(b) or (c) or both] mechanistic pathways by which it follows.

Finally, we would like to emphasize that our dynamical investigation has rationalized a direct comparison between the theoretical and experimental results and restructured the DEA schemes for 3′-dCMPH molecule through a more rigorous approach in the field of electron-molecule scattering phenomenon for a larger molecular network. However, inclusion of other dynamical modes like glycosidic (N–C) along with C–O damage mode in 3′-dCMPH is possible, but the electronic structure calculations for obtaining these PE curves will be computationally very demanding. Performing quantum dynamical calculations of these modes simultaneously in DNA damage would require the use of more rigorous methods like multi-configurational time dependent Hartree (MCTDH) approach [19]. However, this is beyond the scope of the present investigation. Alternatively, we have investigated these

dynamical modes in one dimensional analysis using LCP-TDWP approach in the low energy region discussed in chapter 4.

We hope our findings from time-dependent calculations offer a threshold for further investigations and the algorithm described here can be applied to investigate LEE induced scattering in DNA and other DNA fragments.

References

[1] L. A. Khalfin, Zh. Eksper. Teor. Fiz. **33**, 1371 (1957).

[2] H. Jakobvits, Y. Rothschild, and J. Levitan, Am. J. Phys. **63**, 439 (1995).

[3] S. R. Wilkinson, C. F. Bharucha, M. C. Fischer, K. W. Madison, P. R. Morrow, N. Qian, M. Sundaram, and M. G. Raizen, Nature, **387**, 575 (1997).

[4] E. J. Heller and R. C. Brown, J. Chem. Phys. **79**, 3336 (1983).

[5] Renjith B., S. Bhowmick, M. K. Mishra, and M. Sarma, J. Phys. Chem. A **115**, 13753 (2011).

[6] S. Bhowmick, Renjith B., M. K. Mishra, and M. Sarma, J. Chem. Phys **137**, 064310 (2012).

[7] M. J. Frisch, G. W. Trucks, H. B. Schlegel, et al., *GAUSSIAN 03*, Revision E.01, Gaussian,Inc., Wallingford, CT, 2004.

[8] R. Barrios, P. Skurski, and J. Simons, J. Phys. Chem. B **106**, 7991 (2002).

[9] L. D. Landau and E. M. Lifshitz, *Quantum Mechanics, 3rd ed.* (Pergamon Press, Oxford, U.K., 1977).

[10] R. Marom, C. Levi, T. Weiss, S. Rosenwaks, Y. Zeiri, R. Kosloff, and I. Bar, J. Phys. Chem. A **114**, 9623 (2010).

[11] M. Smyth and J. Kohanoff, J. Am. Chem. Soc. **134**, 9122 (2012).

[12] R. Bhaskaran and M. Sarma, J. Chem. Phys **139**, 045103 (2013).

[13] C. C. Marston and G. G. Balint-Kurti, J. Chem. Phys. **91**, 3571 (1989).

[14] J. Gu, J. Wang, and J. Lesczynski, J. Am. Chem. Soc. **128**, 9322 (2006).

[15] J. Simons, Acc. Chem. Res. **39**, 772 (2006) and references therein.

[16] J. N. Bardsley and J. M. Wadehra, Phys. Rev. A **20**, 1398 (1979).

[17] F. Martin, P. D. Burrow, Z. Cai, P. Cloutier, D. Hunting, and L. Sanche, Phys. Rev. Lett. **93**, 068101 (2004).

[18] M. Sarma, S. Adhikari, and M. K. Mishra, J. Chem. Phys. **126**, 044309 (2007).

[19] *Multidimensional Quantum Dynamics: MCTDH Theory and Applications*, edited by H.-D. Meyer, F. Gatti, and G. A. Worth (Wiley-VCH, Weinheim, 2009).

Chapter 4

Glycosidic bond cleavage in 2′-deoxycytidine-3′-monophosphate

4.1 Introduction

In previous chapters, we have modeled the capture of low energy electron (LEE) at the cytosine nucleobase center and the subsequent transfer of the electron to the highly flexible DNA backbone sugar-phosphate region of high electron affinity [1–3]. The implementation of local complex potential-time dependent wavepacket (LCP-TDWP) approach to polyatomic systems like biomolecules was one of the prime concern in those investigations [1–3]. Our findings were in accordance with the previous results [4, 5]. The oligonucleotide 2′-deoxycytidine-3′-monophosphate (3′-dCMPH) has been subjected exclusively for the LEE induced 3′ C–O bond cleavage. We found that SSB may occur due to the attack of a 0.5–1 eV LEE which appeared as the lowest π^* shape resonance state in the cross section spectrum [3]. The lifetime of the metastable state varies among different 3′ C–O bound vibrational energy levels and thus the probability for occurring SSB from each of these eigenstates [3].

Numerous degrees of freedom are existing in the LEE induced dissociation process which may contribute to DNA damage and one such in 3′-dCMPH molecule is the glycosidic N–C bond scission [6]. It was reported from previous studies on deoxycytidine and its analogous fragments that the base release may get initiated in the low energy (0–3 eV) regime [6–8].

However, this pathway is not a preferred channel in comparison with the phosphodiester 3′ C–O bond lesion due to the high activation energy barrier associated with the former channel [8]. Therefore, we would like to utilize our LCP-TDWP approach to examine the cytosine base release in the chosen cytidine nucleotide 3′-dCMPH [9] and thereby deduce the bond selectivity during LEE induced DNA damage.

A brief overview of the molecular modeling and the quantum dynamical calculation is provided in the next section. A comparative assessment between various forms of DNA damage, those from the present along with the previous experimental and theoretical findings are provided in the Results and Discussion section. We conclude the chapter with the assertion that the glycosidic bond cleavage is lesser prominent than the SSB within this molecule.

4.2 Computational Method

The complexity of DNA or even its short single-strand chain imposes a great challenge to apply quantum mechanical methods for the investigation of LEE induced bond breaking in DNA. Therefore, in a "bottom-up" approach, one may consider its isolated constituents such as simple nucleobases, nucleosides, or nucleotides or a combination of them. The only thing one needs to consider while modeling the moiety is the presence of an electron attachment site alongwith the probable dissociative channel. In this regard, we have considered a molecule 2′-deoxycytidine-3′-monophosphate, in short 3′-dCMPH (Fig. 4.1), comprising of a cytosine base, a ribose sugar, and the phosphate group counter-balanced by a proton at the negative center. The radical centers generated during excision from DNA were neutralized by adding hydrogens. The molecule contains the electron attachment sites as the base, sugar or the phosphate center and the 3′ C–O or glycosidic N–C bonds as the most probable fragmentation pathways. An electron is attached to the lowest unoccupied molecular orbital (LUMO) of the neutral system to obtain the anionic molecule. Geometry optimization were performed for both the neutral and anionic systems at the Hartree-Fock (HF) and second-order Møller-Plesset perturbation theory (MP2) methods with the 6-31+G(d) basis set available in Gaussian

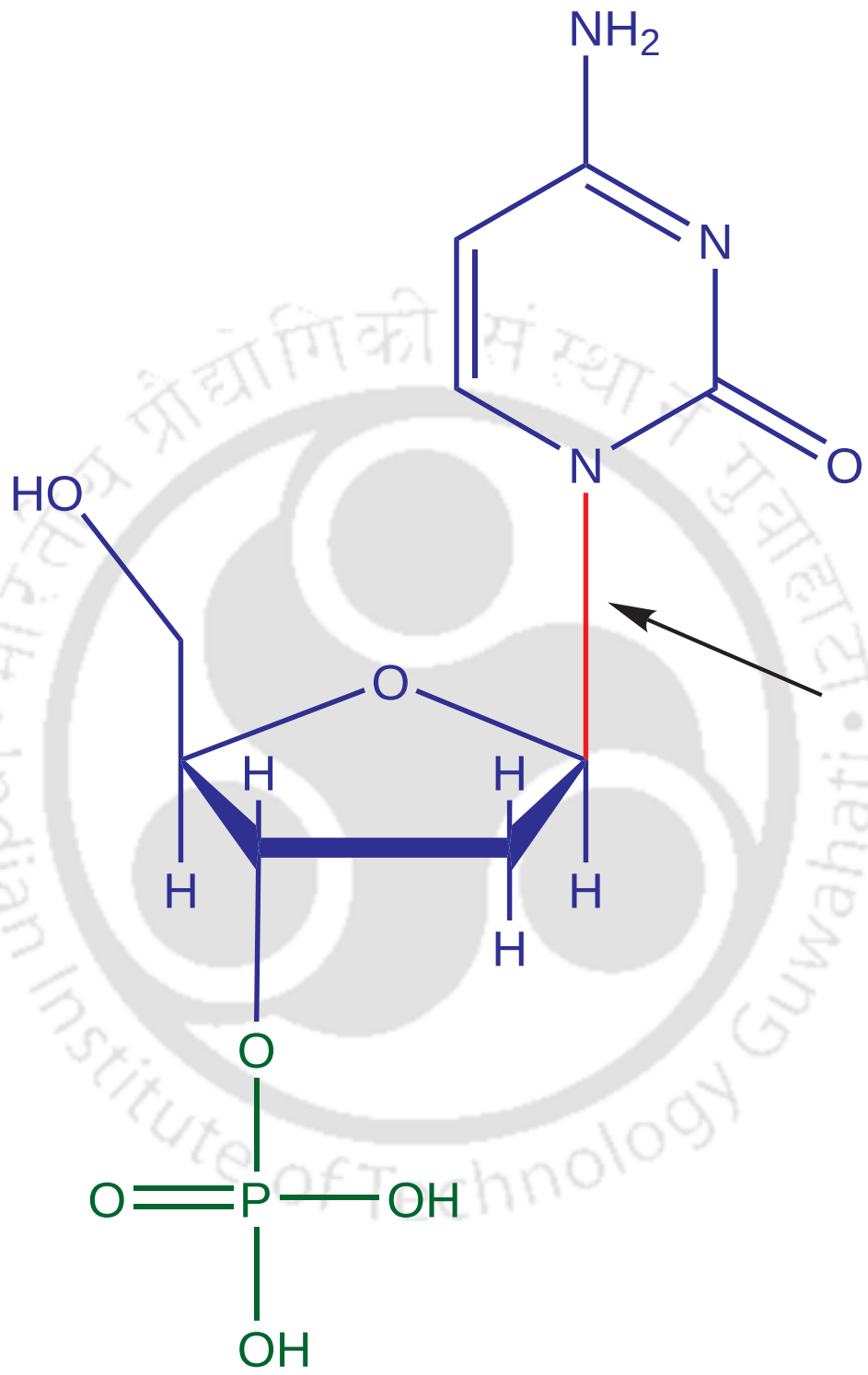

Fig. 4.1 The pyrimidine nucleotide 2′-deoxycytidine-3′-monophosphate (3′-dCMPH) excised from DNA double helix, neutralized by adding hydrogens at the radical centers and a proton at the phosphate negative center with the N–C bond cleavage marked with an arrow.

03W package [10]. The optimized structures were further used for the quantum mechanical calculation of the adiabatic potential energy (PE) curves for the neutral [$E_A(R)$] and anionic [$E_{A^-}(R)$] systems (A = 3′-dCMPH) using Gaussian 09 suite [11]. More details of this gas phase system can be found in chapter 2. Moreover, one can reasonably model the system *in vivo* in a manner considering (a) solvation, (b) neutralizing the phosphate center with positive ions like Na^+ and K^+, and (c) base π stacking and so forth. However, as mentioned earlier, we have not considered these modifications for the present "bottom-up" approach analysis.

In the present work, the calculations are carried out for single vibrational mode corresponding to the glycosidic bond cleavage as the reaction coordinate. However, there are other dissociation channels like the sugar phosphate 3′ C–O bond rupture [in short known as single strand break (SSB)], the sugar ring fragmentation and so forth. We have considered the LEE induced 3′ C–O bond dissociation separately as a 1-D process in chapter 2 and chapter 3 [1–3]. Inclusion of other degrees of freedom along with this phosphodiester bond cleavage channel in 3′-dCMPH molecule needs huge amount of computational work, which is necessary to obtain the corresponding multidimensional complex potential energy surfaces. Moreover, one has to solve the multidimensional Schrödinger equation for an accurate description of the dissociation mechanism. We are currently working on the development of multidimensional [such as 2-dimensional (2D)] nuclear wavepacket dynamics program in our group. To date, multi-dimensional quantum dynamics calculations are limited to small group of chemical systems, e.g., diatomic or triatomic molecules. They possess lesser number of vibrational degrees of freedom compared to polyatomic molecules. In addition, the fragmentation process may take place in a manner where the role of IVR can be neglected due to the heavy atom effect during the LEE induced damage. Therefore, we have chosen to freeze all modes of vibration other than the one corresponding to the reaction coordinate.

Since, our dynamical calculation on the metastable system requires complex potential energy surface, we have modeled (as discussed below) the width function [$\Gamma_{A^-}(R)$] with respect to the inter-nuclear distance. This will be, again, a difficult task to model for scattering involving multidimensional channels. In the present modeling, we have used the same optimized geometries of neutral and anionic systems as there is no structural or vertical

attachment energy change associated with the electron molecule collision process. In other words, the initial localization of the LEE for both the dissociation channels is at the cytosine base only (i.e., we have used the same low energy electron to study both the fragmentation processes). Therefore, we can reasonably treat the coupled dissociation channels separately, within our limitations.

The quantum dynamics of the cytosine base release (N–C bond dissociation) process is governed by the anionic Hamiltonian. The complex potential associated with the metastable state is achieved by modeling $\Gamma_{A^-}(R)$ as an exponential decay which vanishes at the crossing point between neutral and anionic PE curves. Moreover, we have modeled the width function in such a way that the nuclear motion exist only within the lifetime of the shape resonance phenomenon. Our time dependent quantum dynamical calculations involves the propagation of the initial neutral wave packet by solving the time dependent Schrödinger equation (TDSE) using the iterative Lanczos method [12]. The glycosidic N–C bond fragmentation profile [σ(E)] is obtained from the fast Fourier transformation (FFT) [13] of the auto correlation function [14]. Finally, we have calculated the transmission coefficient (T) for the N–C bond tunneling from the bound vibrational levels toward the repulsive region in the anionic PE curve through the avoided crossing [15, 16]. An elaborate discussion of the underpinning quantum mechanical treatment of LCP-TDWP approximation and tunneling can be found in chapters 2 and 3 [1–3].

4.3 Results and Discussions

4.3.1 PE curves, Width functions, and Eigen functions

The optimized structures of both the neutral and anionic systems in HF and MP2 methods are given in the Appendix A (Figs. A1 and A2). It has been found that the equilibrium neutral N–C bond lengths are around 2.74 a_0 (1.45 Å) in both HF and MP2 methods. The corresponding anionic equilibrium bond lengths are elongated slightly to 2.76 a_0 (1.46 Å) and 2.78 a_0 (1.47 Å) respectively in HF and MP2 methods. The adiabatic potential energy (PE) curves generated for the neutral and anionic N–C bonds cleavage from the consonant

Table 4.1 Comparison of various properties/parameters for 3′-dCMPH molecule.

Property/Parameter	HF	MP2
[a]R_{N-C} (Å)	1.456 [b]	1.456 [b]
	1.465 [c]	1.470 [c]
VAE (eV)	0.65	0.38
R_x(Å)	2.16	2.11
δ_1	650	700
α	3.39	3.46
Barrier Height (eV)	2.48	2.14
[d]Barrier Width (Å)	0.28	0.27
$\sigma^{max}_{0\leftarrow 0}$(E) [eV]	0.75	0.46

[a] Equilibrium N-C bond length.
[b] Neutral 3′-dCMPH moiety.
[c] Anionic 3′-dCMPH moiety.
[d] Taken from the fitted curve of Eq. (3.3).

ground states HF and MP2 optimized geometries are provided in Figs. 2(a) and 2(b). This is done by stretching the labeled vibrational mode at 256 equally spaced grid points from 1 a_0 to 10 a_0 keeping all other degrees of freedom of the molecule frozen. We did so for having a direct comparison with that of our previous findings on single strand breaks [1–3] in the same moiety. The electron attachment to this molecule for the cytosine base release is found to be metastable in both the ab initio methods. The vertical attachment energy (VAE) is found to be 0.65 eV at the HF level and around 0.38 eV at the MP2 level of accuracy. The crossing point between the neutral [E_A(R)] and anionic [E_{A^-}(R)] PE curves are respectively noted as 4.08 a_0 (2.16 Å) and 3.99 a_0 (2.11 Å). The N–C bond cleavage is found to surmount a higher barrier of $\approx$ 2.48 eV at the HF level than that at the MP2 level ($\approx$ 2.14 eV). Both these barriers are found to be at almost the same N–C bond length, i.e., at $R_{N-C} \sim$ 3.67 a_0 (1.94 Å). However, the environmental factors like solvent, π stacking, hydrogen bonding, etc. may strongly influence the height of the PE barrier. Inclusion of non-adiabatic effects will subsequently enhance the mechanistic description of LEE induced DNA damages like SSBs or base releases. However, this is beyond the scope of the present investigation. Figs. 4.2(c) and 4.2(d) respectively narrates the modeled width function associated with the metastable

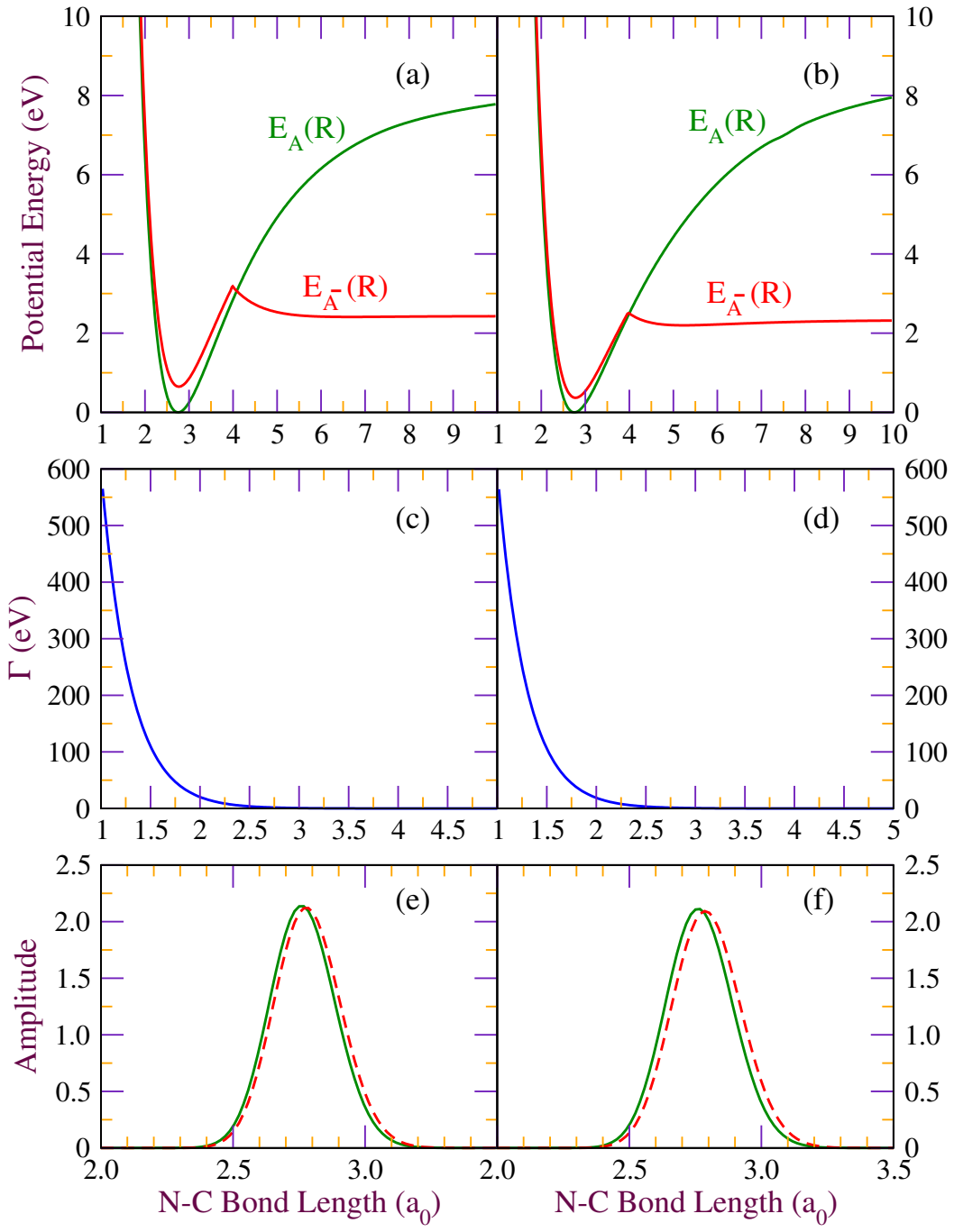

Fig. 4.2 Potential energy curves for the neutral [$E_A(R)$] (green solid line) and the anionic [$E_{A^-}(R)$] (red solid line) 3′-dCMPH molecule computed at the (a) HF/6-31+G(d) and (b) MP2/6-31+G(d) accuracy levels. (c) The width function $\Gamma_{A^-}(R)$ calculated as a decaying exponential function for A=3′-dCMPH, for HF and (d) for MP2. The ground state wavefunctions of neutral and anionic molecules calculated using Fourier grid Hamiltonian method are using (e) HF [Fig. 4.2(a)] and (f) MP2 [Fig. 4.2(b)] PE curves.

resonance for the HF and MP2 potentials. The parameters of Eq. (2.4) [α and δ_1] used for modeling the Γ function are given in Table 4.1. The ground state eigen functions of neutral [ϕ_i(R)] and anionic [χ_i(R)] molecules, calculated using the well known FGH method [17], for HF and MP2 potentials are provided in Figs. 2(e) and 2(f) respectively. A total of 20 bound vibrational states are found for the anionic HF potential energy curve, while the eigen energy levels reduces to 18 for the MP2 anionic potential curve. Different parameters employed for the present calculations are indexed in Table 4.1.

4.3.2 Singly occupied molecular orbitals (SOMOs)

In a shape resonance phenomenon, the vertical Franck-condon transition can be illustrated qualitatively as the attachment of LEE into a formerly empty molecular orbital of the neutral molecule resulting in the formation of a transient negative ion (TNI). This attachment process will not perturb the inner electronic configuration of the neutral target molecule. The qualitative description of the electron transfer process begins at the cytosine base center where the electron attachment takes place. The attachment of LEE to the cytosine disturbs the planarity of the heterocyclic aromatic ring and will try to eject the excess electron in to the N–C anti-bonding σ^* molecular orbital. Once the electron enters in this repulsive channel, the corresponding chemical bond dissociates leaving the electron in to one of the fragment generated. Molecular orbitals occupied by the electron (or SOMOs) during these three stages generated at the correlated MP2 method are shown in Figs. 4.3(a) – 4.3(c). This trend is similar in both the ab initio methods (Please see Figs. A3(a) – A3(c) for the SOMOs generated at the HF/6-31+G(d) accuracy level). It can be seen from Fig. 4.3(a) that the low energy electron attachment takes place at the base π^* orbital at R_{N-C} = 2.78 a_0 (1.47 Å) which subsequently transfers to the N–C anti-bonding σ^* molecular orbital at R_{N-C} = 3.67 a_0 (1.94 Å) and remains situated on the cytosine nucleobase, after the fragmentation, i.e., at R_{C-O} = 5.67 a_0 (3.00 Å). Qualitatively, one may conclude that the LEE induced reduction of 3′-dCMPH at the cytosine center results in the formation of a cytosine anion and a sugar radical along the glycosidic N–C bond dissociation pathway. Similar characteristics were found in the time independent studies of Gu et al. [6] and Li et al. [7] for the LEE

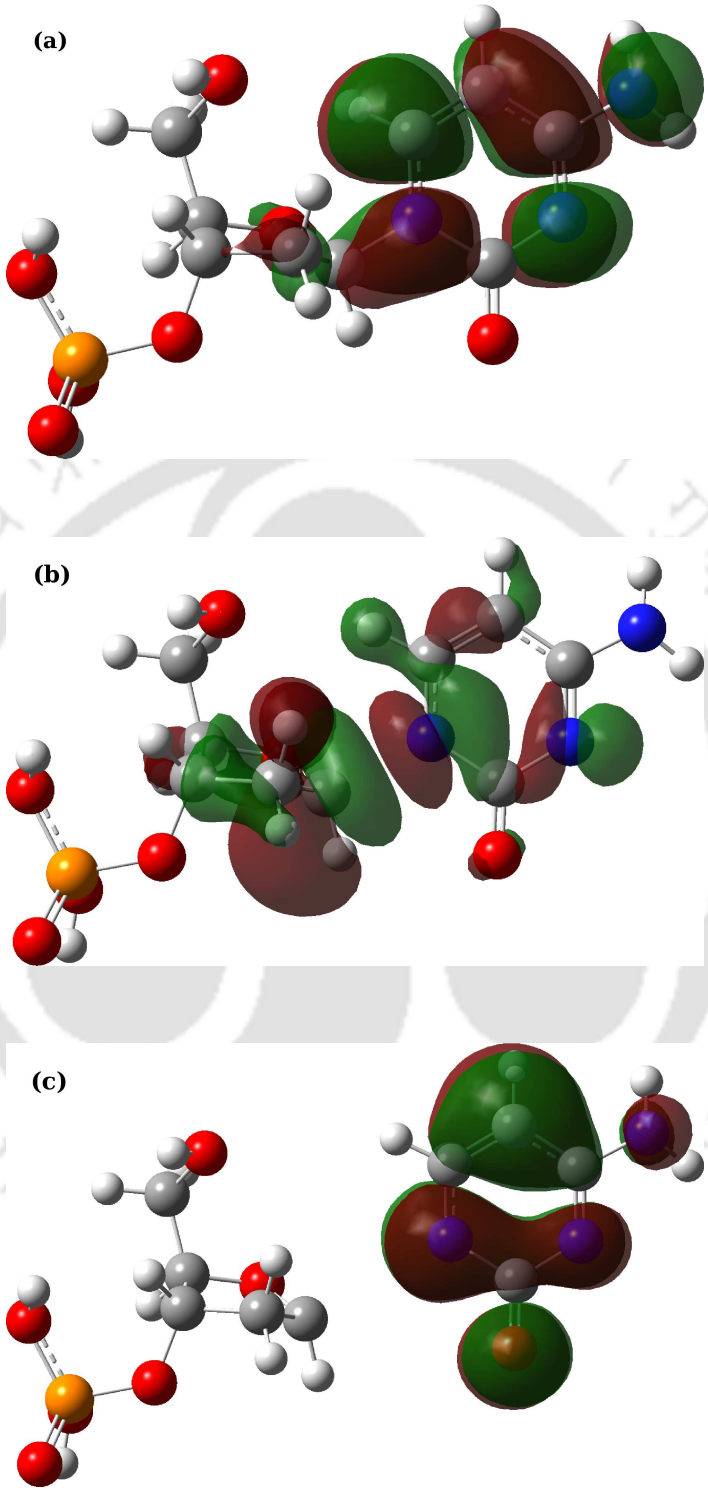

Fig. 4.3 Schematic representation of the singly occupied molecular orbital (SOMO)s generated for anionic 3′-dCMPH moiety for the N-C bond lengths of (a) 2.75 a_0 (1.45 Å), (b) 3.46 a_0 (1.83 Å), and (c) 5.67 a_0 (3.00 Å) at the MP2/6-31+G(d) level of accuracy.

induced glycosidic N–C bond dissociation of 2′-deoxycytidine (dC) molecule. Further, we noted that the MP2/6-31+G(d) optimization of the neutral molecule generate the lowest unoccupied molecular orbital (LUMO) approximately at 1.2 eV, showing the π^* antibonding character on the cytosine base moiety. This energy is close to the already reported [4] electron attachment energy regions in cytosine fragments and therefore, we have carried out our time dependent wave packet dynamics to investigate the unimolecular bond dissociation process at the molecular level. We agree with the fact that higher level correlated methods with larger basis set expansions may improve the description of the dynamics in terms of the resonance energy position and the barrier height determination.

4.3.3 Tunneling

As mentioned in Section 4.3.1, the anionic PE curves [E_{A^-}(R) in Figs. 4.2(a) and 4.2(b)] have a hyperbolic cosine barrier [15] as discussed in chapter 3. Fitting of our potential to the analytical potential [Eq. (3.3)] enable us to determine the width of the barrier ("a"), which is otherwise difficult to compute. The best fitted values of "U_0" and "a" (both in HF and MP2) are provided in Table 4.1.

Fig. 4.4 compares the modeled potential with the calculated HF potential in 4(a) and MP2 potential in 4(b). Moreover, it has been seen from our previous calculations on the 3′ C–O bond cleavage in this moiety [1–3] that the bound vibrational levels embedded in E_{A^-}(R) can tunnel through the barrier towards the repulsive region. For uniformity, we have designated the anionic PE curve into three regions, in which (i) the bound vibrational levels where the LEE gets trapped is labeled as Region 1, (ii) Region 2 is the area under the PE barrier, and (iii) the repulsive state of the potential as Region 3. The transmission coefficient values for the glycosidic N–C bond tunneling have been calculated utilizing the parameters used for the analytical curve fitting for the hyperbolic cosine barrier and the following equation [16]

$$T = \frac{\sinh^2(\pi k/a)}{\sinh^2(\pi k/a) + cosh^2[\frac{1}{2}\pi\sqrt{K-1}]}, \tag{4.1}$$

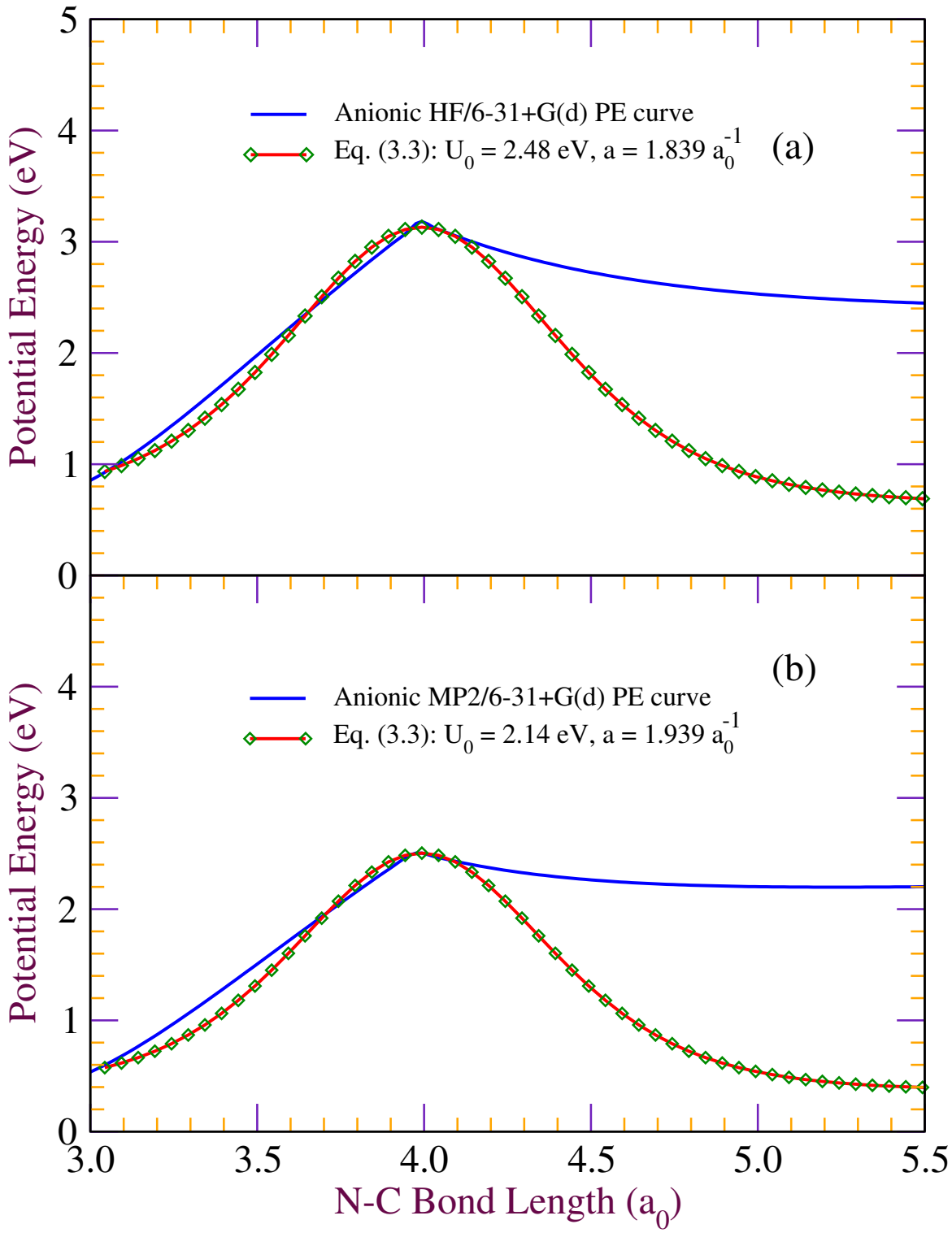

Fig. 4.4 Comparison of analytical hyperbolic cosine curves fitted using Eq. (3.3) with the anionic PE curves of (a) Fig. 4.2(a), and (b) Fig. 4.2(b).

where $K = 8mU_0/\hbar^2a^2$ with "m" being the reduced mass of the N–C bond. The transmission coefficient values for the N–C bond tunneling from each of the bound vibrational levels are tabulated in Table 4.2. It can be seen from the transmission coefficient values that tunneling

Table 4.2 Transmission coefficient (T) calculated using Eq. (4.1)

Vibrational State (χ_i)	Vibrational Energy χ_i(E) [eV]		Transmission Coefficient (T)	
	HF	MP2	HF	MP2
0	0.723	0.438	2.46×10^{-32}	9.19×10^{-34}
1	0.870	0.576	9.68×10^{-29}	9.86×10^{-30}
2	1.014	0.712	1.75×10^{-25}	3.23×10^{-26}
3	1.157	0.846	1.72×10^{-22}	4.49×10^{-23}
4	1.298	0.978	1.02×10^{-19}	3.24×10^{-20}
5	1.437	1.107	3.98×10^{-17}	1.37×10^{-17}
6	1.573	1.234	1.08×10^{-14}	3.79×10^{-15}
7	1.708	1.360	2.14×10^{-12}	7.23×10^{-13}
8	1.841	1.484	3.21×10^{-10}	1.00×10^{-10}
9	1.972	1.605	3.75×10^{-08}	1.05×10^{-08}
10	2.101	1.724	3.50×10^{-06}	8.60×10^{-07}
11	2.227	1.841	2.66×10^{-04}	5.65×10^{-05}
12	2.352	1.957	1.65×10^{-02}	3.03×10^{-03}
13	2.475	2.070	0.47	0.12
14	2.596	2.181	0.97	0.84
15	2.715	2.290	0.99	0.99
16	2.832	2.396	0.99	0.99
17	2.947	2.491	0.99	0.99
18	3.058	-	0.99	-
19	3.161	-	0.99	-

is completely hindered from lower vibrational levels. However, it attains a maximum probability at the top of the barrier. Essentially the same pattern follows in both the ab initio methods (Please see Fig. A4 of the Appendix A). The reason for this "S-type" tunneling [15] pattern may be understood as the gradual increase in the successive vibrational energy and the steady decrease in the corresponding width if one moves from the bottom to top of the anionic PE curve. One may conclude from these findings that the glycosidic bond cleavage via tunneling is less apparent from the lowest π^* shape resonance region (< 1 eV).

Therefore, we argue that the contribution of quantum mechanical tunneling towards the base release induced by LEE is significant only from those metastable states which are formed (thermally) in the higher vibrational energy region ($>$ 2 eV). This effect may be observed via maximizing the population at the respective regions. The effect of tunneling during LEE induced cytosine base release process is provided for the first time from our time-dependent quantum mechanical investigations.

4.3.4 Wave-packet propagation, Life time, and Cross section

As per the discussions in sections 4.3.1, 4.3.2 and 4.3.3, both the HF and MP2 results have similar characteristics and it can be seen that inclusion of electron correlation considerably improves the description of the low energy electron induced glycosidic bond lesion processes. Therefore, quantum dynamical TDWP computations utilizing the ab initio results from MP2 calculations are provided in the subsequent sections. Results from HF calculations are provided in Appendix A. The ground vibrational state of the neutral molecule (ϕ_0), i.e., the initial wave packet in both HF and MP2 methods, has been propagated from time t = 0–198 fs under the effect of the anionic Hamiltonian [H_{A^-}(R)] using the iterative Lanczos method [12]. It can be seen from the time propagation profile plotted in Fig. 4.5 (Fig. A5 of Appendix A for HF results) that the metastable state decays slowly as time progresses, and moves towards the right turning point of the PE curve. The characteristics of both the profiles are quite similar. Particularly, at about t = 10–12 fs, the probability amplitude reduces to small values ($2\text{x}10^{-6}$). This time is less than what is required for a single N–C bond vibration ($\sim$ 31 fs). Therefore, we can classify this type of resonance to follow an "impulse" model [18]. The auto correlation function $\langle\chi_0(R)|\psi_0(R,t)\rangle$ [Fig. 4.6(a)] characterized during the time propagation clearly shows the exponential decay of the metastable state (both HF and MP2) ensuring the shape resonance associated with the LEE attachment. The corresponding fragmentation profile [$\sigma_{0\leftarrow 0}$(E)] computed using the fast Fourier transformation of the auto correlation function is provided in Fig. 4.6(b). The cross section [$\sigma^{max}_{0\leftarrow 0}$(E)] maximum in HF method is seen at 0.75 eV and that of MP2 method is at 0.46 eV. It is noteworthy to mention here that the electron attachment to the cytosine base is found at 0.8 eV in the investigations

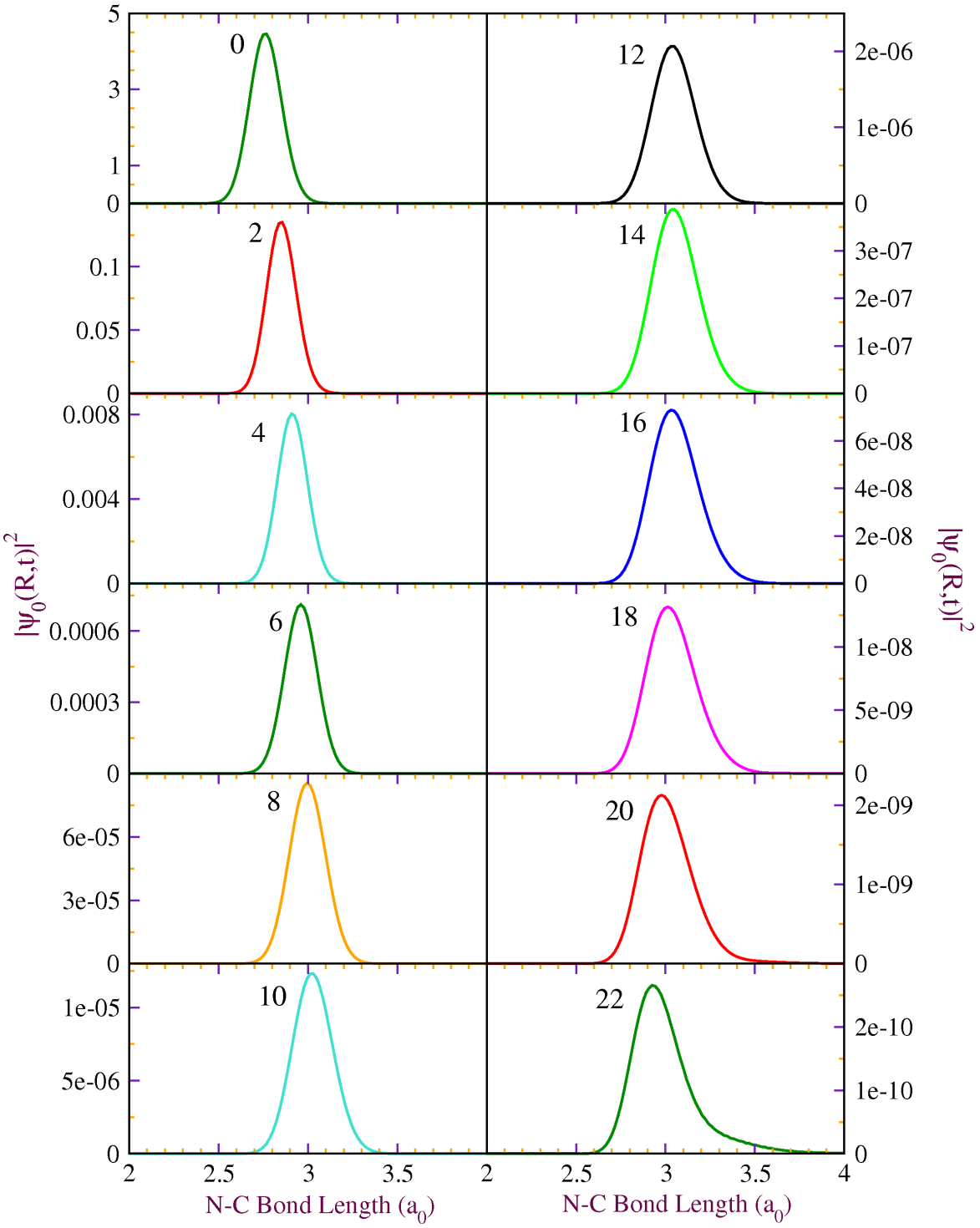

Fig. 4.5 Plots of wave packet propagation from time t = 0–22 fs for the ground state wave function ϕ_0(R) of the target 3′-dCMPH molecule in MP2/6-31+G(d) method under the effect of anionic Hamiltonian.

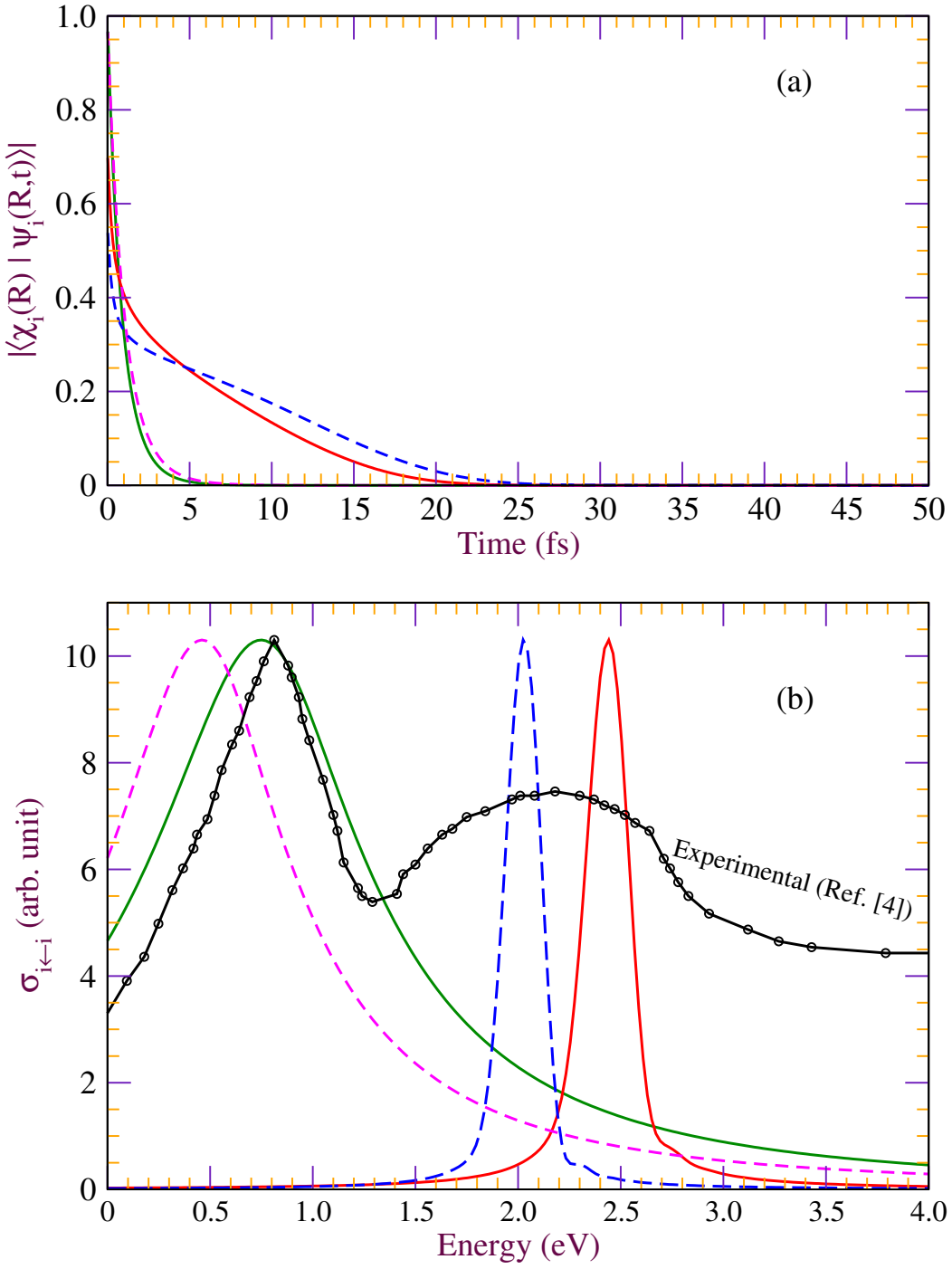

Fig. 4.6 (a) Auto correlation functions $|\langle\chi_i(R)|\psi_i(R,t)\rangle|$ from our HF/6-31+G(d) [(i=0, green solid line) and (i=13, red solid line)] and MP2/6-31+G(d) [(i=0, magenta dashed line) and (i=13, blue dashed line)] calculation on 3′-dCMPH molecule, (b) comparison of corresponding cross section profile $\sigma_{i\leftarrow i}$(E) for 3′-dCMPH molecule [(i=0, green solid line) and (i=13, red solid line) for HF and (i=0, magenta dashed line) and (i=13, blue dashed line)] with the available experimental spectrum [4] (black solid line with circles).

of Anusiewicz et al. on ss dCMPH trimer unit [19]. They found the barrier for the N–C bond cleavage requires an energy of 1.86 eV (43 kcal/mol). The lowest π^* shape resonance state for pure gas phase cytosine base is found to be at 0.32 eV in electron transmission spectroscopy analysis [20]. The changes in our calculated cross section values may be attributed to the modification of the base with the sugar and phosphate group attached to it. These fragmentation profiles are normalized with the available experimental cross section spectrum [4] for the single strand breaks in plasmid DNA molecule. This is mainly due to the metastable state formed in the π^* shape resonance energy region (0–3 eV) responsible for both the single strand and glycosidic bond rupture processes are the same. Additionally, the cross section profile is structure-less, thereby demonstrating the *impulse* [18] model resonance in accordance with our earlier investigations and justifying the time evolution plots of Fig. 4.5 and Fig. A3.

We have also calculated the fragmentation profile arising from the higher vibrational levels (χ_i), where the effect of tunneling in LEE induced glycosidic N–C bond rupture is significant. In particular, the wavepacket propagation, auto-correlation and fragmentation profile from the χ_{13} state of MP2 (same for HF) has been analyzed for cytosine base release and is described below.

As mentioned earlier, the wave packet propagation of the initial state ψ_{13}(R, t = 0) = ϕ_{13} (R) has been computed, using Lanczos scheme [12]. It can be seen from the snapshots provided in Fig. 4.7 (Please see Fig. A6 in the Appendix A for HF results) that the nodes of the initial wave function (t = 0 fs) reduces to zero within 10 fs. Subsequent profiles shows the propagation of the wavepacket towards the repulsive region of the σ^* state. The characteristics of tunneling may be visualized at $\sim$ 20–25 fs in the region 2 as an exponential decay of the TNI. The metastable state possess a lifetime of about 55 fs when using MP2 potential (about 35–40 fs in HF), much longer than what we have seen from the ground vibrational state ($\sim$ 10–12 fs). The calculated auto-correlation function, $\langle \chi_{13}(R) | \psi_{13}(R,t) \rangle$ in Fig. 4.6(a) depicts the maximum overlap when the propagation starts, and decays to negligible values at t = 30– 50 fs. Finally, the fragmentation profile calculated from the χ_{13} state exhibits a maximum at 2.44 eV in HF method and 2.02 eV energy at MP2 method. The

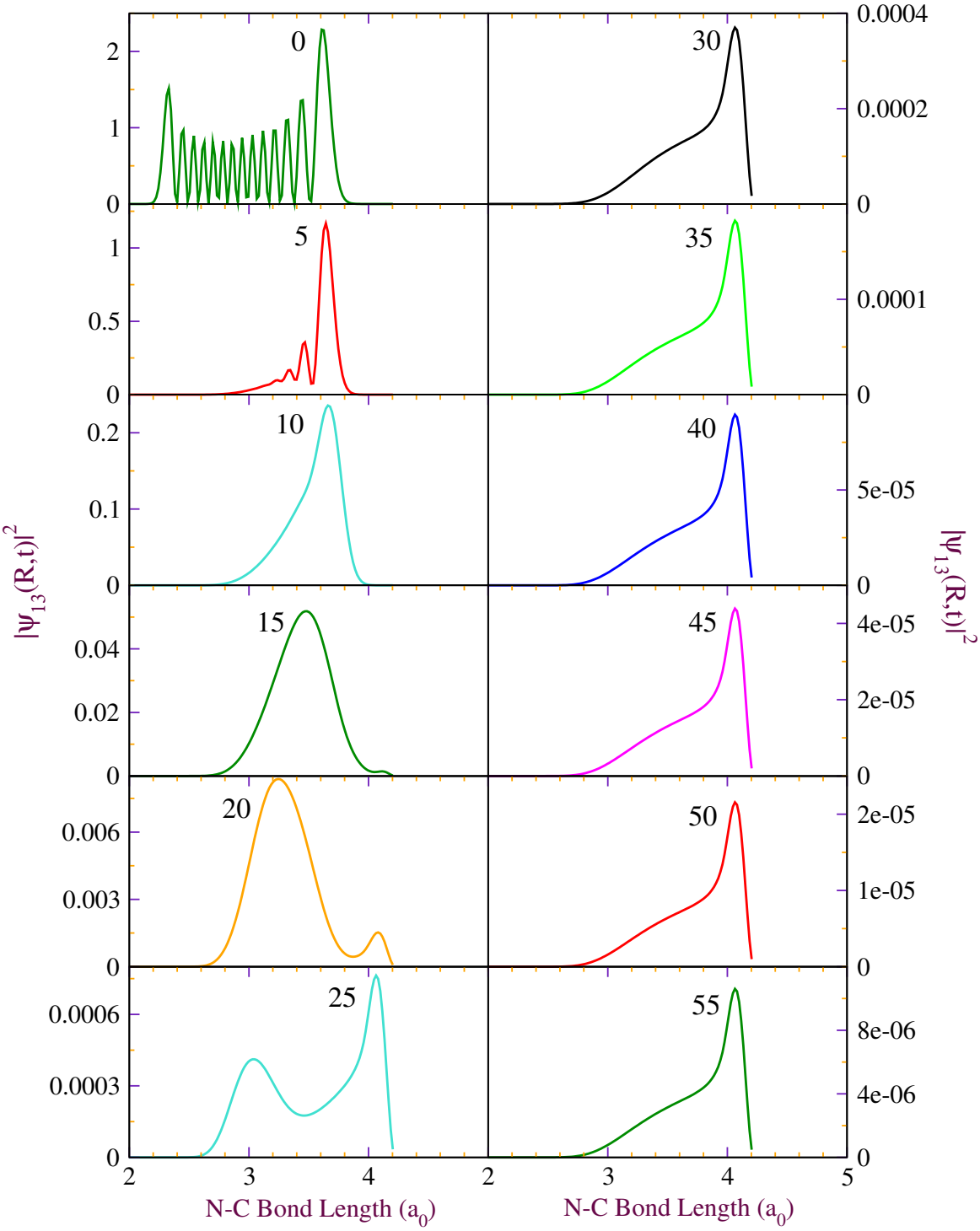

Fig. 4.7 Same as Fig. 4.5 except the target initial wave function is the thirteenth excited vibrational state [ϕ_{13}(R)].

structure less feature of the spectrum in Fig. 4.6(b) once again enables us to infer the *impulse model* [18] classification of electron collision with this DNA fragment. The maximum of this cross section spectrum has now been shifted to the higher energy region. This signifies the pronounced glycosidic N–C bond tunneling in the vibrational eigenstates of the 3′-dCMPH molecule above 2 eV energy.

4.3.5 Comparison with 3′ C–O bond dissociation

Low energy electron scattering off 3′-dCMPH molecule shows similarities between the two fragmentation processes, viz. the backbone sugar-phosphate 3′ C–O bond and the glycosidic N–C bond rupture. The electron attachment to the target takes place at the π^* shape resonance state in the 0.4–0.8 eV energy region. In both the dissociation processes, the molecule didn't get enough time to execute even a single vibration. Significant enhancement in DNA damage occur via tunneling from the higher energy vibrational levels in the two bond breaking events. Moreover, the vertical attachment energy determined for the formation of TNI is similar in both the ab initio methods. On the other hand, there are marked differences if one carefully examine these two DNA damage processes induced by low energy electron. A hyperbolic cosine barrier exist in the anionic PE curve generated at the ab initio HF level for the glycosidic N–C bond cleavage, which was absent in the anionic PE curve generated at the same level of accuracy for the SSB process [1]. The transfer of LEE from the π^* orbital of the base to the σ^* orbital of the 3′ C–O bond requires an activation energy of 1.18 eV for SSB at the MP2 level. However, the glycosidic bond rupture needs 0.96 eV energy more than what is required for the SSB. This implies the N–C bond dissociation is less favored in comparison with the strand break due to the high activation energy barrier ($\sim$ 2.14 eV at the MP2 level) associated with the cytosine base release event. Comparing the ground eigen state wave functions of both neutral and anionic systems, it should be noted here that the anionic vibrational state is slightly moved towards the right turning point in both the ab initio methods for the glycosidic bond breaking channel. The reverse trend can be seen in the SSB. The transfer of LEE from the cytosine base π^* orbital to the 3′ C–O σ^* orbital during single strand breaks clearly depicts the effective "atomic orbital overlap" between

the C_6 center of the base and the $C_{3'}$ center of the ribose sugar (Fig. 4.8). However, such an

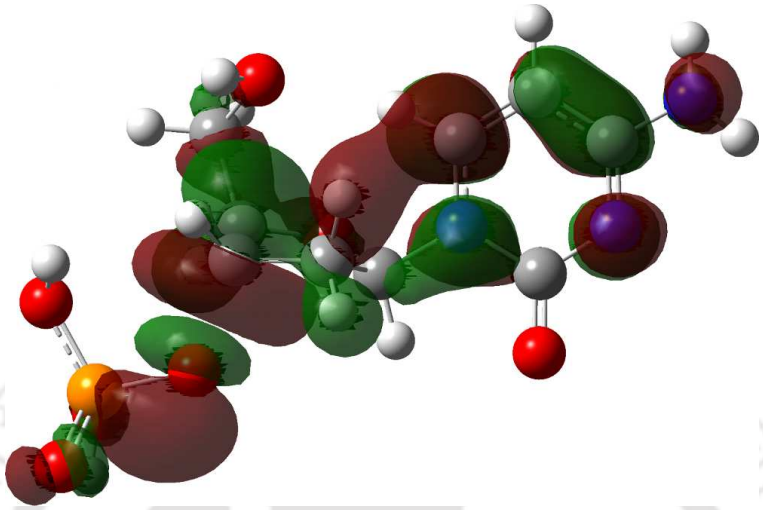

Fig. 4.8 Singly occupied molecular orbital (SOMO) generated for the anionic 3′-dCMPH moiety for the 3′ C-O bond lengths of 3.67 a_0 (1.94 Å) [at the barrier height] showing the effective atomic overlap between C_6 center of the base and the C_3' center of the sugar.

effective overlapping during the electron transfer process have not been seen either in HF or in MP2 level [Fig. 4.3(b)] descriptions of cytosine base release within this DNA fragment. The absence of "effective atomic orbital overlap"may be result of the high activation energy barrier for the base release. The lifetime of the decaying state is found to be larger for SSB than that for the N–C bond scission. It implies the attachment of LEE at the cytosine base and π^* shape resonance state hastens the loss of phosphate group from the 3′-dCMPH molecule. The large electron affinity of the phosphate group may also play a significant role during such an instant electron transfer mediated unimolecular dissociation. The phenomenon of quantum tunneling shows characteristic difference in the threshold for LEE induced SSB and cytosine base release damages within this molecule. SSBs may occur preferably in the 1–2 eV energy regime whereas the rupture of glycosidic bond via tunneling requires LEEs of above 2 eV. Our calculations are in conformity with the previous investigations [19] and suggests that the glycosidic N–C bond is the least preferred channel compared to the phosphodiester C–O bond for the damage, after attaching a low energy electron.

4.4 Concluding Remarks

The present study draws attention to our earlier investigations on low energy electron induced single strand breaks in 3′-dCMPH molecule. Various degrees of freedom exist within this moiety which may likely play a major role during the electron induced damage to DNA. However, it is very difficult to incorporate all these vibrational modes together for a quantitative description of the damage using time-dependent quantum mechanical calculations. Instead, we have investigated the probable dissociation channels individually and provide a reasonable explanation for this complex bio-chemical change on the basis of a comparative assessment. Notable findings of the present investigation follows:

(a) The π^* shape resonance state present in the cytosine nucleobase can act as LEE receiver and may play a major role in LEE induced single strand breaks, and cytosine base release.

(b) The activation energy barrier for the glycosidic N–C bond cleavage is higher than that for the 3′ C–O bond rupture. Therefore, it is unlikely that the electron captured at the cytosine base π^* orbital will transfer to the glycosidic N–C bond σ^* orbital via the atomic orbital overlap.

(c) The metastable species formed below 1 eV possess a very short lifetime for the glycosidic bond scission which is comparable with the auto-detachment lifetime.

(d) The role of tunneling during the cytosine base release is seen only at the higher energy regime, i.e., above 2 eV.

(e) The electron-molecule scattering occur in 3′-dCMPH molecule is classified as the "impulse model" [18] resonance phenomenon.

The findings of the present investigation encourage us to employ the LCP-TDWP approach to layer network of biomolecules for gaining insight in the mechanistic picture during LEE induced damage to biomolecules. One such case we have treated in an analogous molecule known as 2′-deoxycytidine-5′-monophosphate (in short 5′-dCMPH) is provided in chapter 5.

References

[1] Renjith B., S. Bhowmick, M. K. Mishra, and M. Sarma, J. Phys. Chem. A **115**, 13753 (2011).

[2] S. Bhowmick, Renjith B., M. K. Mishra, and M. Sarma, J. Chem. Phys **137**, 064310 (2012).

[3] R. Bhaskaran and M. Sarma, J. Chem. Phys **139**, 045103 (2013).

[4] F. Martin, P. D. Burrow, Z. Cai, P. Cloutier, D. Hunting, and L. Sanche, Phys. Rev. Lett. **93**, 068101 (2004).

[5] J. Gu, J. Wang, and J. Lesczynski, J. Am. Chem. Soc. **128**, 9322 (2006).

[6] J. Gu, Y. Xie, and H. F. Schaefer III, J. Am. Chem. Soc. **127**, 1053 (2005).

[7] X. Li, L. Sanche, and M. D. Sevilla, Radiat. Res. **165**, 721 (2006).

[8] J. Simons, Acc. Chem. Res. **39**, 772 (2006) and references therein.

[9] R. Bhaskaran and M. Sarma, J. Chem. Phys **141**, 104309 (2014).

[10] M. J. Frisch, G. W. Trucks, H. B. Schlegel, et al., *GAUSSIAN 03*, Revision E.01, Gaussian,Inc., Wallingford, CT, 2004.

[11] M. J. Frisch, G. W. Trucks, H. B. Schlegel, et al., *GAUSSIAN 09*, Revision D.01, (Gaussian,Inc. Wallingford, CT, 2013).

[12] C. Leforestier, R. H. Bisseling, C. Cerjan, M. D. Feit, R. Friesner, A. Guldberg, A. Hammerich, G. Jolicard, W. Karrlein, H.-D. Meyer, N. Lipkin, O. Roncero, and R. Kosloff, J. Comput. Phys. **94**, 59 (1991).

[13] D. Kosloff and R. Kosloff, J. Comput. Phys. **52**, 35 (1983).

[14] J. Zhang, D. G. Imre, and J. H. Frederick, J. Phys. Chem. **93**, 1840 (1989).

[15] R. Marom, C. Levi, T. Weiss, S. Rosenwaks, Y. Zeiri, R. Kosloff, and I. Bar, J. Phys. Chem. A **114**, 9623 (2010).

[16] L. D. Landau and E. M. Lifshitz, *Quantum Mechanics, 3rd ed.* (Pergamon Press, Oxford, U.K., 1977).

[17] C. C. Marston and G. G. Balint-Kurti, J. Chem. Phys. **91**, 3571 (1989).

[18] J. N. Bardsley and J. M. Wadehra, Phys. Rev. A **20**, 1398 (1979).

[19] I. Anusiewicz, J. Berdys, M. Sobczyk, P. Skurski, and J. Simons, J. Phys. Chem. A **108**, 11381 (2004).

[20] K. Aflatooni, G. A. Gallup, and P. D. Burrow, J. Phys. Chem. A **102**, 6205 (1998).

Chapter 5

Single strand breaks in 2′-deoxycytidine-5′-monophosphate

5.1 Introduction

It has been well understood that low energy electron (LEE) can attach to DNA/DNA fragments [1] in any one of the components like (i) nucleobase, [2] (ii) sugar, [3] (iii) phosphate group [4] or, as a dipole bound state (DBS) [5] outside the molecular framework. The LEE attachment to the target may lead to either the formation of a metastable state [also known as transient negative ion (TNI)] or an electronically stable anionic species. Metastable states, usually lie above their parent neutral state (negative electron affinity) and are often referred to as "resonance" and exist only for a very short period of time. The TNI plays a prominent role during LEE induced damage to bio-molecules like DNA, causing mutagenesis to the organisms [6, 7]. Hence, a large number of secondary electrons which are produced as a result of the interaction of primary ionizing radiation with living cells [8, 9] offer a critical threat to the metabolic activities [7]. Crossed electron-molecular beam experiment on gas phase 2′-deoxycytidine-5′-monophosphate (5′-dCMP) molecule (without neutralization) [10] concludes that (a) LEE can attach to either the nucleobase cytosine, sugar unit, or the phosphate group, and (b) the contribution towards SSBs varies with respect to each of these sites where the LEE gets attached. A near 0 eV electron can attach to the backbone phosphate

group resulting in *ca.* 60% of the strand breaks, while a near 1 eV LEE can induce SSB (*ca.* 15%) after attaching to the cytosine nucleobase. The remaining 25% damage is due to the electron initially localized at the ribose sugar unit. The study noted the formation of entire phosphate ion (PO_4^-) due to two overlapping resonances peaking near 0 eV and 1 eV [10]. On the contrary, theoretical investigation of Bao et al. on modeled 5′-dCMPH moiety (where one of the generated radical center is terminated with methyl group) in both gas phase and aqueous medium suggested the plausibility of a near 0 eV electron attachment exclusively at the nucleobase region [11]. In addition, they also pointed out that the rate of SSB in gas phase is more, compared to that of in aqueous environment [11]. Owing to the discrepancy found in the theoretical and the recent experimental findings, here we present the results obtained from our local complex potential based time dependent wave packet (LCP-TDWP) calculations for this molecule in detail. Our objective is to look into the possible LEE attachment sites within this building block (5′-dCMPH) of life and deduce the characteristic fragmentation profiles which may help to understand *the role of shape resonance states* during LEE induced SSB.

A short description of the electronic structure calculations and the wave packet propagation scheme is mentioned in Section 5.2. Section 5.3 discusses the role of shape resonance state during LEE induced SSB in 5′-dCMPH. The major outcome from this investigation concludes this chapter.

5.2 Computational Method

5.2.1 Geometry optimization and Potential energy scan

Before explaining the details of the time dependent quantum mechanical aspects, let us briefly discuss about the modeled gas phase system 2′-deoxycytidine-5′-monophosphate, in short 5′-dCMPH (Fig. 5.1) for LEE induced SSB considered in the present investigation. The selected nucleotide is excised from a portion of double stranded DNA contains the pyrimidine base cytosine, the ribose sugar, and the phosphate group. This fragment possesses the LEE attachment sites and the site where the strand breaks occur. Electro-neutrality in *in vivo* DNA is offered by the presence of alkali metal counter cations like Na^+ or K^+ to the negative

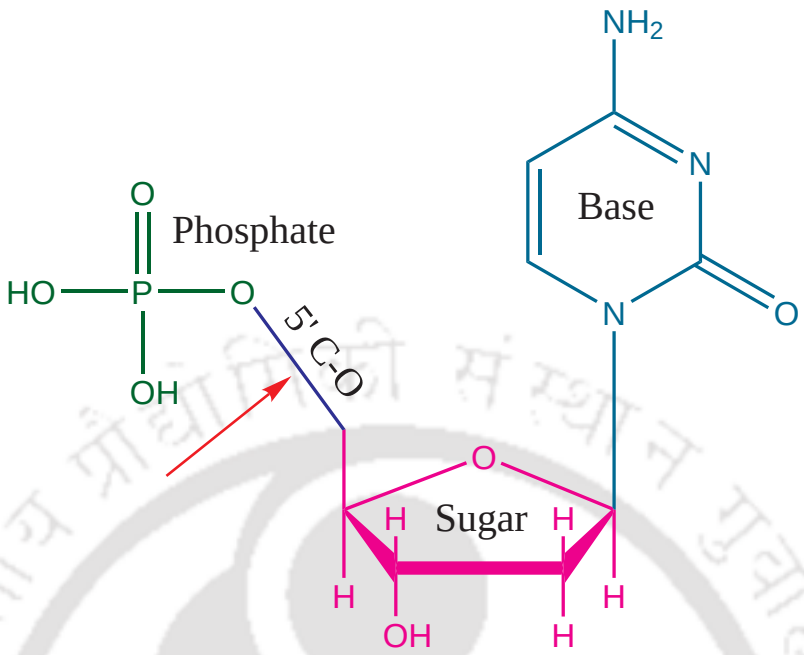

Fig. 5.1 The Base-Sugar-Phosphate unit of 2′-deoxycytidine-5′-monophosphate (5′-dCMPH) neutralized by adding hydrogens at the radical center and a proton at the phosphate negative center. The bond undergoing cleavage is marked with a red arrow.

center of the phosphate group. However, we have chosen two hydrogens and a proton to neutralize the modeled system for relatively smooth attachment of the incoming low energy electron. The neutral and anionic systems were optimized initially at the Hartree-Fock (HF) and later at the correlated second-order Møller Plesset perturbation theory (MP2) methods at the 6-31+G(d) accuracy level. The optimized geometries were used to compute the potential energy (PE) curves for the target [E_A(R)] and anionic [E_{A^-}(R)] systems (where A = 5′-dCMPH), those are the necessary ingredients for our wave packet propagation calculations. The labeled 5′ C–O bond of Fig. 5.1 has been compressed/stretched within the interval of 1-10 a_0 for 256 equally spaced grid points for both the neutral and anionic systems, keeping all other degrees of freedom of the molecule frozen. GAUSSIAN 09 package of programs [12] have been used in all of the electronic structure calculations presented here.

5.2.2 Quantum dynamical calculations

The local complex potential (LCP) formalism for describing the dynamics of the nuclei of a metastable anion is briefly explained below. Since, it is computationally very difficult to consider the quantum multi-dimensional analysis of relevant biological molecular network, we have considered the one-dimensional 5′ C–O bond dissociation channel in the gas phase 5′-dCMPH molecule (Fig. 5.1). Anionic species is obtained by adding an electron to the lowest unoccupied molecular orbital (LUMO) of the neutral molecule (A), which in the present context known as TNI [A^-]. The anionic Hamiltonian for the 5′ C–O bond dissociation in LCP-TDWP method is expressed as in Eq. (2.2). The local complex potential term is [13, 14] coined by two necessary ingredients for our time dependent quantum mechanical calculations. The first term is the PEs of the anion [$E_{A^-}(R)$] which is obtained using G09 program suite [12] as discussed in the section 5.2.1 and the other unknown quantity $\Gamma_{A^-}(R)$ is computed as an exponential function [please see Eq. (2.4)].

The first step of our molecular quantum dynamical calculation is the computation of the grid representation of the wave function of the neutral (A) [ϕ_i(R)] and anionic (A^-) [χ_i(R)] systems at time t = 0, utilizing the extremely efficient Fourier grid Hamiltonian (FGH) [15] method. The initial wave packet prepared so is then propagated for a finite time limit in space employing the iterative Lanczos based diagonalization scheme [16] to find out the final quantum state distribution. The time dependent Schrödinger equation, which is the pillar for any gas phase and condensed phase quantum dynamical calculations have been used for solving the wave packet propagation sequence in which the performance of the fast Fourier transform (FFT) [17] technique to determine the effect of kinetic energy operator in the anionic Hamiltonian $H_{A^-}(R)$ is well appreciated. Fourier transformation of the auto correlation function gives the fragmentation profile [σ(E)] which is one of the prime objective of our investigation and compared with the available experimental cross-section spectra.

Finally, there may be a possibility of coupling between the valence π^* shape resonance state and the repulsive σ^* state within the system which may influence as an avoided crossing of the 5′ C–O bond and give rise to a hyperbolic cosine barrier in the anionic PE curve.

This will allow the 5′ C–O bound vibrational levels to tunnel toward the repulsive region through the barrier. The transmission coefficient, T, [18, 19] under this circumstance can be computed using any one of the equations as represented in Eq. (3.3) or (3.4). More details of the theoretical method can be found in chapters 2 and 3.

5.3 Results and Discussions

5.3.1 Optimized geometries and PE curves

The HF and MP2 optimized structures of neutral and anionic systems are provided in Figs. B1 and B2 of the Appendix B. The equilibrium neutral 5′ C–O bond [R_{C-O} = 2.703 a_0 (1.430 Å) at HF and 2.754 a_0 (1.457 Å) at MP2] is found to be shortened than that of the anion [R_{C-O} = 2.718 a_0 (1.438 Å) at HF and 2.767 a_0 (1.464 Å) at MP2] in both the ab-initio methods. The PE curves calculated for neutral [E_A(R)] and anionic [E_{A^-}(R)] 5′-dCMPH moieties from the optimized structures (Figs. B1 and B2) using G09 codes [12] at the HF and MP2 methods with 6-31+G(d) accuracy levels are shown in Figs. 5.2(a) and 5.2(b) respectively. It is clear from these figures that the anion formed is metastable (vertical attachment energy (VAE) is 0.59 eV at HF and 0.35 eV at MP2) at both these methods. Careful inspection of the anionic PE curves enable us to infer that the barrier position in HF [$R_{C-O} \sim$ 3.84 a_0 (2.03 Å)] and MP2 methods [$R_{C-O} \sim$ 3.78 a_0 (1.99 Å)] are almost similar, though the barrier heights differ as 2.14 eV in the former and 1.70 eV in the latter methods respectively.

Since, both HF and MP2 methods results shows similar characteristics especially the formation of metastable anionic state after the LEE attachment, therefore, we focus on the results of time dependent quantum mechanical calculations carried out for the correlated MP2 potential energy curves. Important findings of dynamical calculations on HF potentials are also discussed at the appropriate places.

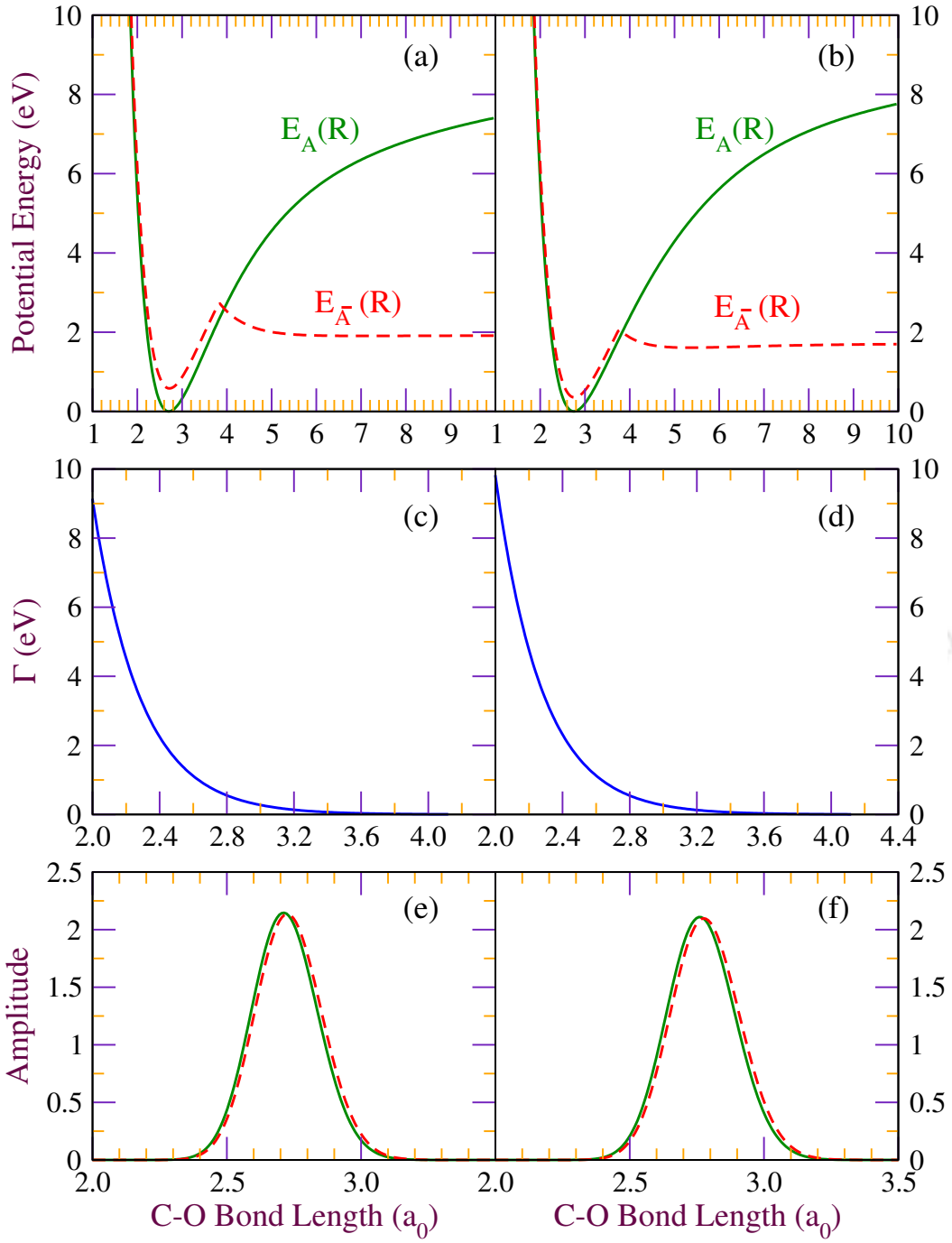

Fig. 5.2 Potential energy curves for the neutral [$E_A(R)$] (green solid line) and the anionic [$E_{A^-}(R)$] (red solid line) 5′-dCMPH molecule computed at the (a) HF/6-31+G(d), and (b) MP2/6-31+G(d) accuracy level. The width function $\Gamma_{A^-}(R)$ calculated as an exponential function for (c) HF, and (d) MP2 potentials of 5′-dCMPH moiety. The ground state eigenfunctions are shown in (e) for HF [green solid line for neutral and red dashed line for anion], and (f) for MP2 [green solid line for neutral and red dashed line for anion] potentials respectively.

5.3.2 Width functions and Vibrational eigen functions

The crossing point (R_x) between the neutral and anionic PE curve in MP2 method is 3.83 a_0 (2.02 Å) [3.94 a_0 (2.08 Å) in HF method]. Time dependent calculations have been done on a curtailed slice of E_A(R) and E_{A^-}(R) ranging from R_{C-O} = 1.88 – 4.12 a_0 with 256 equally discretized points in both the *ab initio* methods. The width function [Γ_{A^-}(R)] is calculated at each grid points for MP2 potential by choosing an optimal values of α = 3.61 and δ_1 = 490 (α = 3.50 and δ_1 = 370 for HF potential) which ensures the metastability of the short lived resonance intermediate state. A plot of Γ_{A^-}(R) at each grid points with respect to the 5′ C–O bond distance (R_{C-O}) is shown in Figs. 5.2(c) and 5.2(d) for HF and MP2 potentials respectively. The width function goes nearly to zero at the crossing point (R_x) as mentioned in section 5.2.2.

We have, then, computed the vibrational eigenfunctions of the neutral [ϕ_i(R)] and anionic [χ_i(R)] systems to get the dynamical aspects of LEE induced single strand breaks in 5′-dCMPH moiety. Implementation of the FGH method [15] on the anionic PE curve [E_{A^-}(R)] revealed fifteen bound vibrational states for MP2 potential and eighteen bound vibrational levels for HF potential. The ground vibrational levels of both the neutral and anionic systems are shown in Figs. 5.2(e) and 5.2(f) respectively for HF and MP2 potentials. It is to be noted here that the anionic wave functions are slightly move forward to the right turning point of the PE curve.

The hyperbolic cosine barrier seen in E_{A^-}(R) for both the HF and MP2 methods may be a result of the coupling between the valence π^* shape resonance state on the cytosine and the repulsive σ^* state on the 5′ C–O bond within the system, thereby allowing the 5′ C–O bond to follow an avoided crossing pathway. Consequently, the probability of 5′ C–O bond tunneling from the higher anionic bound vibrational levels through this barrier towards the repulsive region may be very high. Therefore, we have divided the vibrational energy levels [χ_i(R)] of MP2 anionic potential into two regions, those with energy (i) below 1.5 eV [$\chi_{i=0-9}$(R)] and (b) above 1.5 eV [$\chi_{i=10-14}$(R)]. Similarly for HF anionic potential with energy (i) below 1.5 eV [$\chi_{i=0-10}$(R)] and (b) above 1.5 eV [$\chi_{i=11-17}$(R)]. This classification will enable us to

focus on the effect of quantum tunneling during LEE induced SSB in 5′-dCMPH molecule which, to the best of our knowledge, has not appeared in the literature yet.

5.3.3 SSB from the ground vibrational level [ϕ_0(R)]

Quantitative treatment of LCP-TDWP approach comprises of three steps in which in the first step, wave packet propagation of the initial bound vibrational state (ϕ_0 in the present context) has been carried out from time t = 0 – 198 fs under the effect of the metastable anionic Hamiltonian [H_{A^-}(R)]. Fig. 5.3 depicts a few plots of this quantum state evolution for MP2 potential (please see Fig. B3 of Appendix B for HF potential) at t = 0 – 22 fs in the interval of 2 fs where we can see (i) the progress of the metastable state with maximum amplitude when propagation starts, and goes to negligible values by t = 20 fs with the amplitude being reduced to 4x10^{-6} and (ii) the movement of the wave function towards the right turning point of the anionic PE curve characterizing the *impulse model* resonance in e-DNA scattering. This is further ensured from the life time of the metastable anion (18 – 20 fs) which is less than what is required for a C–O bond single vibration ($\sim$ 33 fs). Similar trend can be seen in HF results (please see Fig. B3 of Appendix B).

We further proceed to the second step of the quantitative analysis where we have analyzed the auto correlation function $\langle\chi_0(R)|\psi_0(R,t)\rangle$ [Fig. 5.4(a)] which clearly exhibits the maximum overlap during the initial time of propagation and nullifies near about t = 15 – 20 fs. The fragmentation profile [$\sigma_{0\leftarrow0}$(E)] is computed from the Fourier transformation of the auto correlation function in the final step and is compared with the experimental results [10] of gas phase 5′-dCMP molecule investigation (shoulder near 1 eV) as shown in Fig. 5.4(b). The calculated $\sigma_{0\leftarrow0}$(E) spectrum from this investigation is in accordance with the experimental profile [10]. The maximum in the fragmentation profile [$\sigma^{max}_{0\leftarrow0}$(E)] for our time-dependent wavepacket calculation is seen at 0.44 eV for MP2 potential [magenta solid line of Fig. 5.4(b)] and at 0.67 eV [blue solid line of Fig. 5.4(b)] for the HF potential. These peak positions are in the reasonable error limit of the maximum yield observed for the condensed phase plasmid DNA experiment (0.8 eV) [20]. The structure-less feature of the

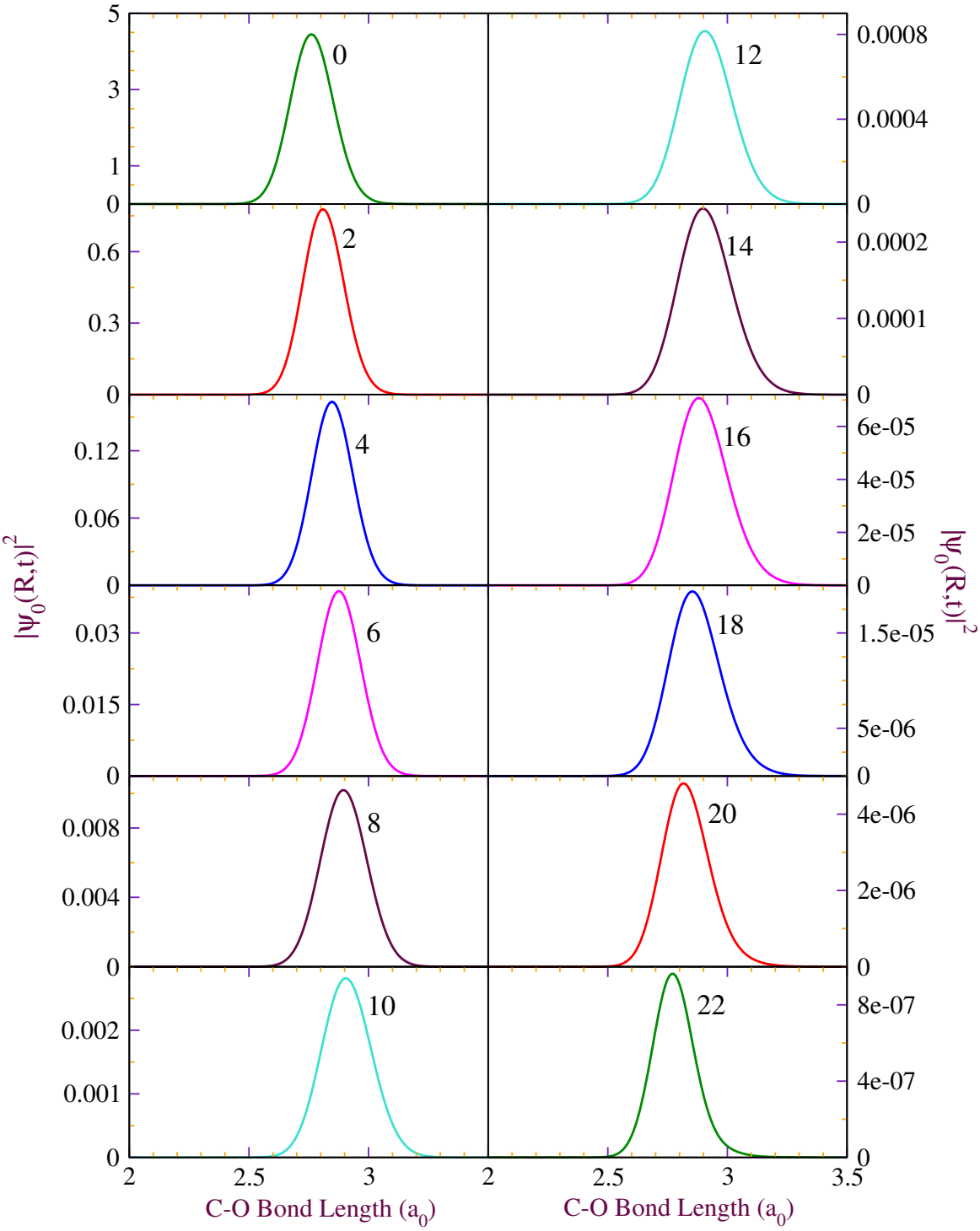

Fig. 5.3 Plots of wave packet propagation from time t = 0–22 fs for the ground state wave function ϕ_0(R) of the target 5′-dCMPH molecule under the effect of anionic Hamiltonian.

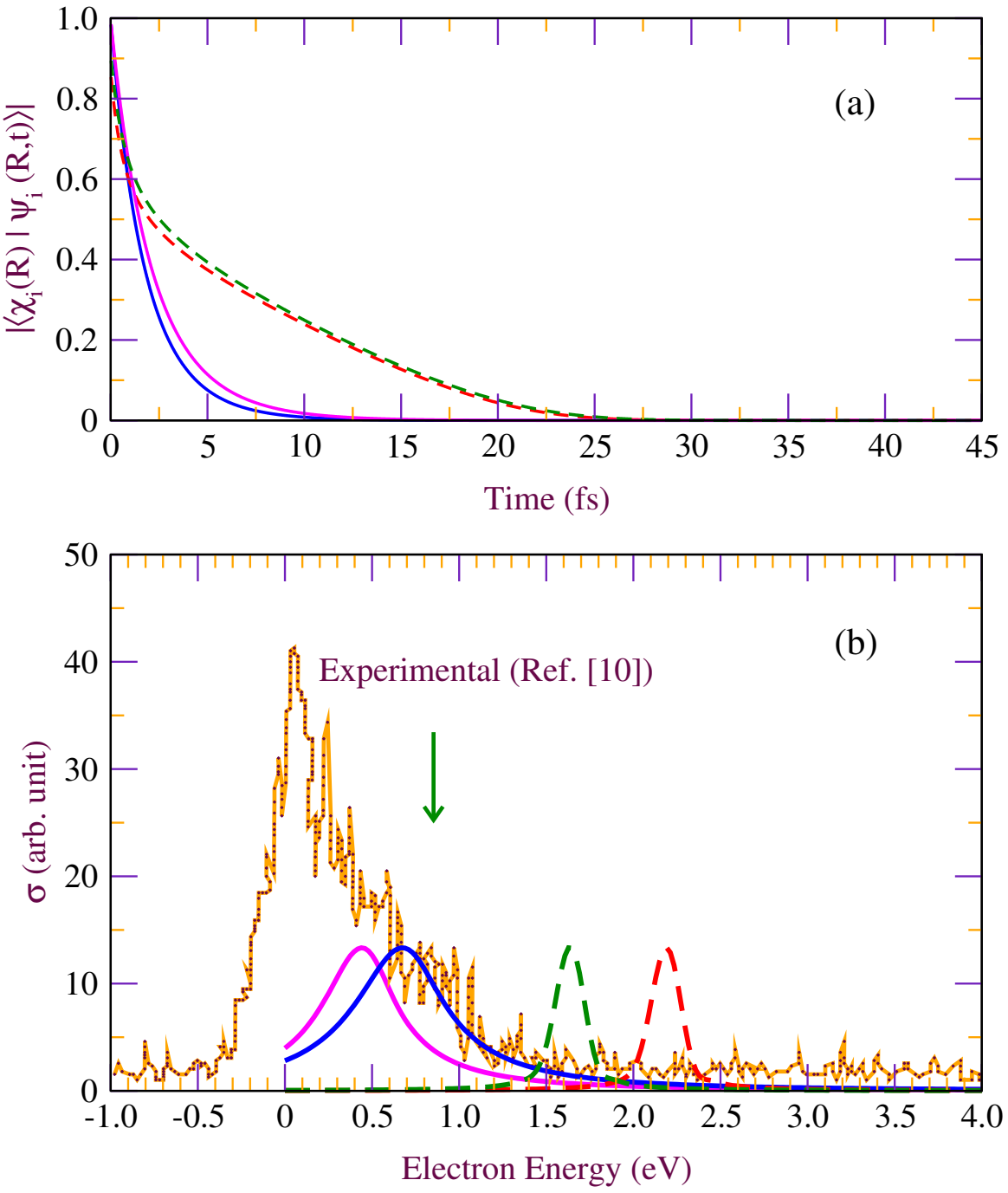

Fig. 5.4 (a) Auto correlation functions $|\langle\chi_i(R)|\psi_i(R,t)\rangle|$ calculated from wave packet propagation for 5′-dCMPH molecule at (i) HF/6-31+G(d) level (i=0, blue solid line and i=12, red dashed line), and (ii) MP2/6-31+G(d) level (i=0, magenta solid line and i=10, green dashed line) and, (b) comparison of corresponding $\sigma_{i\leftarrow i}$(E) for 5′-dCMPH molecule with the experimental profile [10] where the shoulder near 1 eV is labeled with an arrow.

calculated fragmentation profile, here, further confirms the *impulse*[14] model behavior of the shape resonance process corroborating the time evolution plots of Fig. 5.3.

As mentioned earlier, the role of quantum mechanical tunneling phenomenon during the sugar phosphate 5′ C–O bond lesion may not be ruled out. Hence, we investigated the effect of tunneling during LEE induced SSB within this molecule for the first time and discussed in the following subsection 5.3.4.

5.3.4 SSB due to the C–O bond tunneling

The anionic PE curve [E_{A^-}(R)]s of Figs. 5.2(a) and 5.2(b) have barriers around 3.0 – 5.0 a_0 of the 5′ C–O bond length. We have divided E_{A^-}(R) into three regions. Region 1 is the potential well where the LEE gets trapped forming the metastable state (or known as shape resonance state), Region 2 is the area under the barrier, and the repulsive asymptotic part of the potential designates as Region 3.

To proceed for the transmission coefficient calculation, we have made use of Eq. (4.1) which is solely depending upon the value of the constant K. However, since the barrier in E_{A^-}(R) is not symmetric, therefore, it is difficult to find out the value of width parameter (a) which is the full width at the half maximum (FWHM) of the anionic PE curve. We have used a modeled hyperbolic cosine barrier of the following form [19] to get the a value as:

$$U(R) = \frac{U_0}{\cosh^2(aR)} \tag{5.1}$$

where R corresponds to the 5′ C–O bond length of the anion. The analytical curve obtained using Eq. (5.1) is reasonably fitted well with the E_{A^-}(R), represented in Figs. 5.5(a) [for HF anionic potential] and 5.5(b) [for MP2 anionic potential]. The value of K is found to be greater than one and thus, we have calculated the transmission coefficient (T) of the 5′ C–O bond tunneling from each of the fifteen bound vibrational levels ($\chi_{i=0-14}$) of MP2 anionic potential using Eq. (4.1). The best fitted values of "U_0" and "a" are taken as 1.70 eV and 2.13 ${a_0}^{-1}$ respectively for MP2 potential ("U_0"= 2.14 eV and "a"= 1.89 ${a_0}^{-1}$ for HF calculation).

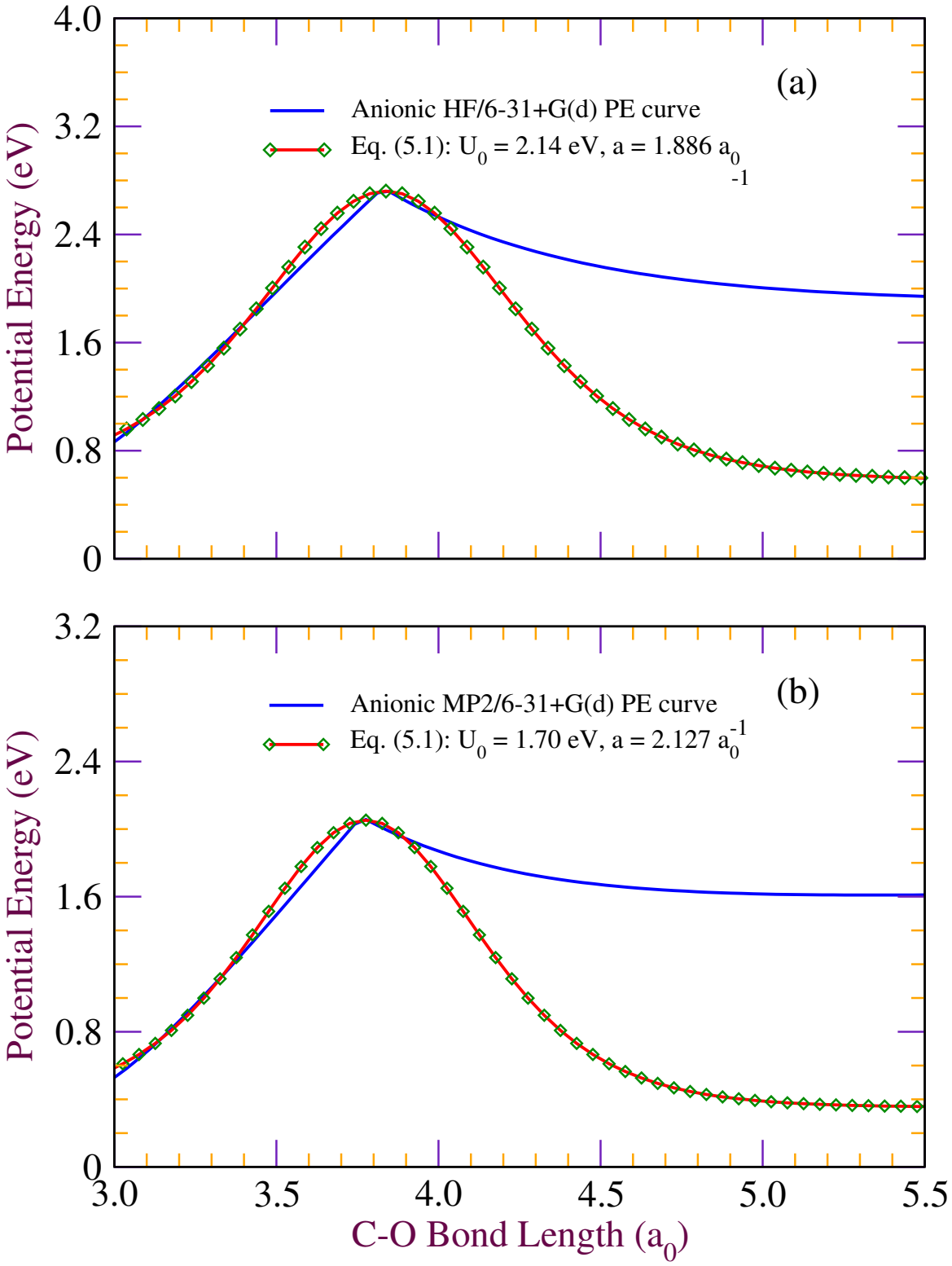

Fig. 5.5 (a) Comparison of analytical hyperbolic cosine curves fitted using Eq. (5.1) with the anionic PE curves of (a) Fig. 5.2(a) and (b) Fig. 5.2(b).

The variation of the tunneling probability against each of the anionic vibrational energies of HF and MP2 potentials are provided in Table 5.1 and Fig. B4 of the Appendix B.

It can be seen from Table 5.1 and Fig. B4 that the probability of tunneling is completely

Table 5.1 Transmission coefficient (T) calculated using Eq. (4.1)

Vibrational State (χ_i)	Vibrational Energy χ_i(E) [eV]		Transmission Coefficient (T)	
	HF	MP2	HF	MP2
0	0.65	0.42	1.95×10^{-29}	3.11×10^{-26}
1	0.79	0.55	8.59×10^{-26}	1.50×10^{-22}
2	0.93	0.68	1.65×10^{-22}	2.49×10^{-19}
3	1.07	0.81	1.66×10^{-19}	1.90×10^{-16}
4	1.20	0.93	9.84×10^{-17}	8.02×10^{-14}
5	1.33	1.05	3.76×10^{-14}	2.11×10^{-11}
6	1.46	1.18	9.94×10^{-12}	3.73×10^{-09}
7	1.59	1.30	1.89×10^{-09}	4.75×10^{-07}
8	1.72	1.42	2.71×10^{-07}	4.54×10^{-05}
9	1.84	1.54	3.01×10^{-05}	3.38×10^{-03}
10	1.97	1.65	2.66×10^{-03}	0.17
11	2.09	1.76	0.16	0.91
12	2.21	1.88	0.92	0.99
13	2.32	1.96	0.99	0.99
14	2.44	1.99	0.99	0.99
15	2.55	-	0.99	-
16	2.63	-	0.99	-
17	2.67	-	0.99	-

suppressed from the lower vibrational levels [$\chi_{i=0-9}$(R) for MP2 and $\chi_{i=0-10}$(R) for HF anionic potentials]. However, at the χ_{10} state of MP2 potential (χ_{11} state of HF potential) a sudden jump in "T" is seen and that "T" becomes significant in the higher vibrational levels [$\chi_{i=11-14}$(R)] which may eventually contribute towards SSB. This characteristic tunneling behavior seen as “S-shaped” curve in Fig. B4 is already found in other investigations [19]. The surge in the transmission probabilities may be attributed to the increase in anionic vibrational energies from lower to higher vibrational states which allow the C–O bond to tunnel towards the dissociative region of the E_{A^-}(R). Therefore, contribution of quantum mechanical tunneling of the 5′ C–O bond in SSB induced by LEE is prominent only from the metastable state formed in any one of the higher lying energy ($>$ 1.5 eV) levels. Quantum

mechanical tunneling of 5′ C–O bond from the upper lying states in *in vivo* DNA may be observed experimentally by achieving maximum population at these energy levels.

Further, to analyze the effect of quantum tunneling quantitatively from the higher vibrational levels ($\chi_{i=10-14}$) where T values are significant, we have chosen the χ_{10} state of E_{A^-}(R) of MP2 calculation (χ_{12} state of E_{A^-}(R) of HF calculation). The quantitative algorithm for wave packet propagation, auto correlation, and cross-section profile calculations have utilized the same as that mentioned in the earlier sub-section 5.3.3.

The wave packet motion of the initial state ψ_{10}(R, t=0) = ϕ_{10} (R) has been computed using Lanczos scheme [16] and a few of them are provided in Fig. 5.6 (see Fig. B5 for HF potential). The time evolution plots of Fig. 5.6 reveals that the ten nodes of the initial wave function (t = 0 fs) reduces to four nodes within 5 fs. Subsequent profiles show no nodes. Interestingly, there is a signature of shoulder and subsequent exponential decay of the wave function in the 20–25 fs plots. This feature is seen between $R_{C-O} \sim$ 3.2–4.2 a_0 lies in the Region 2 ($R_{C-O} \sim$ 1.7–2.2 Å, tunneling region) of the Fig. 5.2(b) and may indicate quantum tunneling of the 5′ C–O bond from the χ_{10} state to the dissociative region. In addition, the metastable state at this vibrational state possesses a life-time of $\sim$ 60–65 fs which is much longer than that from the ground vibrational state ($\sim$ 18–20 fs). The larger spatial spread of the eigenfunction at χ_{10} may be the reason for the longer life-time. These findings are also supported by the calculated auto-correlation function $\langle\chi_{10}(R)|\psi_{10}(R,t)\rangle$ of Fig. 5.4(a) where the overlap is maximum at the initial time and reduces gradually to negligible values at t = 50 fs. Finally, the fragmentation profile is calculated from the χ_{10} state exhibits a maximum at the 1.62 eV energy (2.19 eV for χ_{12} state of HF potential). The structure less feature of the spectrum in Fig. 5.4(b) once again enables us to infer the *impulse model* [14] classification of electron collision with this DNA fragment. The maximum of this spectrum has now been shifted to the higher energy region of the experimental maxima (0.83 eV in the condensed phase plasmid DNA investigation [20] and near 1 eV in the gas phase investigation of 5′-dCMP moiety [10]). This, thus, signifies pronounced 5′ C–O bond tunneling in the vibrational eigenstates of the 5′-dCMPH molecule above 1.5 eV energy. Our

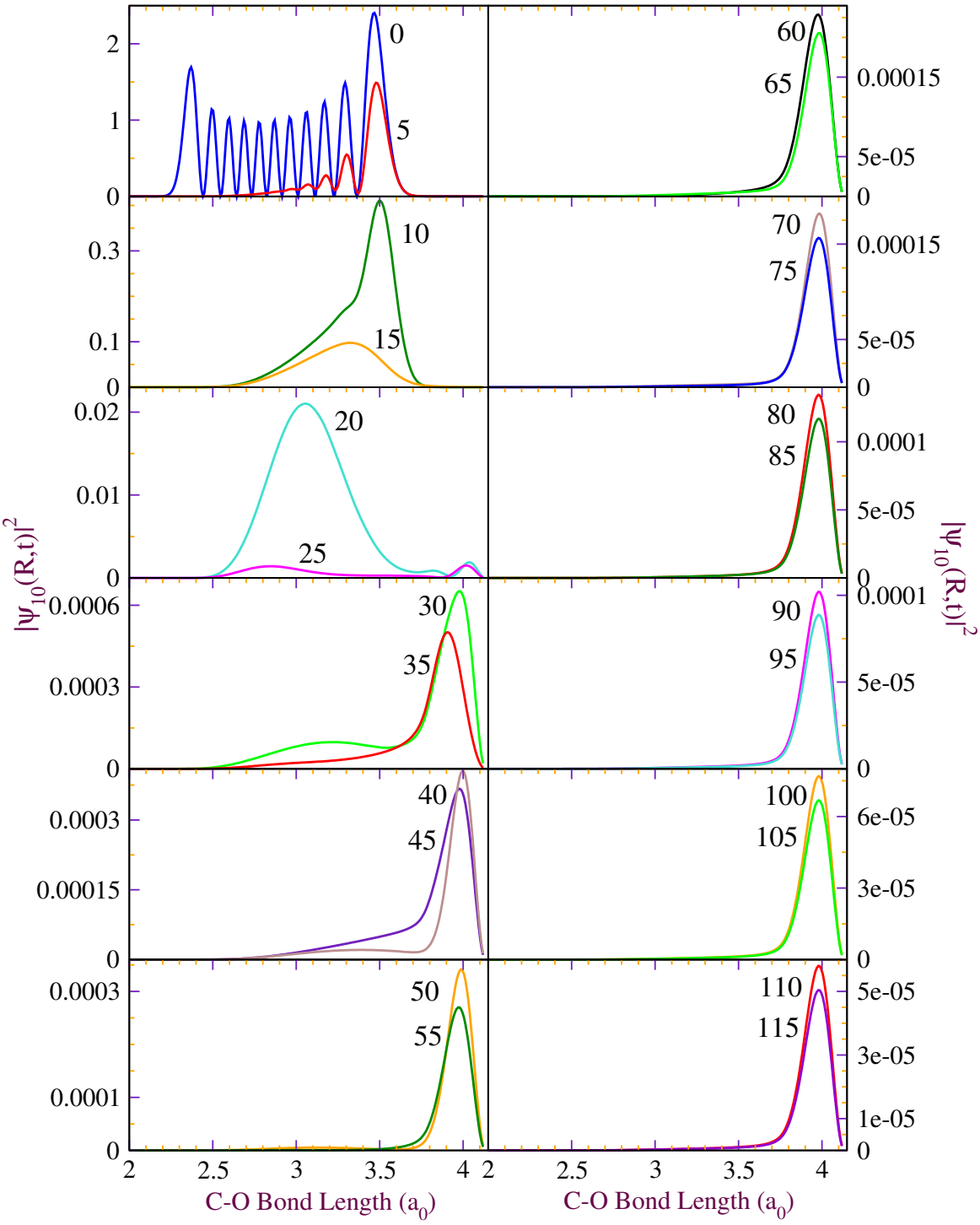

Fig. 5.6 Same as Fig. 5.3 except the target initial wave function is the tenth excited vibrational state [ϕ_{10}(R)].

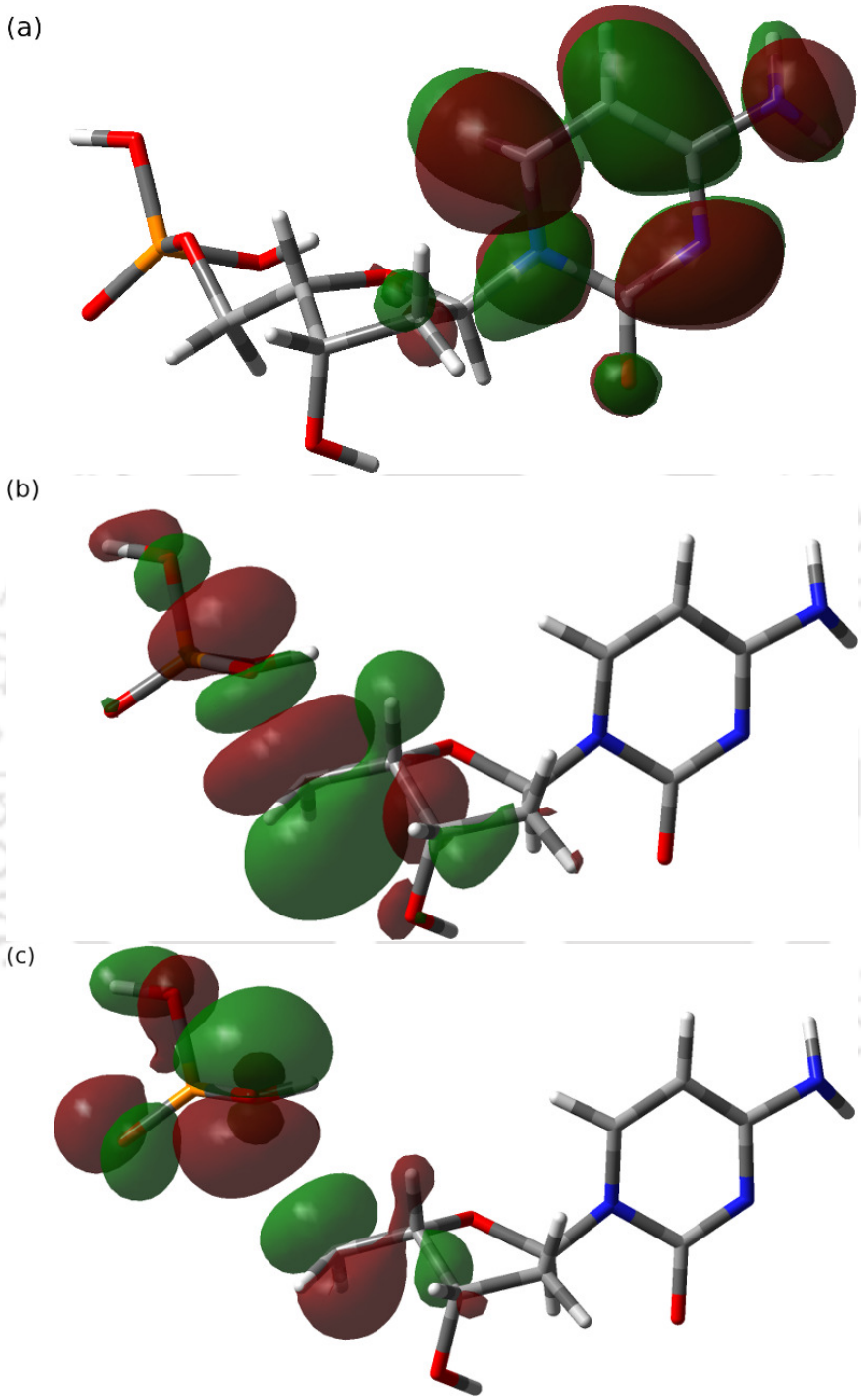

Fig. 5.7 Singly occupied molecular orbital (SOMO)s generated at the MP2/6-31+G(d) accuracy level for anionic 5′-dCMPH moiety for the 5′ C–O bond lengths of (a) 2.75 a_0 (1.45 Å), (b) 3.69 a_0 (1.95 Å), and (c) 5.67 a_0 (3.00 Å).

quantum dynamical predictions are reasonable with the available experimental observations [10, 20].

Apart from the quantitative approach discussed above, qualitative analysis from a series of generated molecular orbitals at MP2/6-31+G(d) accuracy level along the 5′ C–O potential energy curve shows the electron transfer pathway from the pyrimidine base to the back-bone phosphate P=O π^* orbital. The lowest unoccupied molecular orbital (LUMO) of the neutral 5′-dCMPH molecule at equilibrium C–O bond length [R_{C-O} = 2.75 a_0 (1.45 Å)] represents the π^* character located on cytosine base. Electron attachment to this molecular orbital does not alter it's π^* character on the base indicating a direct LEE attachment site in this nucleotide [Fig. 5.7(a)]. Singly occupied molecular orbital (SOMO) at the barrier height, R_{C-O} = 3.69 a_0 (1.95 Å) [Fig. 5.7(b)] shows the transfer of LEE to the C–O σ^* orbital. Once the LEE enters in to this repulsive state, it results in the rupture of the sugar-phosphate 5′ C–O bond producing highly stable phosphate anion and the pyrimidine nucleoside radical. This is evident from the SOMO generated at R_{C-O} = 5.67 a_0 (3.00 Å) as shown in Fig. 5.7(c) [Please see Fig. B6 for the similar trend in SOMOs generated at HF/6-31+G(d) accuracy level]. Thus, we state that the excess charge transfer originates from the base π^* orbital to the phosphate P=O π^* orbital through the valence 5′ C–O σ^* orbital. The large electron affinity ($\sim$ 5 eV) of the phosphate group [21] may facilitate the charge transfer process within a short period of time [22].

Both the qualitative and quantitative analysis for LEE induced SSB in 5′-dCMPH molecule assures the role of *shape resonance* state present at the cytosine nucleobase.

5.4 Concluding Remarks

We have provided the role of shape resonance state during LEE induced single strand breaks (SSBs) in a modeled DNA fragment 2′-deoxycytidine-5′-monophosphate (5′-dCMPH) in this investigation. The major outcome of our combined electronic structure and local complex potential based time dependent wave packet calculations are:

(a) LEE ($\sim$ 1 eV) can attach to the pyrimidine nucleobase cytosine leading to the formation

of π^* shape resonance state.

(b) SSB can occur either from the ground vibrational levels (energy below 1.5 eV) of the metastable state or from the higher energy vibrational levels (above 1.5 eV) via quantum mechanical tunneling of the 5′ C–O bond.

(c) The metastable species possess a life-time of $\sim$ 18–20 fs at the ground vibrational level. The dissociation of 5′ C–O bond takes place even before it gets time to execute single vibration.

(d) We can compare the calculated cross section spectrum in a reasonable manner with those of the available experimental [10, 20] observations for the first time.

The main features of the present investigation suggest the low energy electron attachment and subsequent decay of the metastable state occurs within a femtosecond time scale. In this ultrafast electron induced phenomenon, *shape resonance* state possess a major role. However, as suggested by Kopyra et al.,this is only a part (15 %) of the total SSB formation within this molecule [10]. The other major pathway (60 %) leading to 5′ C–O bond fragmentation is the initial localization of LEE at the phosphate center of the nucleotide [10]. The likely mechanism of charge transfer for this pathway has been investigated on a modeled DNA fragment called sugar-phosphate-sugar (SPS) molecule and is discussed in the next chapter. Finally, we hope our findings offer a threshold for further investigations in other nucleotide units or DNA fragments for LEE induced damage and the LCP-TDWP approach can help to bring about the characteristics features of the electron scattering off DNA and DNA fragments.

References

[1] I. Baccarelli, I. Bald, F. A. Gianturco, E. Illenberger, and J. Kopyra, Phys. Rep. **508**, 1 (2011) and references therein.

[2] K. Aflatooni, G. A. Gallup, and P. D. Burrow, J. Phys. Chem. A **102**, 6205 (1998).

[3] S. Ptasinska, S. Denifl, P. Scheier, and T. D. Mark, J. Chem. Phys. **120**, 8505 (2004).

[4] X. Li, M. D. Sevilla, and L. Sanche, J. Am. Chem. Soc. **125**, 13668 (2003).

[5] A. M. Scheer, K. Aflatooni, G. A. Gallup, and P. D. Burrow, Phys. Rev. Lett. **92**, 068102 (2004).

[6] L. Sanche, Eur. Phys. J. D **35**, 367 (2005).

[7] L. Sanche, Chem. Phys. Lett. **474**, 1 (2009).

[8] S. M. Pimblott and J. A. LaVerne, Radiat Phys Chem **76**, 1244 (2007).

[9] E. Alizadeh and L. Sanche, Chem. Rev. **112**, 5578 (2012) and references therein.

[10] J. Kopyra, Phys. Chem. Chem. Phys. **14**, 8287 (2012).

[11] X. Bao, J. Wang, J. Gu, and J. Leszczynski, Proc. Natl. Acad. Sci. U.S.A. **103**, 5658 (2006).

[12] M. J. Frisch, G. W. Trucks, H. B. Schlegel, et al., *GAUSSIAN 09*, Revision D.01, (Gaussian,Inc. Wallingford, CT, 2013).

[13] L. Dubé and A. Herzenberg, Phys. Rev. A **20**, 194 (1979).

[14] J. N. Bardsley and J. M. Wadehra, Phys. Rev. A **20**, 1398 (1979).

[15] C. C. Marston and G. G. Balint-Kurti, J. Chem. Phys. **91**, 3571 (1989).

[16] C. Leforestier, R. H. Bisseling, C. Cerjan, M. D. Feit, R. Friesner, A. Guldberg, A. Hammerich, G. Jolicard, W. Karrlein, H.-D. Meyer, N. Lipkin, O. Roncero, and R. Kosloff, J. Comput. Phys. **94**, 59 (1991).

[17] D. Kosloff and R. Kosloff, J. Comput. Phys. **52**, 35 (1983).

[18] L. D. Landau and E. M. Lifshitz, *Quantum Mechanics, 3rd ed.* (Pergamon Press, Oxford, U.K., 1977).

[19] R. Marom, C. Levi, T. Weiss, S. Rosenwaks, Y. Zeiri, R. Kosloff, and I. Bar, J. Phys. Chem. A **114**, 9623 (2010).

[20] F. Martin, P. D. Burrow, Z. Cai, P. Cloutier, D. Hunting, and L. Sanche, Phys. Rev. Lett. **93**, 068101 (2004).

[21] J. Simons, Acc. Chem. Res. **39**, 772 (2006) and references therein.

[22] J. Gu, J. Wang, and J. Lesczynski, J. Am. Chem. Soc. **128**, 9322 (2006).

Chapter 6

Electron attachment to sugar-phosphate-sugar fragment

6.1 Introduction

The effect of low energy electron (LEE) attachment to the modeled cytidine nucleotides [1–4] and the likely involved mechanism for the DNA damage, so far, have been discussed in the previous chapters. It is not so surprising that the nucleobase cytosine can attract LEEs at energies below 1 eV since it possess three π^* shape resonance states in which the lowest has an energy 0.32 eV [5]. Rather, the electron transfer rate [6] and the mechanistic pathway involved during the damage process is quite exciting. Our quantum mechanical treatment indicates the plausible route toward the sugar-phosphate C–O bond fragmentation as the LEE transfer from the π^* orbital of the base to the σ^* orbital of the C–O bond which is going to be dissociated [1–4]. However, as suggested by Kopyra and co workers [7], there are other electron attachment sites present within the DNA components such as the phosphate or the sugar moiety other than the nucleobase. Single strand breaks (SSBs) arise due to the initial localization the electron at these sites are at higher percentage level (60 % at phosphate site, and 25 % at the sugar site). Therefore, to model these alternative pathways, we have considered sugar-phosphate-sugar (SPS) fragment model [8] in this chapter. Our purpose is to identify the possible electron attachment site within this molecule and to determine the

possible mechanistic pathway leading to SSBs in the absence of cytosine base. Theoretical investigations of Li et al. [8] on this modeled fragment came up with the remarks that the LEE attachment (0 eV) may takes place at π^* orbital of the phosphate group and the electron transfer subsequently takes place to the 3′ or 5′ C–O σ^* orbitals followed by dissociation of the corresponding chemical bond. These calculations were questioned, however, by Simons and co-workers [9] and they computed the LEE attachment in SPS moiety at the Hartree Fock level. According to them, an electron having an energy above 2 eV can attach to the P=O π^* orbital. Later, Burrow et al. questioned the existence of π^* orbital (above 2 eV) on the phosphate group [10]. These controversial remarks are not resolved even qualitatively till date. On account of this, here we have investigated the quantitative treatment of electron driven SSB using our LCP-TDWP approach.

Modeling of the SPS molecule and the possible fragmentation schemes are discussed in the method section. The major findings of our quantum dynamical calculations are explained in the Results and Discussions section. Salient features of this investigation concludes the chapter.

6.2 Computational Method

In the present investigation, we have studied the LEE induced SSBs in modeled SPS molecule [8] as shown in Fig. 6.1. The fragment has excised from DNA double helix and the generated radical centers were neutralized by adding hydrogens to it. The negative center of the phosphate group is neutralized by adding a proton. If these centers were not neutralized, they may obscure the electron attachment leading to the incorrect electronic state of the system. An electron is attached to the lowest unoccupied molecular orbital (LUMO) of the neutral system to obtain the anionic molecule. The scheme provided in Fig. 6.1 consists of two fragmentation channels. The LEE attachment may take place either at the sugar site or at the phosphate group [7] giving rise to the fragmentation of either sugar-phosphate 3′ C–O or 5′ C–O bonds. In both the cases, a sugar radical and highly stable phosphate centered anions are formed. Geometry optimizations were performed for both the neutral and anionic systems

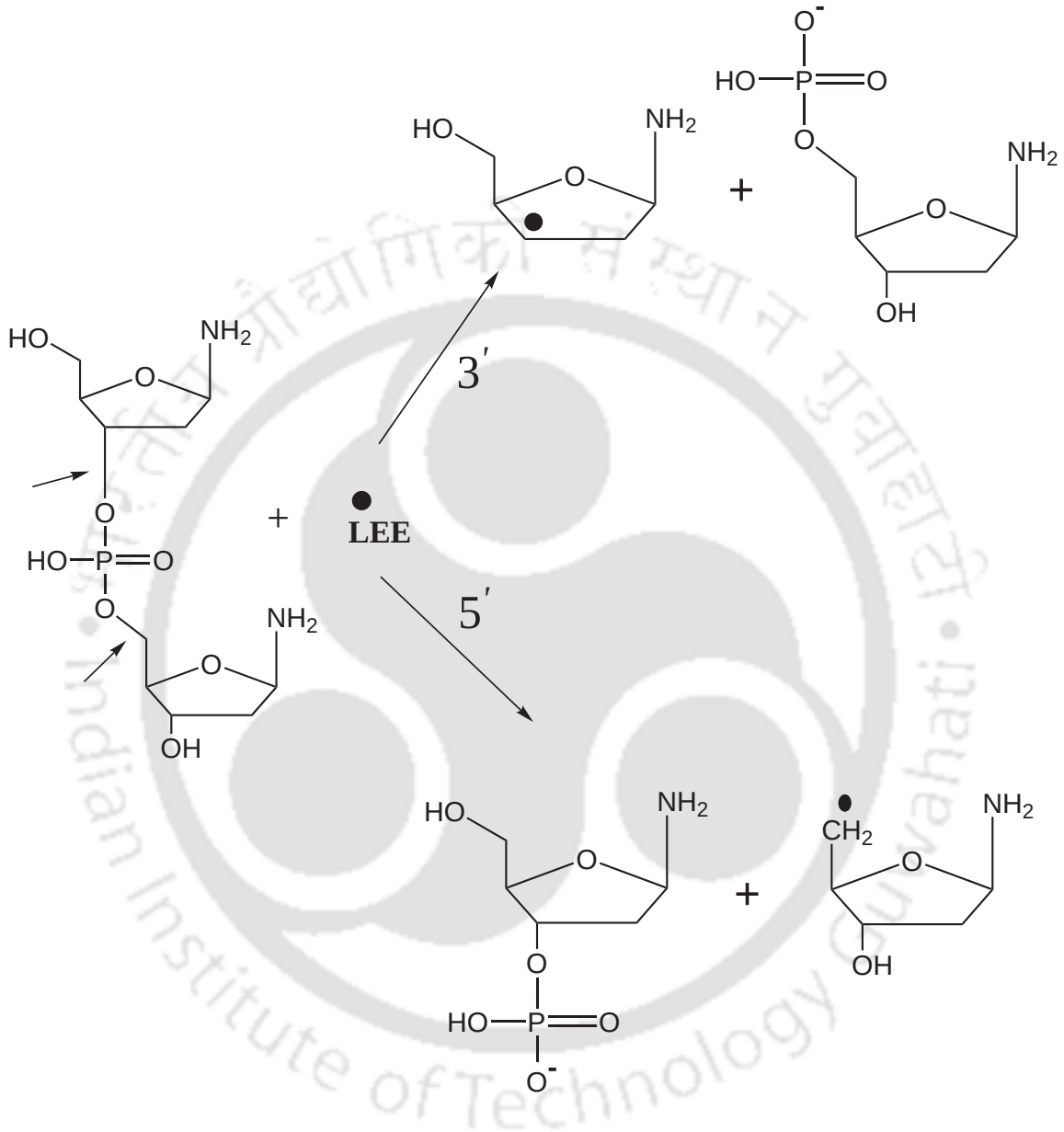

Fig. 6.1 Schematic representation of low energy electron (LEE) induced single strand break (SSB) in a modeled sugar-phosphate-sugar (SPS) fragment excised from DNA double helix. The radical centers were neutralized by adding hydrogens and the negative charge by a proton at the phosphate center. The 3′ C–O and 5′ C–O bonds undergoing dissociation are labeled with arrows. The fragmented products can be seen as the sugar radical and the stable phosphate centered anion in both the bond lesion processes.

at the second-order Møller-Plesset perturbation theory (MP2) with the 6-31+G(d) basis set available in Gaussian 09 package [11]. The optimized structures were further used for the quantum mechanical calculation of the adiabatic potential energy (PE) curves for the neutral [E_A(R)] and anionic [E_{A^-}(R)] systems (A = SPS molecule) using G09. More details of the local complex potential based quantum mechanical approach has already been discussed in chapter 2 and chapter 3 [1–3]. Furthermore, we have investigated 3′ C–O and 5′ C–O bond dissociation channels separately.

6.3 Results and Discussions

Potential energy curves generated at the MP2/6-31+G(d) accuracy level for the neutral [E_A(R)] and anionic [E_{A^-}(R)] systems are shown in Figs. 6.2(a) [for 3′ C–O bond] and 6.2(b) [for 5′ C–O bond] respectively. The width functions [calculated using Eq. (2.4)] associated with the metastable state formed during the LEE induced 3′ C–O and 5′ C–O bonds dissociation are shown in Figs. 6.2(c) and 6.2(d) successively. The ground state eigenfunctions calculated using FGH method [12] are shown in Figs. 6.2(e) and 6.2(f). Fig. 6.2(e) represents the wavefunction the neutral [ϕ_i(R)] and anionic [χ_i(R)] for MP2 potentials in Fig. 6.2(a). Similarly, Fig. 6.2(f) corresponds to the eigenvectors for neutral and anionic MP2 potentials provided in Fig. 6.2(b). The following characteristics have been noted for these two different fragmentation channels:

(1) At the equilibrium geometries, the neutral 3′ C–O bond is found to be more elongated than that of the corresponding anionic molecule. However, there is no notable differences for the 5′ C–O bond length in neutral and anionic optimized moieties.

(2) The vertical attachment energy (VAE) is the same for both the SSB channels. In addition, the potential energies at the equilibrium geometries of both the neutral and anionic SPS molecules is similar in 3′ C–O and 5′ C–O bonds dissociation. This is in accordance with the findings of Sanche and co-workers [8].

(3) The potential energy landscape changes considerably as we move from the equilibrium C–O bond distance to the larger C–O bond lengths. This is obviously reflected in the barrier

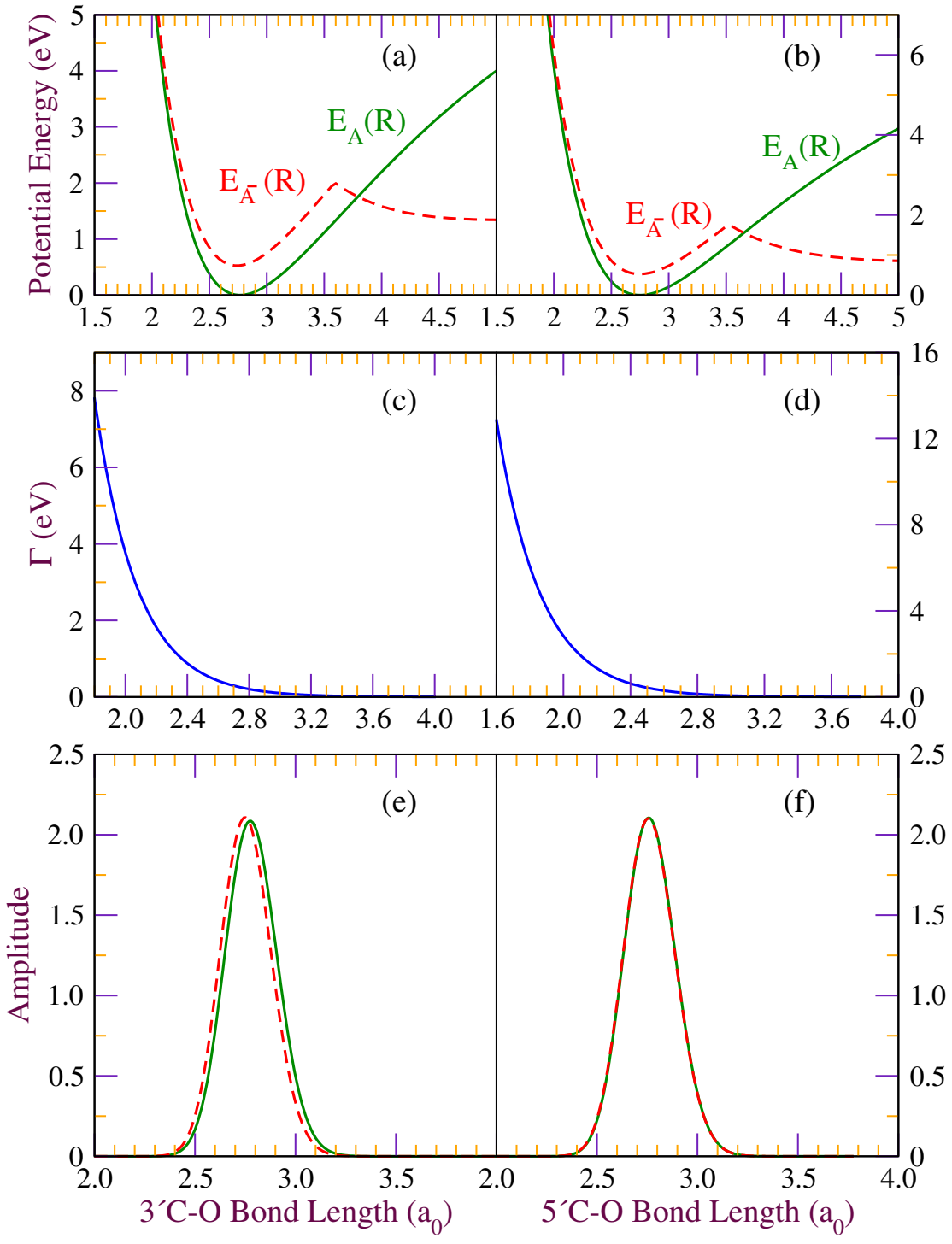

Fig. 6.2 Potential Energy curves generated for neutral (green line) and anionic (red line) moieties for the 3′ and 5′ C–O bonds dissociation are shown in (a) and (b) respectively. The width function associated with the metastable states in (a) and (b) are shown in Figs. (c) and (d) respectively. Figs. (e) and (f) correspond to the neutral and anionic ground state eigenfunctions of PE curves in (a) and (b).

Table 6.1 Comparison of various properties/parameters for SPS molecule.

Property/Parameter	3′ C–O bond	5′ C–O bond
[a]R_{C-O} (Å)	1.464 [b]	1.455 [b]
	1.450 [c]	1.454 [c]
VAE (eV)	0.53	0.53
R_x(Å)	2.00	1.92
δ_1	200	200
α	3.64	3.78
Barrier Height (eV)	1.46	1.22
[d]Barrier Width (Å)	0.38	0.35
$\sigma^{max}_{0\leftarrow 0}$(E) [eV]	0.60	0.60

[a] Equilibrium C–O bond length.
[b] Neutral SPS moiety.
[c] Anionic SPS moiety.
[d] Taken from the fitted curve of Eq. (3.3).

position of the anionic potential [E_{A^-}(R)]s, which is different for the two different C–O bonds fragmentation processes. In addition, the barrier height for the two anionic PE curves are different in which 5′ C–O PE curve is found to have lesser height (1.22 eV) than that for the 5′ C–O PE curve (1.46 eV).

(4) Interestingly, there is crossing (R_x) between the neutral and anionic PE curves for the two separate bond lesion channels and is found to be different in both the cases (please see Table 6.1 for details).

(5) The δ_1 value chosen for the calculation of the width function is the same for both the dissociation processes.

(6) The neutral ground state eigenfunction is slightly shifted forward compared to the anionic wavefunction in 3′ C–O bond dissociation. However, both the neutral and anionic ground eigenstate wavefunctions are overlapped in the case of 5′ C–O fragmentation channel.

(7) There are a total of 14 bound vibrational energy levels found for the MP2 anionic 3′ C–O PE curve. However, the anionic potential for 5′ C–O mode contains only 11 bound vibrational energy states.

(8) Furthermore, the E_{A^-}(R) of both 3′ C–O and 5′ C–O modes contains a hyperbolic cosine

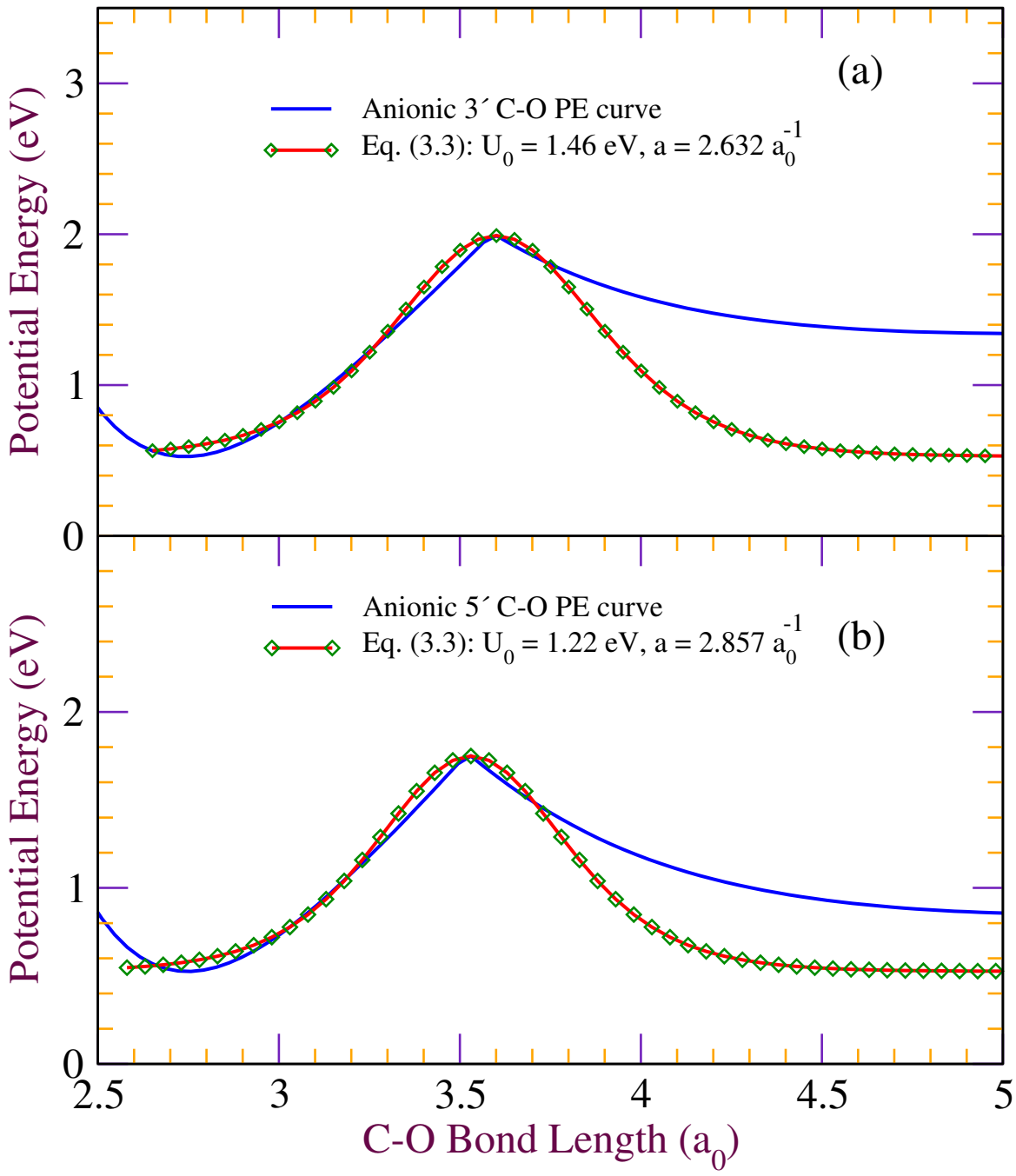

Fig. 6.3 (a) The modeled hyperbolic cosine barrier is compared with the MP2 PE curve [E_{A^-}(R)] for 3′ C–O dissociation. Curves in (b) represent the best fitted analytical potential modeled using Eq. (3.3) compared with the anionic MP2 potential [E_{A^-}(R)] for 5′ C–O bond dissociation.

barrier around 3.5 a_0.

As discussed in previous chapters, since it is difficult to calculate the width ("a") of the barrier (full width at half maximum) which is used for the computation of transmission coefficient "T" [Eq. (4.1)], we have analytically modeled a hyperbolic cosine barrier using Eq. (3.3). The modeled hyperbolic curve are compared with the anionic MP2 potentials of Figs. 6.2(a) and 6.2(b) and respectively shown in Figs. 6.3(a) and 6.3(b). This modeling enable us to identify the width ("a") of the barrier in both the C–O bonds rupture processes. Table 6.1 listed above contains the necessary input parameters used for our quantum dynamical calculations.

6.3.1 Tunneling

As discussed in previous chapters, we have calculated the tunneling transmission coefficient (T) [13] using Eq. (4.1) for both the LEE induced SSB channels. Table 6.2 listed shows the variation of C–O bond tunneling probabilities from each of the bound anionic vibrational energy levels of the two different MP2 PE curves. It can be seen from the Table 6.2

Table 6.2 Transmission coefficient (T) calculated using Eq. (4.1)

Vibrational State (χ_i)	Vibrational Energy χ_i(E) [eV]		Transmission Coefficient (T)	
	3′ C–O	5′ C–O	3′ C–O	5′ C–O
0	0.59	0.59	1.58×10^{-14}	1.97×10^{-26}
1	0.72	0.72	6.24×10^{-12}	4.59×10^{-22}
2	0.86	0.86	1.33×10^{-09}	6.19×10^{-19}
3	0.99	0.98	1.80×10^{-07}	5.46×10^{-16}
4	1.12	1.11	1.66×10^{-05}	3.30×10^{-14}
5	1.24	1.23	1.13×10^{-03}	0.61
6	1.37	1.36	5.59×10^{-02}	0.98
7	1.49	1.48	0.71	0.99
8	1.61	1.59	0.98	0.99
9	1.73	1.67	0.99	0.99
10	1.79	1.72	0.99	0.99
11	1.87		0.99	
12	1.94		0.99	
13	1.98		0.99	

that tunneling is completely hindered from the lower energy vibrational levels. However, significant contribution of C–O tunneling to SSB is seen only from the higher energy vibrational states (typically above 1.1 eV). In addition, the characteristic "S-type tunneling" [14] is also seen from the tabulated transmission coefficient values.

Moreover, we can also notice from Table 6.2 that χ_7 state of 3′ C–O and χ_5 state of 5′ C–O MP2 PE curves have non-negligible contribution toward SSB. Therefore we have further computed the fragmentation profile for LEE induced SSB from these excited vibrational levels in addition to the ground vibrational level of each of the anionic PE curves.

6.3.2 Molecular orbital analysis

Singly occupied molecular orbitals (SOMOs) generated at various 3′ and 5′ C–O bonds distances showing the electron transfer leading to the rupture of the sugar-phosphate backbone C–O bond are provided in Fig. 6.4. It should be noted that the SOMO generated at the anionic equilibrium geometry of SPS molecule for both the C–O bond dissociation process are the same and is given in Fig. 6.4(a). We can infer from the SOMO at the anionic equilibrium C–O bond distance [around 2.75 a_0 (1.45 Å)] that the electron attaches at the phosphate center, although the molecular orbital exhibits diffuse character. It is difficult to predict the nature of the orbital [π^* or σ^*] at the equilibrium SPS geometry. Calculations of Simons and co-workers [9] came up with the fact that the direct attachment of LEE (2.5–3 eV) will take place at the phosphate P=O π^* orbital. However, according to Burrow et al. [10] such π^* orbital (above 2 eV) does not exist in phosphate group. Instead, there exists a σ^* orbital of energy below 1 eV. The same is argued by Kumar and co-workers through their time-dependent density functional theory (TD-DFT) calculations [15]. On the other hand, experimental findings suggested that the direct electron attachment at the phosphate group will take place near 0 eV [7]. In such cases, vibrational Feshbach resonance (VFR) may have a major role during the LEE transfer which has to be investigated further using special theoretical techniques. Our present MP2/6-31+G(d) investigation suggest that the electron attachment may take place at the phosphate group. However, we cannot conclude the nature of the orbital shown in Fig. 6.4(a) since the orbital calculated is slightly diffused around the

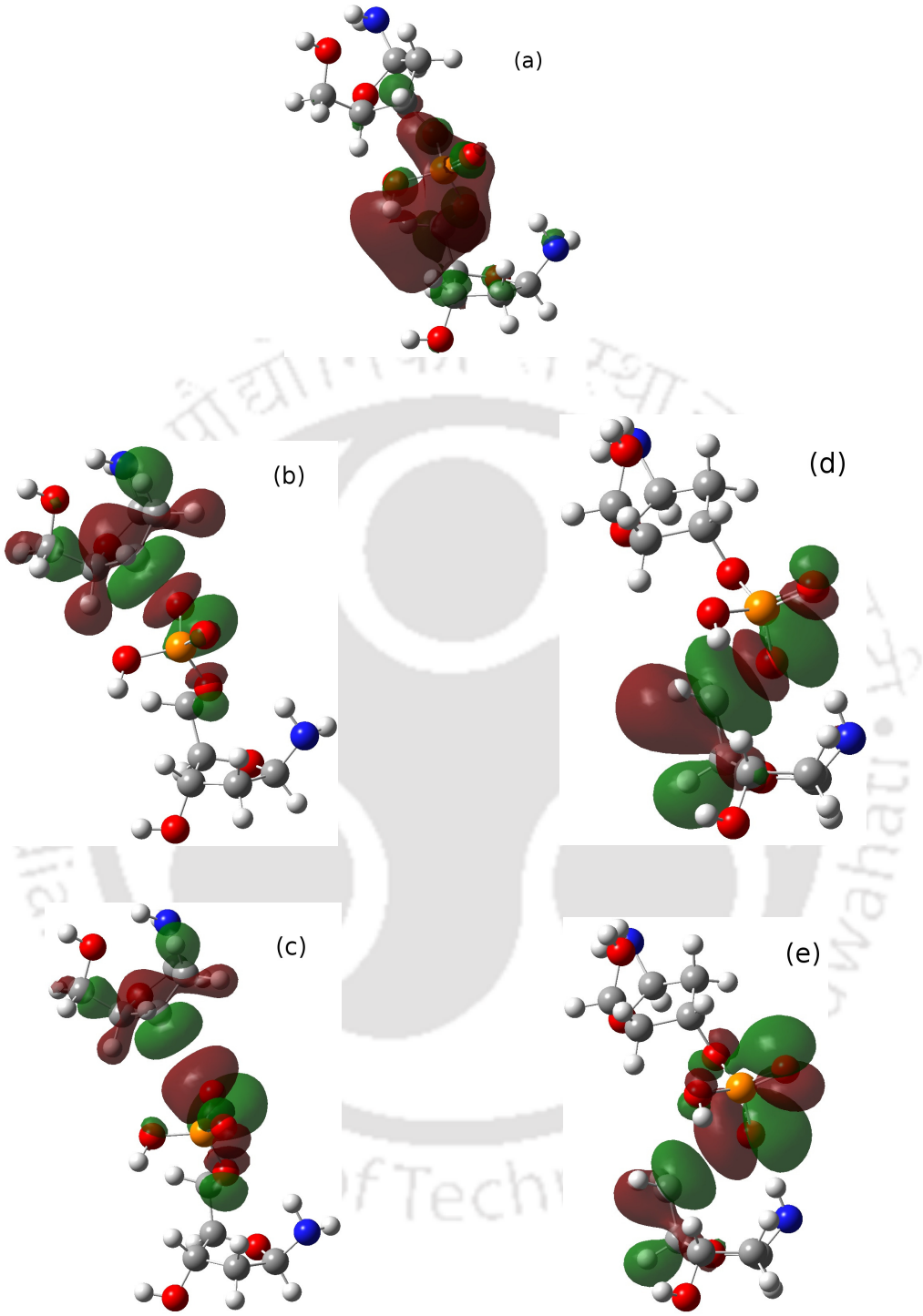

Fig. 6.4 Singly occupied molecular orbital (SOMO)s generated at various stages of 3′ and 5′ C–O bonds dissociation for the anionic SPS molecule. (a) Electron residing around phosphate group at equilibrium C–O bond length 2.75 a_0 (1.45 Å). (b) and (c) represent the location of the electron generated at 3.59 a_0 (1.90 Å) and 5.67 a_0 (3.00 Å) 3′ C–O bond lengths. The orbitals at the same 5′ C–O bond lengths are shown in (d) and (e) successively.

phosphate region. On the other hand, since the anionic PE curve near the equilibrium C–O bond distance shows a bound state characteristics for π^* orbital (and also the metastable behavior), we believe that the electron resides on the π^* orbital of the phosphate group rather than the σ^* orbital. Further, Figs. 6.4(b) shows the electron migration from the equilibrium P=O π^* orbital to the σ^* orbital of the 3′ C–O bond [at the barrier height 3.59 a_0 (1.90 Å)] during the dissociation. The 3′ C–O bond fragmented products are seen in Fig. 6.3(c) where the excess electron located on the phosphate group. The electron transfer during 5′ C–O bond dissociation is found to be in the similar way and is shown in Figs. 6.4(d) [barrier height] and 6.4(e) [after fragmentation]. The characteristics of the metastable state formed and the time-dependent behavior of the state calculated from our quantum dynamical calculations are discussed in details below.

6.3.3 Time-dependent analysis

In general, the quantum mechanical treatment of LEE induced 3′ C–O and 5′ C–O bonds dissociation (both for the ground and excited vibrational levels) is carried out through the wavepacket propagation algorithm as discussed in chapters 2 and 3. The time evolved states has been computed using Eq. (2.1) for both the ground and excited vibrational states. Fig. 6.5 shows a few snapshots of the time evolved states of ϕ_0(R) for 3′ C–O bond dissociation in SPS molecule. As found in our earlier investigations, the wavepacket has maximum amplitude before the propagation. However, the amplitude diminishes slowly as the propagation proceeds and probability reduces to zero within 40–45 fs. We can also see that the wavepacket moves slowly toward the right turning point of the PE curve. Similarly Fig. 6.6 represents the time evolved states of ground state eigen function [ϕ_0(R)] for LEE induced 5′ C–O dissociation in SPS moiety. The characteristics of the time evolved states follows the same pattern as with that of 3′ C–O bond dissociation. However, it should be noted here that the metastable state possess a life time of $\sim$ 55 fs for 5′ C–O bond dissociation which is higher than that for the 3′ C–O bond dissociation (40–45 fs) within the SPS fragment. In addition, we emphasize here that the lifetime of these two metastable states are longer than that for the TNI formed at the nucleobase center (18–20 fs) [3] in 3′-dCMPH and 5′-dCMPH

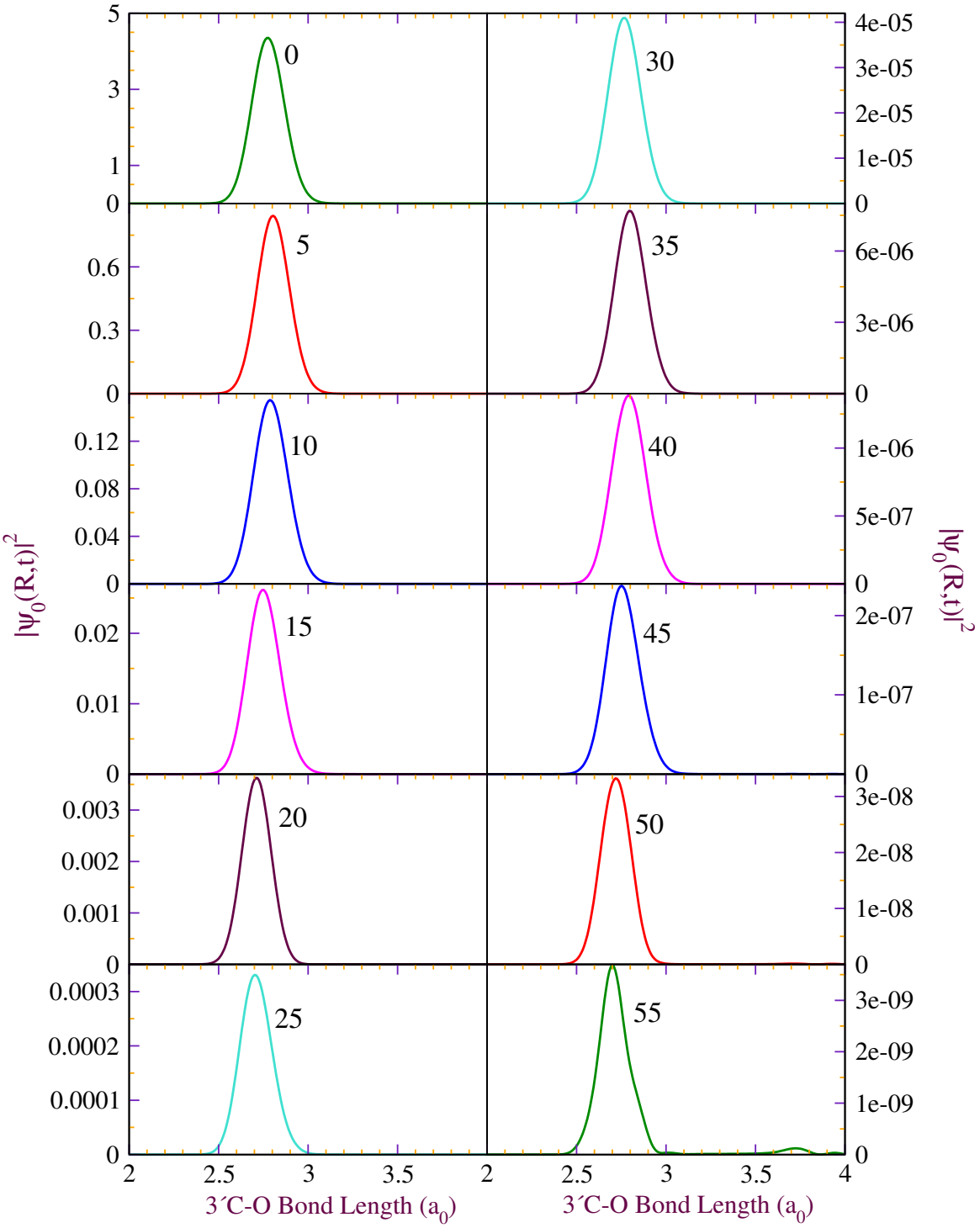

Fig. 6.5 Snapshots of the propagated wavepacket for the ground vibrational state [ϕ_0(R)] of 3′ C–O anionic potential from time t = 0 to 55 fs at 5fs interval.

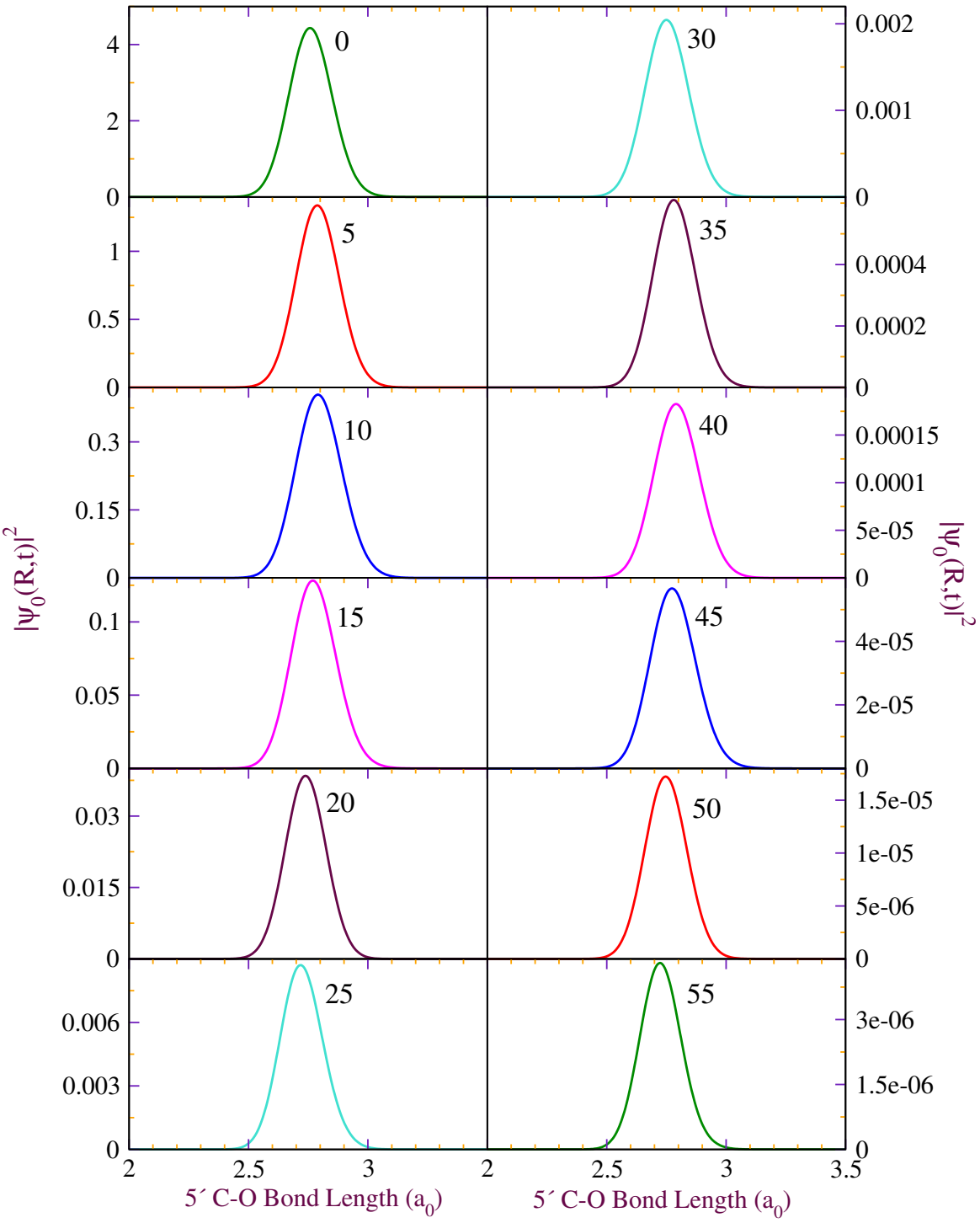

Fig. 6.6 Same as Fig. 6.5 except the target initial wave function is the ground vibrational state [ϕ_0(R)] of 5′ C–O bond dissociation.

molecules. Therefore, we can expect a higher LEE induced dissociation rate for the initial resonance state formed at the phosphate center. The same characteristics is alternatively suggested in Kopyra's work (i.e., 60% dissociation for initial electron localization at the phosphate group) [7].

In the same way, the time evolved states [$\psi_i(R,t)$] for excited state wave functions [where i=7 for 3′ C–O and i=5 for 5′ C–O dissociation] are given in Figs. 6.7 and 6.8 respectively. It can be seen from Fig. 6.7 that the initial wavepacket has maximum amplitude before the propagation and the number of nodes in the wavepacket reduces from six (at time t = 0 fs) to one nodes within 10 fs. Thereafter, the state evolved without any node. At about 30 fs the wavepacket started to bifurcate. We can identify the exponential decay of the time evolved metastable state in the Region 2 [$R_{C-O} \sim$ 3.2–4.2 a_0 ($R_{C-O} \sim$ 1.7–2.2 Å, tunneling region)] during 30–40 fs in these plots. Further, the metastable state from this excited region possesses a life-time of $\sim$ 60–70 fs which is much longer than that we found for the corresponding ground vibrational state ($\sim$ 40–45 fs). In passing, we have also calculated the time evolved states $\psi_i(R,t)$ for the fifth excited vibrational state of 5′ C–O PE curve. The characteristics of the propagated states seen in Fig. 6.8 are the same which we found in the Fig. 6.7 for the 3′ C–O bond dissociation. The metastable state has a lifetime of $\sim$ 55 fs. The longer lifetime in these excited states may be due to the fact that these eigen functions have larger spatial spread [20], which may translate into a longer life-time of the respective metastable anion.

Further, we have calculated the auto correlation function [$\langle\chi_i(R)|\psi_i(R,t)\rangle$] from the propagated wave packet. Fig. 6.9(a) depicts the computed auto correlation functions for the different fragmentation pathways. From the Fig. 6.9(a), in general, we can see that the overlap of the wavepacket with that of the anionic vibrational eigenfunction is maximum before the propagation start. However, the overlap gradually decreases as time proceeds. The overlap is negligible after a period of 35 fs (for i=0) for both the 3′ and 5′ C–O bond dissociations. For the excited vibrational levels (i=7 for 3′ C–O and i=5 for 5′ C–O) the overlap reduces to zero near t = 50 fs. Finally, the fragmentation spectra have been calculated via the fourier transformation of the autocorrelation function which is then compared with the available experimental spectrum [7] for the LEE induced SSB from the phosphate group.

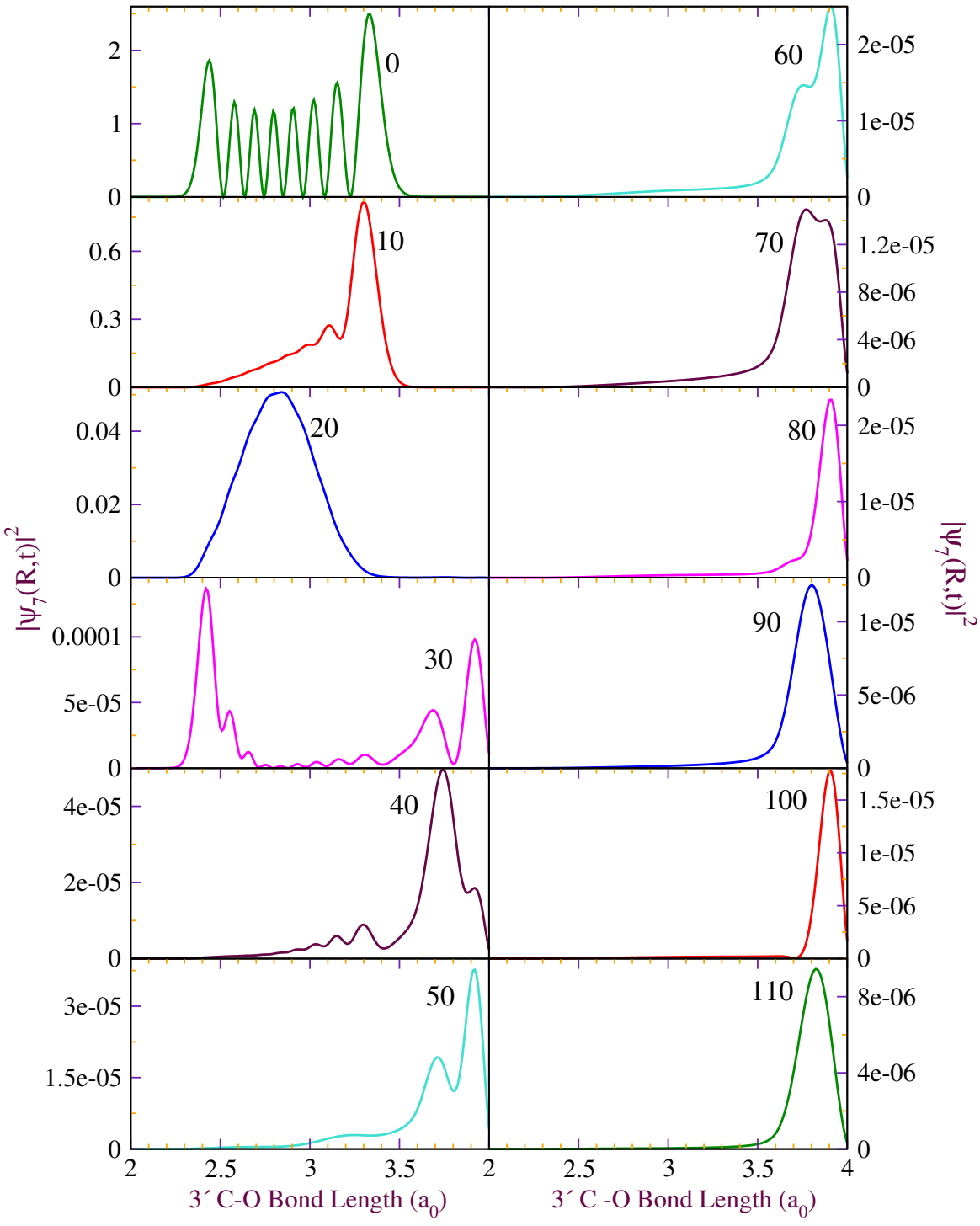

Fig. 6.7 The time evolution plots of seventh excited vibrational state [ϕ_7(R)] for 3′ C–O bond breaks showing at regular intervals of 10 fs.

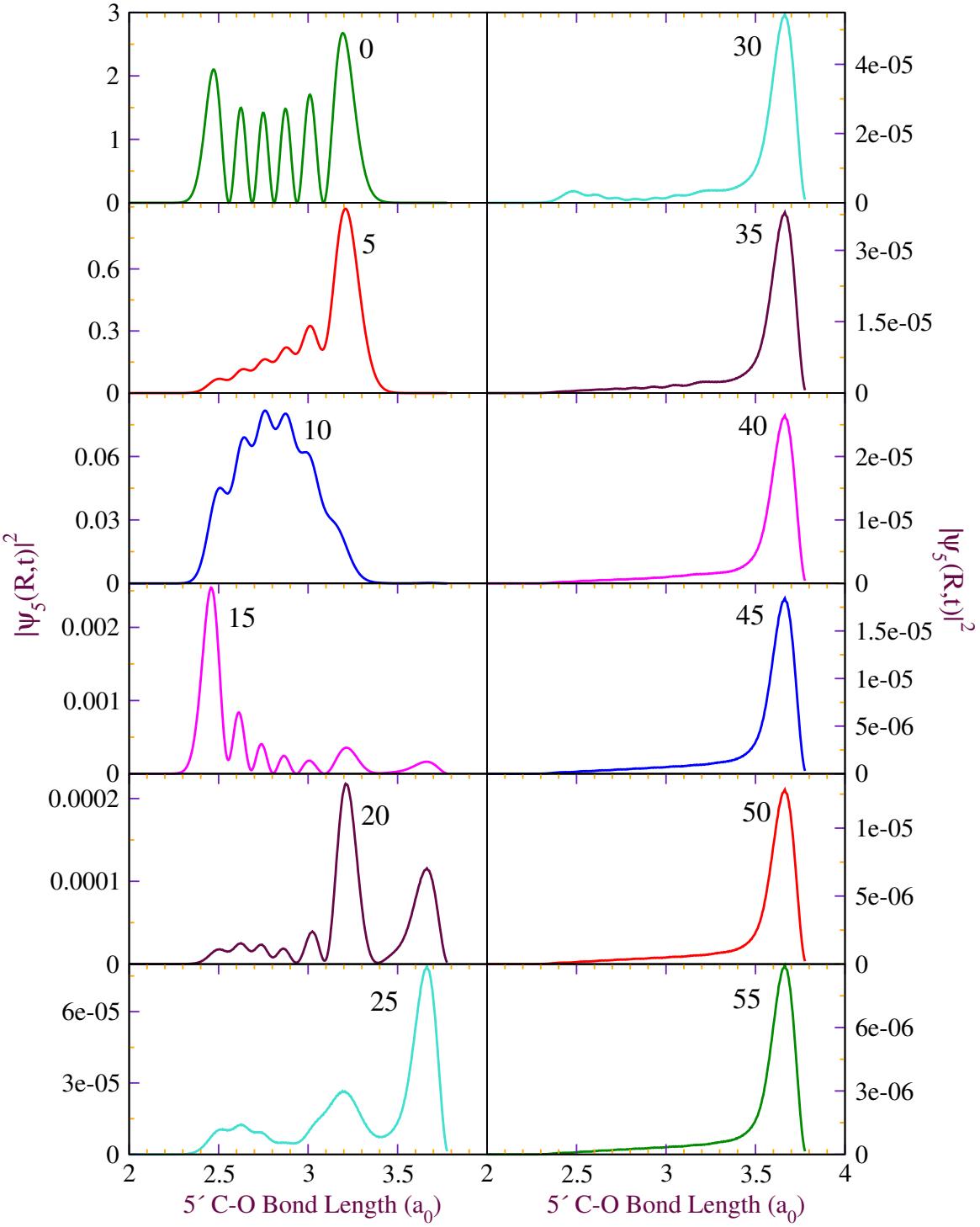

Fig. 6.8 Same as in Fig. 6.7 except the target initial wave function is the fifth excited vibrational state [ϕ_5(R)] for 5′ C–O bond dissociation.

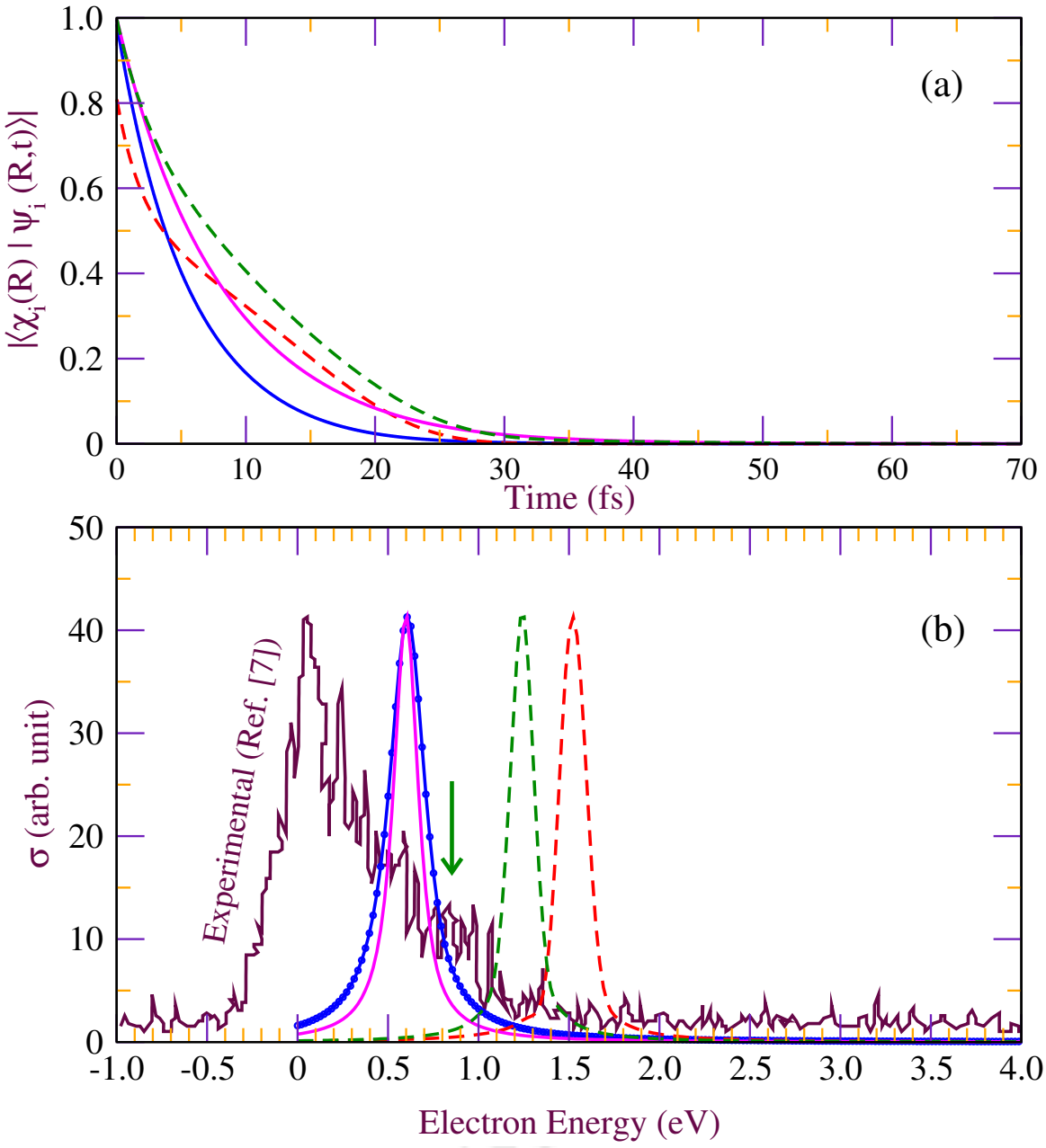

Fig. 6.9 (a) Auto correlation functions $|\langle\chi_i(R)|\psi_i(R,t)\rangle|$ from MP2/6-31+G(d) calculation for 3′ [(i=0, blue solid line) and (i=7, red dashed line)] and 5′ [(i=0, magenta solid line) and (i=5, green dashed line)] C–O bond breaks in SPS molecule, (b) comparison of corresponding cross section profile [$\sigma_{i\leftarrow i}$(E)]s for SPS molecule [(i=0, blue solid line) and (i=7, red dashed line) for MP2 and (i=0, magenta solid line) and (i=5, green dashed line)] with the available experimental spectrum [7] (maroon solid line).

The fragmentation profiles calculated for the ground and excited state vibrational levels for both 3′ C–O and 5′ C–O dissociation channels are shown in Fig. 6.9(b). The ground state cross-section exhibits a maximum at the 0.52 eV for both 3′ C–O and 5′ C–O dissociation modes whereas the peak is shifted to higher energies [1.5 eV for i=7 (3′ C–O) and 1.24 eV for i=5 (5′ C–O)] for the excited state dissociation pathways. The structure less feature of all these fragmentation spectra once again confirms the *impulse model* [16] classification of LEE induced resonance scattering in SPS moiety. Our quantum dynamical findings are in line with the available experimental observations [7, 17]. Compared to 3′ C–O and 5′ C–O dissociation channels, 5′ C–O bond rupture may prefer LEEs initially attached to phosphate group, whereas 3′ C–O bond lesion may prefer LEEs localized at cytosine center. These findings encourage us to suggest that the "charge induced dissociation" [19] is the prominent way for the ultrafast electron transfer processes taking place at the physical stage of radiation induced DNA damage.

6.4 Concluding Remarks

The present study focuses on the low energy electron attachment to a modeled sugar-phosphate-sugar molecule without the presence of a nucleobase site to investigate the likely involvement of resonance states in DNA subunits like sugar and phosphate groups during single strand breaks. We have treated the two competing 3′ C–O and 5′ C–O bonds dissociation channels separately. We have employed the local complex potential based time-dependent approach (LCP-TDWP) to deduce the mechanistic pathway during the bond lesion. We then compared our calculated results with the available experimental and theoretical findings. The major remarks of our present investigation are:

(a) We found a shape resonance state present at the phosphate group which can attract LEEs and induce single strand breaks (either 3′ C–O or 5′ C–O bond rupture).

(b) Since the activation energy barrier for the 5′ C–O bond dissociation is lesser than that for the 3′ C–O bond rupture, dissociation at the 5′ C–O site will be preferred over 3′ C–O fragmentation.

(c) The metastable states formed at the phosphate center possess a longer lifetime ($\sim$ 40–45 fs) compared to the TNI formed at the cytosine nucleobase center ($\sim$ 18–20 fs).

(d) The quantum tunneling of the C–O bond leading to SSBs is seen only at the higher energy regimes, i.e., above 1.5 eV.

(e) The resonant electron scattering in SPS molecule is classified as the "impulse model" [16] resonance phenomenon.

It is quite encouraging for us to implement the LCP-TDWP technique in chemically modified compounds to investigate the ultrafast electron induced dissociation process. Though the technique has some limitations, we have successfully computed the characteristics of TNI during the bond breaking phenomenon.

References

[1] Renjith B., S. Bhowmick, M. K. Mishra, and M. Sarma, J. Phys. Chem. A **115**, 13753 (2011).

[2] S. Bhowmick, Renjith B., M. K. Mishra, and M. Sarma, J. Chem. Phys **137**, 064310 (2012).

[3] R. Bhaskaran and M. Sarma, J. Chem. Phys **139**, 045103 (2013).

[4] R. Bhaskaran and M. Sarma, J. Chem. Phys **141**, 104309 (2014).

[5] K. Aflatooni, G. A. Gallup, and P. D. Burrow, J. Phys. Chem. A **102**, 6205 (1998).

[6] R. Barrios, P. Skurski, and J. Simons, J. Phys. Chem. B **106**, 7991 (2002).

[7] J. Kopyra, Phys. Chem. Chem. Phys. **14**, 8287 (2012).

[8] X. Li, M. D. Sevilla, and L. Sanche, J. Am. Chem. Soc. **125**, 13668 (2003).

[9] J. Berdys, I. Anusiewicz, P. Skurski, and J. Simons, J. Am. Chem. Soc **126**, 6441 (2004).

[10] P. D. Burrow, G. A. Gallup, and A. Modelli, J. Phys. Chem. A **112**, 4106 (2008).

[11] M. J. Frisch, G. W. Trucks, H. B. Schlegel, et al., *GAUSSIAN 09*, Revision D.01, (Gaussian,Inc. Wallingford, CT, 2013).

[12] C. C. Marston and G. G. Balint-Kurti, J. Chem. Phys. **91**, 3571 (1989).

[13] L. D. Landau and E. M. Lifshitz, *Quantum Mechanics, 3rd ed.* (Pergamon Press, Oxford, U.K., 1977).

[14] R. Marom, C. Levi, T. Weiss, S. Rosenwaks, Y. Zeiri, R. Kosloff, and I. Bar, J. Phys. Chem. A **114**, 9623 (2010).

[15] A. Kumar and M. Sevilla, Chem. Phys. Chem. **10**, 1426 (2009).

[16] J. N. Bardsley and J. M. Wadehra, Phys. Rev. A **20**, 1398 (1979).

[17] F. Martin, P. D. Burrow, Z. Cai, P. Cloutier, D. Hunting, and L. Sanche, Phys. Rev. Lett. **93**, 068101 (2004).

[18] J. Simons, Acc. Chem. Res. **39**, 772 (2006) and references therein.

[19] J. Gu, J. Wang, and J. Lesczynski, J. Am. Chem. Soc. **128**, 9322 (2006).

[20] M. Sarma, S. Adhikari, and M. K. Mishra, J. Chem. Phys. **126**, 044309 (2007).

Chapter 7

Outcome of the present work and future directions

7.1 What we have Calculated

It has been known for long time that interaction of ionizing radiations (IR) with living cells produce large number of low-energy electrons (LEEs) within the cell. LEEs (0–20 eV range) can effectively attach to biomolecules resulting in the formation of very short lived species. These transient negative ion states (TNI) or the so called "resonance" can relax in either of the two ways; either by ejecting the excess electron leading to the undissociated species or by fast uni-molecular decomposition leading toward specific fragments. DNA subunits (nucleobases, sugar, and phosphate group) are found to be attracting these LEEs and impart damage such as single strand breaks (SSBs), double strand breaks (DSBs), nucleobase release, dimer formation and so forth. Surprisingly, the mechanism by which these LEEs induce DNA damages are not fully understood till date. We have initiated our investigation with the objective to implement time dependent wavepacket method for studying the electron induced uni-molecular dissociation in selected DNA fragments and deduce the likely mechanism involved during the LEE induced fragmentation.

We have studied theoretically, for the first time, the comprehensive route to SSB in the following DNA fragments, viz.,

- 2′–deoxycytidine–3′–monophosphate (3′–dCMPH),
- 2′–deoxycytidine–5′–monophosphate (5′–dCMPH) and
- sugar–phosphate–sugar (SPS)

induced by LEE (0–3 eV) scattering using local complex potential based time dependent wave packet (LCP-TDWP) approach. The results obtained from our calculations in the gas phase provide good agreement with experimental observations. We found that

- the LEE can attach to either cytosine nucleobase or at the phosphate group and induce SSB around 0.5–1.0 eV.
- there is significant quantum tunneling of the C–O bond above 1.0 eV.
- the electron transfer takes place from the low lying π^* orbital of cytosine to the P=O π^* orbital of the phosphate group during the strand breaks.
- effective atomic overlap between C_6 center of the base and the C_3' center of the sugar facilitates the "charge induced dissociation" within 18 – 20 fs.
- the lifetime of the metastable species is larger if the LEE attaches to the phosphate group.

In addition, we have also modeled the LEE induced cytosine base release from 3′–dCMPH molecule and found that it is less likely that an electron can favor base release from this fragment. There are a wide range of applications one can find for these electron driven processes in gas phase, at surfaces and interfaces, and in condensed matter. However, the present investigation within certain limitations may be found suitable in the context of chemotherapy for modeling suitable radiosensitizers and suggest the possible mechanism behind the enhancement of DNA damage.

7.2 Future Scope

As we have discussed in previous chapters, we have not included the multidimensional quantum effect during the LEE induced damage to DNA subunits. Therefore, our immediate goal is to include the multidimensional effect and non-adiabatic effect so that we may get a more detailed insight into the dissociation dynamics. It is also very essential to construct a potential energy surface via relaxing other geometrical degrees of freedom. By doing so, we may get a better barrier (avoided crossing) and hence, the number of vibrational states involved during the fragmentation process. Further, inclusion of time dependent approach outside the interaction region is very much essential. In conjunction with autoionization process, we may get a more detailed picture regarding the electron induced dissociation. To mimic the realistic system, one can also consider solvation and inclusion of alkali metal ions while modeling. It will obviously reflect in the actual dissociation dynamics and can deduce the mechanistic pathway leading to damage in a suitable manner. We can also consider the effect of DNA π stacking and hydrogen bonding while modeling. However, treating the quantum aspects will require high computational resources. Modifying the DNA subunits towards LEE attachment and investigate the radiosensitizing capacity is another very interesting field. Investigations along these lines will further help us to understand the effect of electron donating and electron withdrawing groups at the DNA subunits.

The above mentioned perspectives are only few which upon successful investigation will lead us to understand the action of LEE in DNA fragments. With more computing facilities, we can crack those bottlenecks at the earliest. As the famous Physicist Prof. Einstein said, "The whole of science is nothing more than a refinement of everyday thinking".

Appendix A

Supporting information for Chapter 4

I. The optimized structures of neutral and anionic 3′-dCMPH moiety at the (a) HF, and (b) MP2 methods with 6-31+G(d) basis set.

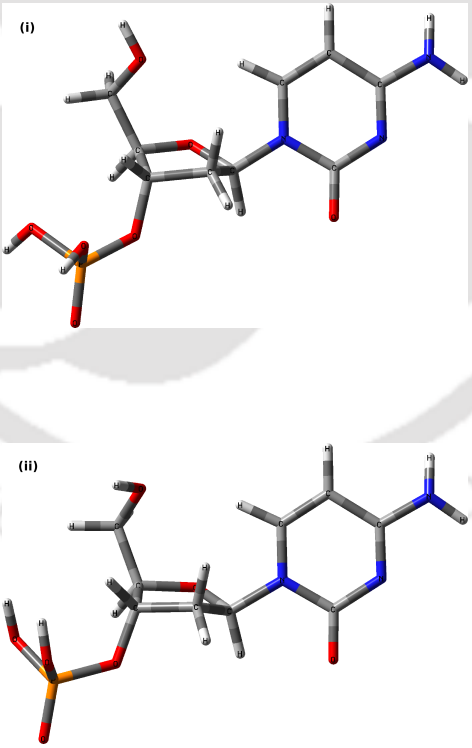

Fig. A1 The optimized structures of (i) neutral and (ii) anionic 3′-dCMPH moiety at the HF/6-31+G(d) accuracy level.

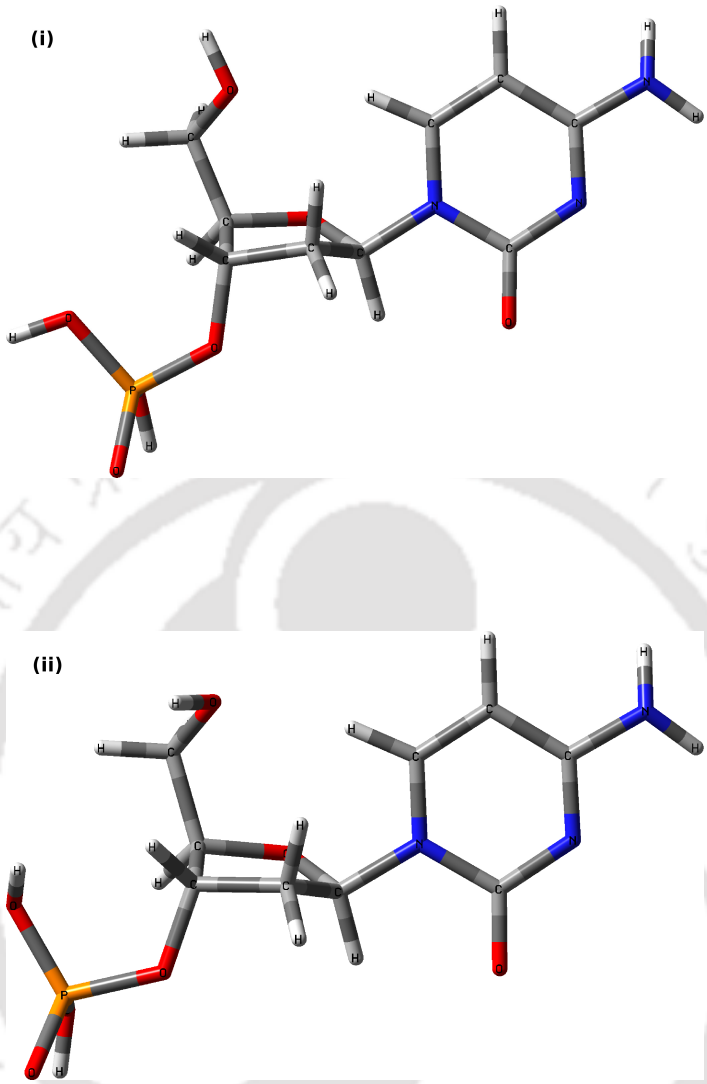

Fig. A2 The optimized structures of (i) neutral and (ii) anionic 3′-dCMPH moiety at the MP2/6-31+G(d) accuracy level.

II. Singly occupied molecular orbitals (SOMOs) generated at the HF/6-31+G(d) level for the glycosidic N–C bond cleavage in 3′-dCMPH molecule.

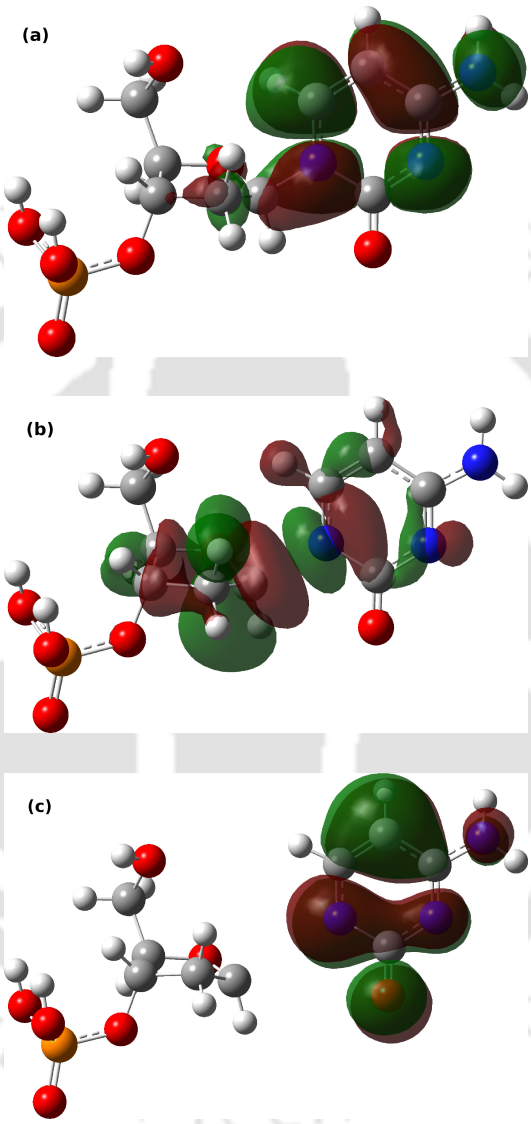

Fig. A3 Singly occupied molecular orbital (SOMO)s generated for anionic 3′-dCMPH moiety for the N–C bond lengths of (a) 2.76 a_0 (1.46 Å), (b) 3.67 a_0 (1.94 Å), and (c) 5.67 a_0 (3.00 Å) at the HF/6-31+G(d) level of accuracy.

III. Plot of transmission coefficient (T) of the N–C bond from the anionic vibrational states (i) $\chi_{i=0-19}$ for the HF, and (ii) $\chi_{i=0-17}$ for the MP2 of 3′-dCMPH moiety.

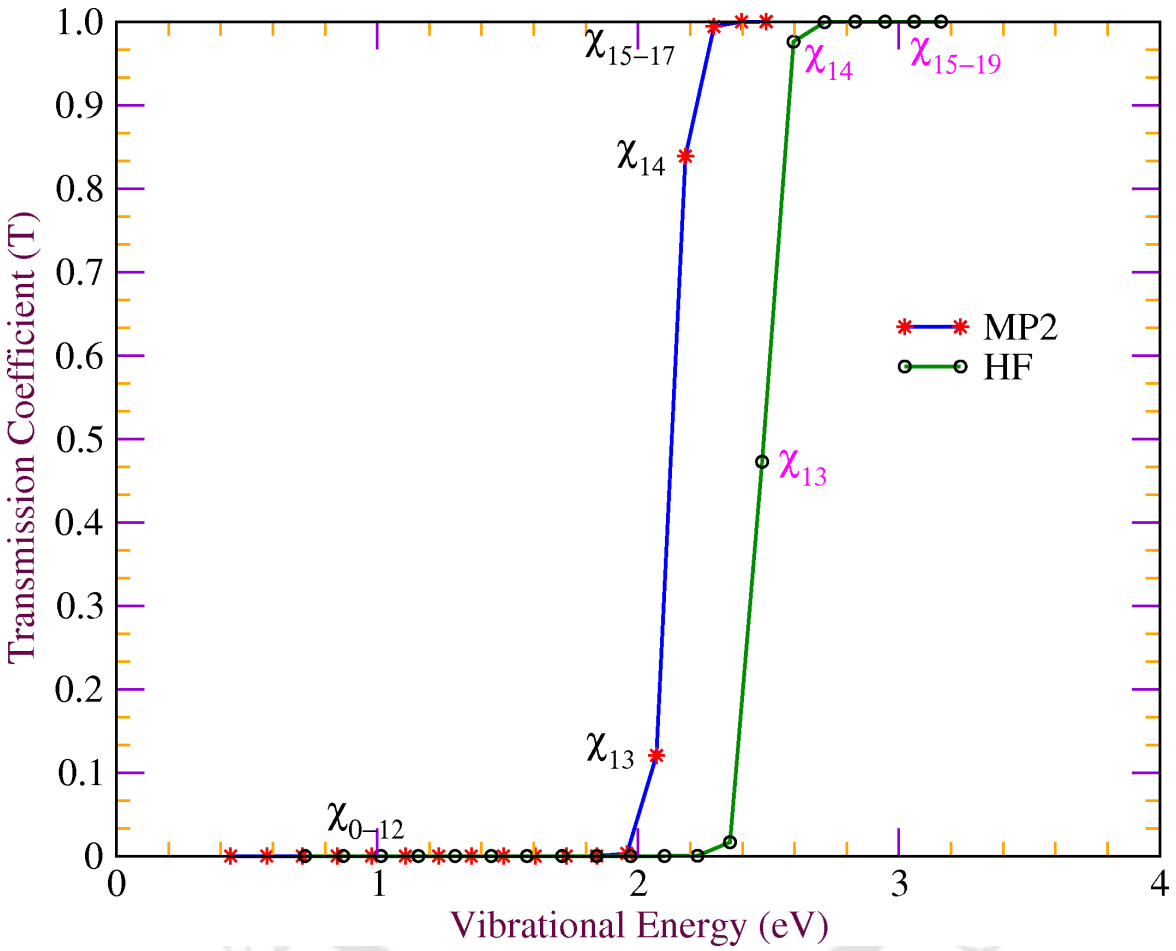

Fig. A4 "S-shaped" Transmission coefficient (T) tunneling curve of the N–C bond from the vibrational states $\chi_{i=0-19}$ (HF, green solid line with black circles), and $\chi_{i=0-17}$ (MP2, blue solid line with red circles) of the curtailed anionic PE curves of Figs. 4.2(a) and 4.2(b) respectively.

IV. Plots of wave packet propagation from time t = 0–22 fs for the ground state wave function ϕ_0(R) of the target 3′-dCMPH molecule in HF method under the effect of anionic Hamiltonian.

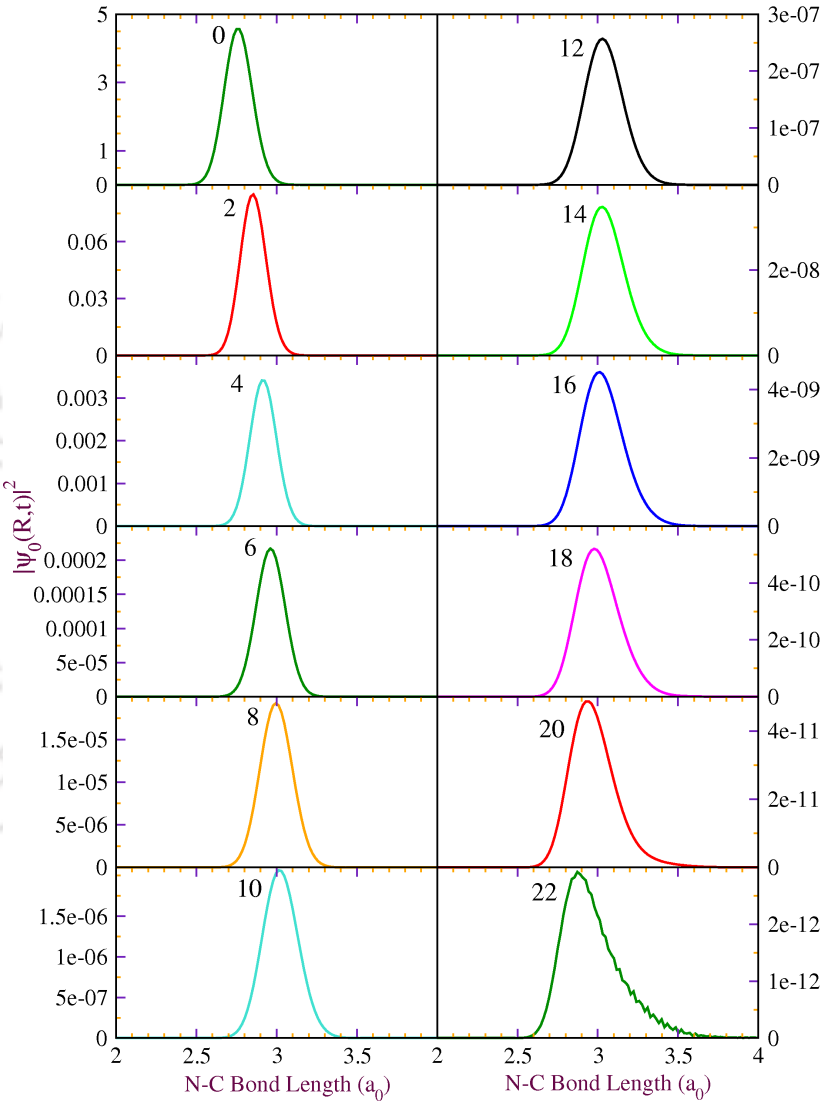

Fig. A5 Plots of wave packet propagation from time t = 0–22 fs for the ground state wave function ϕ_0(R) of the target 3′-dCMPH molecule in HF method under the effect of anionic Hamiltonian.

V. Plots of wave packet propagation from time t = 0–55 fs for the thirteenth excited state wave function ϕ_{13}(R) of the target 3′-dCMPH molecule in HF method under the effect of anionic Hamiltonian.

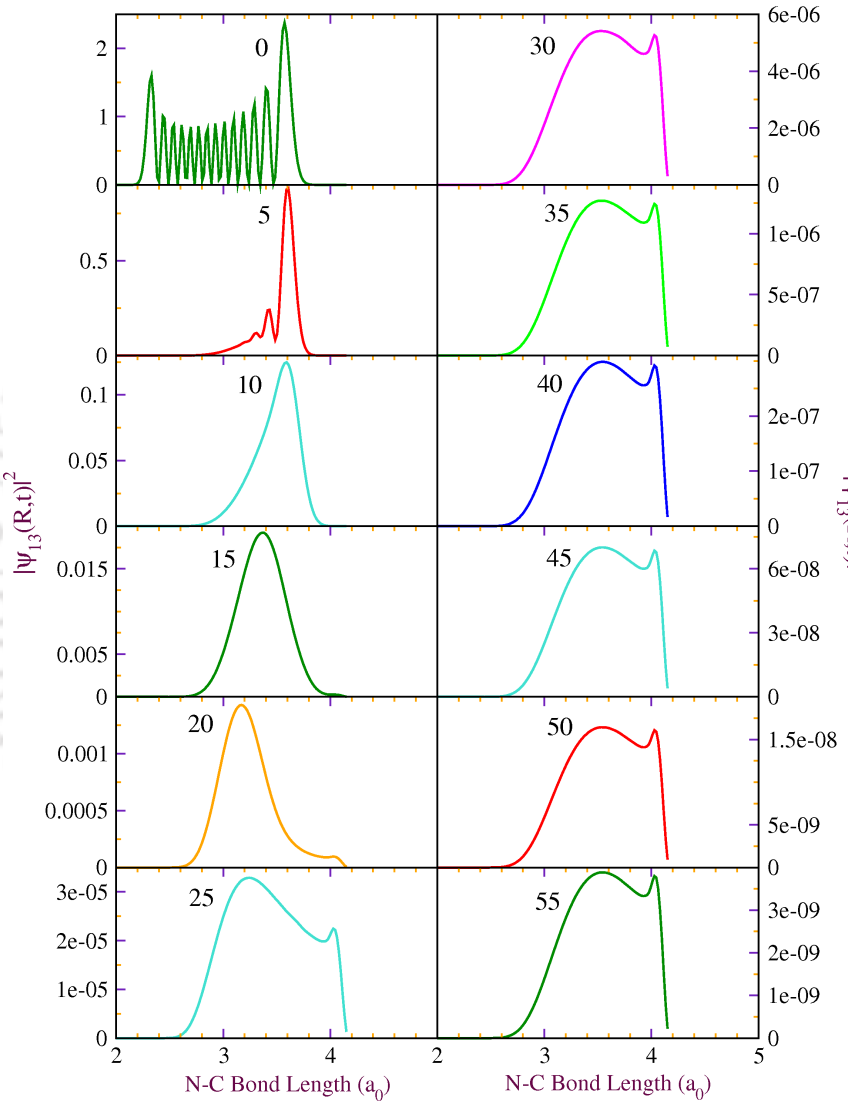

Fig. A6 Plots of wave packet propagation from time t = 0–55 fs for the thirteenth excited state wave function ϕ_{13}(R) of the target 3′-dCMPH molecule in HF method under the effect of anionic Hamiltonian.

Appendix B

Supporting information for Chapter 5

I. The optimized structures of neutral and anionic 5′-dCMPH moiety at the (a) HF, and (b) MP2 methods with 6-31+G(d) basis set.

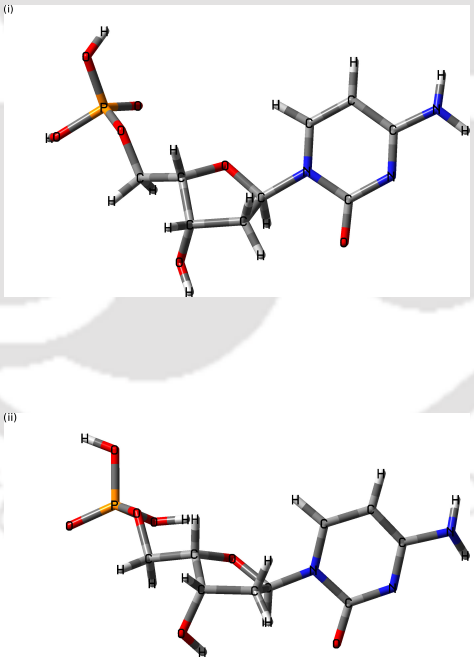

Fig. B1 The optimized structures of (i) neutral and (ii) anionic 5′-dCMPH moiety at the HF/6-31+G(d) accuracy level.

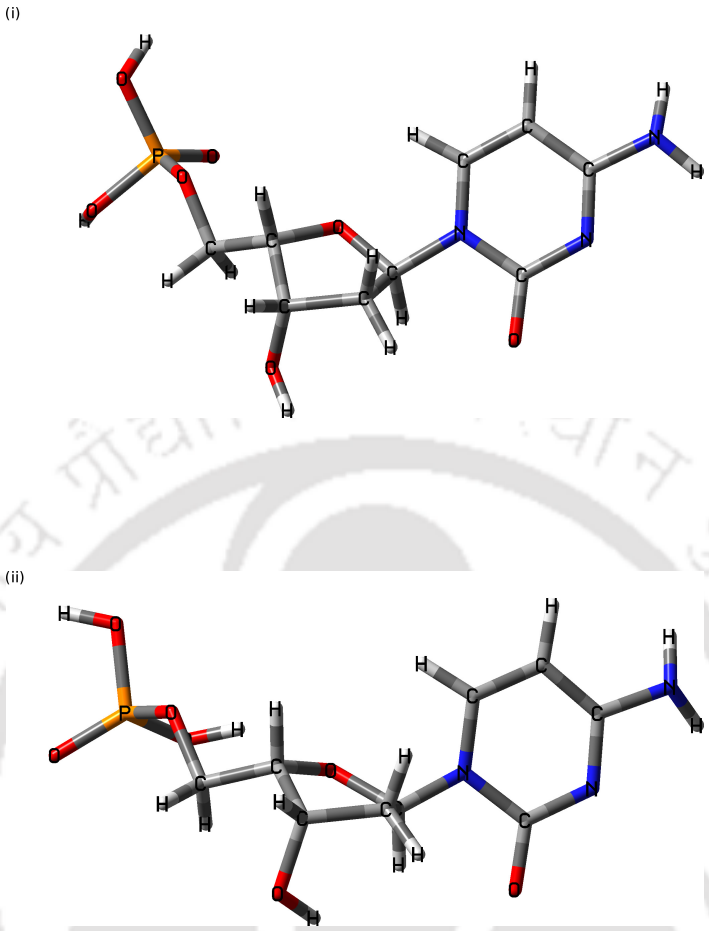

Fig. B2 The optimized structures of (i) neutral and (ii) anionic 5′-dCMPH moiety at the MP2/6-31+G(d) accuracy level.

II. Plots of wave packet propagation from time t = 0–22 fs for the ground state wave function $\phi_0(R)$ of the target 5′-dCMPH molecule in HF method under the effect of anionic Hamiltonian.

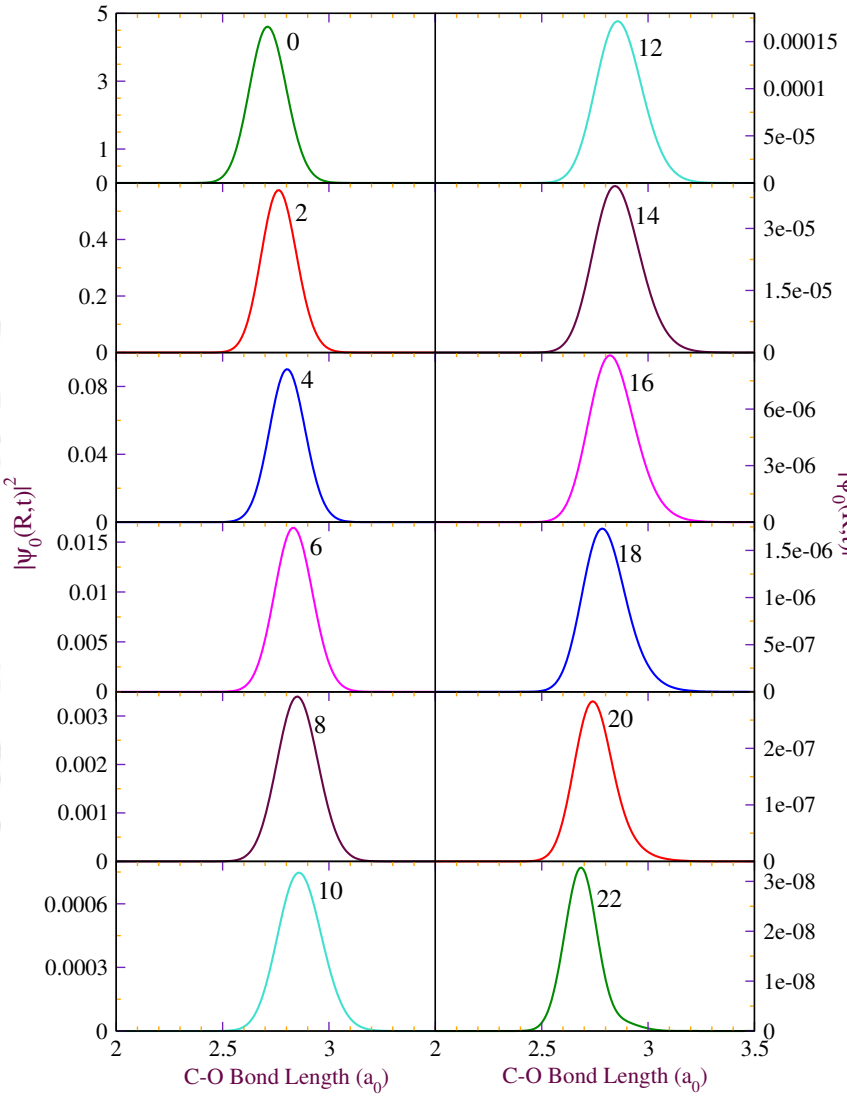

Fig. B3 Plots of wave packet propagation from time t = 0–22 fs for the ground state wave function $\phi_0(R)$ of the target 5′-dCMPH molecule in HF method under the effect of anionic Hamiltonian.

III. Plot of transmission coefficient (T) of the C–O bond from the anionic vibrational states (i) $\chi_{i=0-19}$ for the HF, and (ii) $\chi_{i=0-17}$ for the MP2 of 5′-dCMPH moiety.

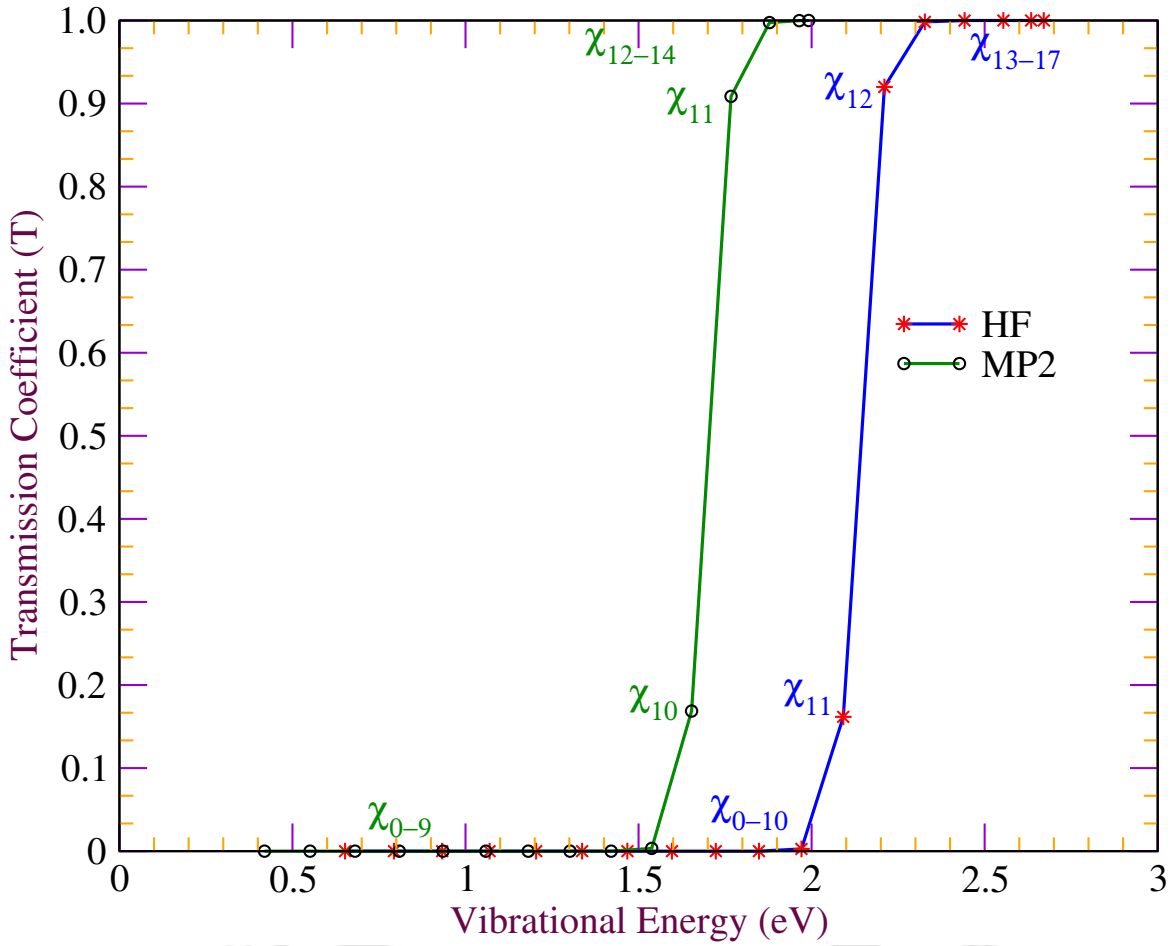

Fig. B4 "S-shaped" Transmission coefficient (T) tunneling curve of the C–O bond from the vibrational states $\chi_{i=0-19}$ (HF, green solid line with black circles), and $\chi_{i=0-17}$ (MP2, blue solid line with red circles) of the curtailed anionic PE curves of Figs. 5.2(a) and 5.2(b) respectively.

IV. Plots of wave packet propagation from time t = 0–55 fs for the twelfth excited state wave function ϕ_{12}(R) of the target 5′-dCMPH molecule in HF method under the effect of anionic Hamiltonian.

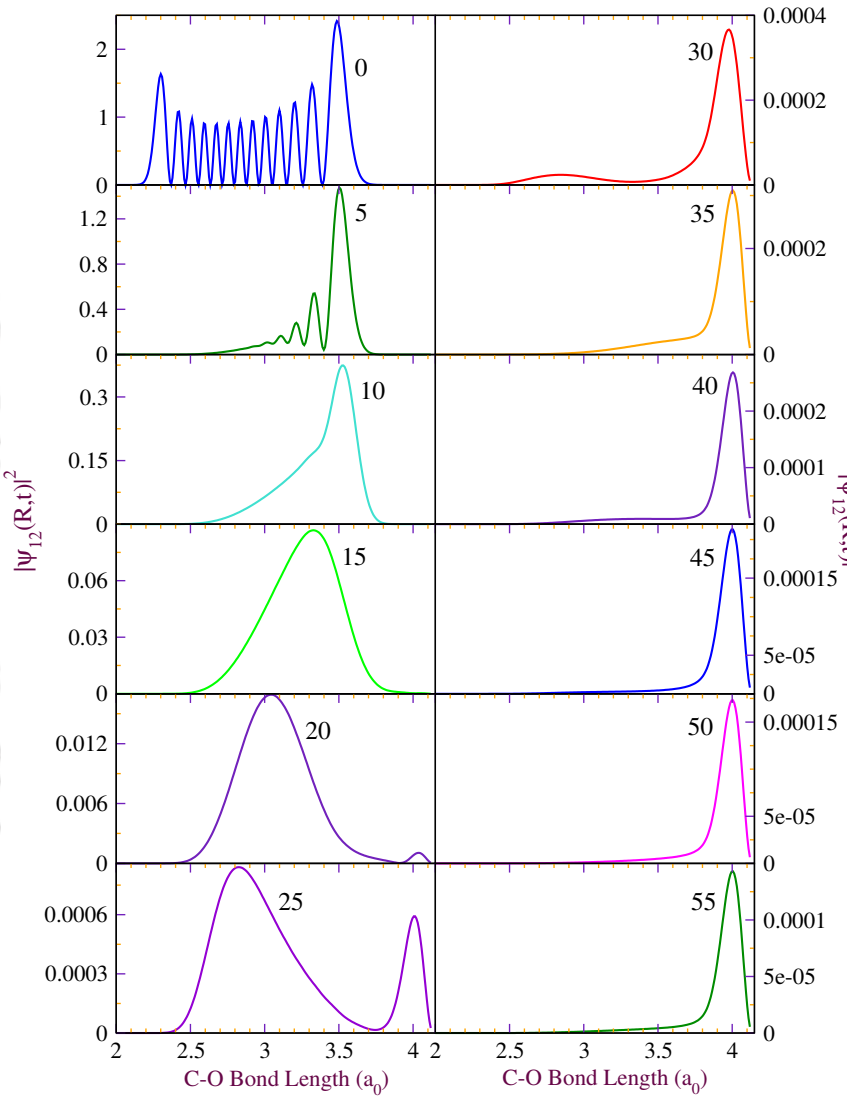

Fig. B5 Plots of wave packet propagation from time t = 0–55 fs for the twelfth excited state wave function ϕ_{12}(R) of the target 5′-dCMPH molecule in HF method under the effect of anionic Hamiltonian.

V. Singly occupied molecular orbitals (SOMOs) generated at the HF/6-31+G(d) level for the glycosidic C–O bond cleavage in 5′-dCMPH molecule.

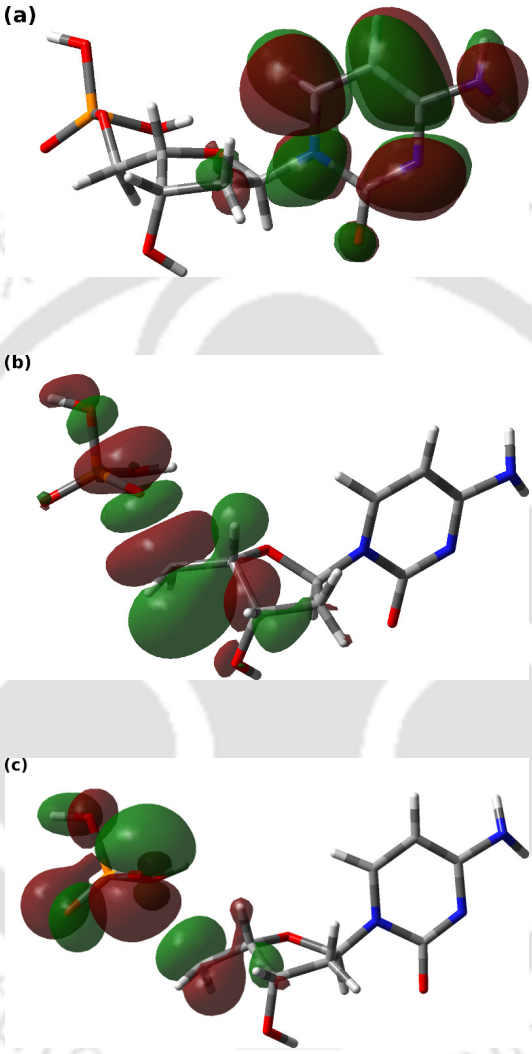

Fig. B6 Singly occupied molecular orbital (SOMO)s generated for anionic 5′-dCMPH moiety for the C–O bond lengths of (a) 2.76 a_0 (1.46 Å), (b) 3.67 a_0 (1.94 Å), and (c) 5.67 a_0 (3.00 Å) at the HF/6-31+G(d) level of accuracy.

Appendix C

Lanczos Scheme

The Schrödinger equation, governing the time evolution, is

$$i\hbar \frac{\partial \Psi(x,t)}{\partial t} = H\Psi(x,t) \tag{C.1}$$

where H is the time independent Hamiltonian in a bounded region of space in d dimensions and takes the form

$$H = \sum_{i=1}^{d} \frac{-\hbar^2}{2\mu} \frac{d^2}{dx_i{}^2} + V(x) \tag{C.2}$$

Let an N function basis $\phi_i(x)_N$ be sufficient to expand $\Psi(x,t)$ to the desired degree of accuracy:

$$\Psi(x,t) = \sum_{i=1}^{N} a_i(t)\phi_i(x) \tag{C.3}$$

Then the time evolution of the wave packet is given exactly by the solution of the Schrödinger equation in this basis. The matrix equation for the $a_i(t)$ is

$$i\hbar S \frac{\partial a(t)}{\partial t} = \mathbf{H}a(t) \tag{C.4}$$

where, for a nonorthogonal but square integrable basis, ϕ_{iN}, the overlap matrix S and Hamiltonian matrix **H** are defined as

$$S_{ij} = \langle \phi_i \mid \phi_j \rangle \tag{C.5}$$

$$\mathbf{H}_{ij} = \langle \phi_i | H | \phi_j \rangle \tag{C.6}$$

The exact solution within this representation is, of course,

$$a(t) = \exp(-\frac{iS^{-1}\mathbf{H}t}{\hbar})a(0) \tag{C.7}$$

with

$$a(0) \equiv S^{-1}b(0) \tag{C.8}$$

$$b_i(0) = \langle \phi_i \mid \Psi(x,0) \rangle \tag{C.9}$$

The exact solution (within the representation) is obtained by diagonalizing S, forming the orthonormal basis, diagonalizing the Hamiltonian in this basis ($S^{-1/2}\mathbf{H}S^{-1/2}$), and computing the coefficient vector a(t) at the desired time t by back transformation from the diagonal representation. For relatively short times and very large N this may be unnecessary and computationally very demanding.

The exact method outlined above is fine for small systems (N < 10^2 - 10^3) but, because the computer time required increases as N^3, one rapidly approaches in practice severe problems for more complex systems. The Lanczos reduced iterative propagation method gives the temporal evolution of the single vector corresponding to the initial state. For an orthonormal basis it is also O (N^2) (a matrix generalization can be used for a set of wave packets if desired).

We can start by noting that the expansion of Eq. (C.7) to the pth order (p < N) will, in general, define p independent vectors in the N-dimensional space:

$$\exp\{-iS^{-1}\mathbf{H}t\}a(0) \simeq \sum_{k=0}^{p-1} \frac{(-it)^k}{k!}(S^{-1}\mathbf{H})^k a(0) \tag{C.10}$$

$$= \sum_{k=0}^{p-1} \frac{(-it)^k}{k!} d_k \tag{C.11}$$

The d_k produced here

$$d_k = (S^{-1}\mathbf{H})d_{k-1} \tag{C.12}$$

$$d_0 \equiv a(0) \tag{C.13}$$

are not orthogonal but are independent if $\Psi(x,0)$ is a linear combination of at least p exact eigenfunctions of $\mathbf{H}$.

The Lanczos procedure systematically yields a set of p S-orthogonal vectors a_p spanning the same subspace as d_p, in terms of which the Hamiltonian now has a tridiagonal form. The procedure, although slightly complicated by the nonorthogonality of the original basis (S $\neq$ I), is quite straightforward. We define

$$S^{-1}\mathbf{H}a_0 = \alpha_0 a_0 + \beta_0 a_1 \tag{C.14}$$

$$S^{-1}\mathbf{H}a_k = \beta_{k-1}a_{k-1} + \alpha_k a_k + \beta_k a_{k+1} \tag{C.15}$$

$$a_0 = a(0) \Big/ \left[a^\dagger(0) S a(0)\right]^{1/2} \tag{C.16}$$

where

$$\alpha_k \equiv a_k^\dagger \mathbf{H} a_k \tag{C.17}$$

$$\beta_{k-1} \equiv a_{k-1}^{\dagger} \mathbf{H} a_k \tag{C.18}$$

The vectors so generated are S orthogonal:

$$a_k^{\dagger} S a_l = \delta_{kl} \tag{C.19}$$

The generation of each new vector requires two operations, one large matrix vector multiplication

$$b = \mathbf{H} a \tag{C.20}$$

and a simple solution of the large set of linear equations (for S $\neq$ I),

$$b_s = S^{-1} b \tag{C.21}$$

If localized basis functions are used, both **H** and S will be sparse. [Note that the iterative solution of Sb_s = b is of order N^2.

The vectors and matrix elements defined in Eqs. (C.14) to (C.18) may be arranged to form a rectangular transformation matrix A_{Nxp} from the basis ϕ_{iN} to the p-dimensional subspace defined by the a_p and the Hamiltonian matrix in this subspace H_p:

$$A_p \equiv \left[a_0 a_1 a_2 ... a_{p-1}\right] \tag{C.22}$$

$$H(p) = \begin{pmatrix} \alpha_0 & \beta_0 & 0 & ... & 0 & 0 \\ \beta_0 & \alpha_1 & \beta_1 & ... & 0 & 0 \\ 0 & \beta_1 & \alpha_2 & ... & 0 & 0 \\ ... & ... & ... & ... & ... & ... \\ 0 & 0 & 0 & ... & \alpha_{p-2} & \beta_{p-2} \\ 0 & 0 & 0 & ... & \beta_{p-2} & \alpha_{p-1} \end{pmatrix} \tag{C.23}$$

We now can solve time dependent Schrödinger equation in this reduced representation. It will be accurate over the time interval 0<t<T for which the truncated expansion, Eqs. (C.10 and C.11), are valid.

Thus we let the vector c(t) (pxl) be the coefficient of the p vectors a_p which are, in turn, coefficients of the basis ϕ_{i_N}. The Lanczos reduced Schrödinger equation is then

$$\frac{\partial c}{\partial t} = -iH_p c \tag{C.24}$$

where

$$C(0) = \begin{pmatrix} 1 \\ 0 \\ 0 \\ . \\ . \end{pmatrix} \tag{C.25}$$

The initial condition, Eq. (C.25), holds because the initial vector a(0) is the initial vector in the Lanczos subspace a(0) [Eq. (C.16)], with proper S normalization. Equation (C.24) is then solved (usually by diagonalization) to give

$$c(t) = \exp\{-iH_p t\} c(0) \tag{C.26}$$

Transformation to the basis representation yields the desired set of basis coefficients

$$a(t) = A_p c(t) \tag{C.27}$$

and the time evolved wave packet, if desired,

$$\Psi(x,t) = \sum_{i=1}^{N} a_i(t)\phi_i(x) \tag{C.28}$$

Appendix D

Copyright and Permissions

Copyright and permission is granted from the respective published journal for reuse all or part of the submitted, accepted or published work in this thesis that the author writes, and the necessary information regarding the same is attached herewith in the subsequent pages. Moreover, the published work is cited at appropriate places in this dissertation. Comprehensive list of publications that are published, accepted, and/or in preparation are provided at the end of the dissertation.

AIP PUBLISHING LLC LICENSE
TERMS AND CONDITIONS

Apr 30, 2015

All payments must be made in full to CCC. For payment instructions, please see information listed at the bottom of this form.

License Number	3618630577866
Order Date	Apr 30, 2015
Publisher	AIP Publishing LLC
Publication	Journal of Chemical Physics
Article Title	Investigation of dissociative electron attachment to 2′-deoxycytidine-3′-monophosphate using DFT method and time dependent wave packet approach
Author	Somnath Bhowmick,Renjith B,Manoj K. Mishra, et al.
Online Publication Date	Aug 9, 2012
Volume number	137
Issue number	6
Type of Use	Thesis/Dissertation
Requestor type	Author (original article)
Format	Print and electronic
Portion	Excerpt (> 800 words)
Will you be translating?	No
Title of your thesis / dissertation	DNA Damage Induced by Low Energy Electrons: A Theoretical Approach
Expected completion date	May 2015
Estimated size (number of pages)	130
Total	0.00 USD
Terms and Conditions	

AIP Publishing LLC -- Terms and Conditions: Permissions Uses

AIP Publishing LLC ("AIPP"") hereby grants to you the non-exclusive right and license to use and/or distribute the Material according to the use specified in your order, on a one-time basis, for the specified term, with a maximum distribution equal to the number that you have ordered. Any links or other content accompanying the Material are not the subject of this license.

1. You agree to include the following copyright and permission notice with the reproduction of the Material:"Reprinted with permission from [FULL CITATION]. Copyright [PUBLICATION YEAR], AIP Publishing LLC." For an article, the copyright and permission notice must be printed on the first page of the article or book chapter. For photographs, covers, or tables, the copyright and permission notice may appear with the Material, in a footnote, or in the reference list.
2. If you have licensed reuse of a figure, photograph, cover, or table, it is your responsibility to ensure that the material is original to AIPP and does not contain the copyright of another entity, and that the copyright notice of the figure, photograph, cover, or table does not indicate that it was reprinted by AIPP, with permission, from another source. Under no circumstances does AIPP, purport or intend to grant permission to reuse material to which it does not hold copyright.
3. You may not alter or modify the Material in any manner. You may translate the Material into another language only if you have licensed translation rights. You may not use the

AIP PUBLISHING LLC LICENSE
TERMS AND CONDITIONS

Apr 30, 2015

All payments must be made in full to CCC. For payment instructions, please see information listed at the bottom of this form.

License Number	3618630259929
Order Date	Apr 30, 2015
Publisher	AIP Publishing LLC
Publication	Journal of Chemical Physics
Article Title	Low energy electron induced cytosine base release in 2′-deoxycytidine-3′-monophosphate via glycosidic bond cleavage: A time-dependent wavepacket study
Author	Renjith Bhaskaran,Manabendra Sarma
Online Publication Date	Sep 10, 2014
Volume number	141
Issue number	10
Type of Use	Thesis/Dissertation
Requestor type	Author (original article)
Format	Print and electronic
Portion	Excerpt (> 800 words)
Will you be translating?	No
Title of your thesis / dissertation	DNA Damage Induced by Low Energy Electrons: A Theoretical Approach
Expected completion date	May 2015
Estimated size (number of pages)	130
Total	0.00 USD
Terms and Conditions	

AIP Publishing LLC -- Terms and Conditions: Permissions Uses

AIP Publishing LLC ("AIPP"") hereby grants to you the non-exclusive right and license to use and/or distribute the Material according to the use specified in your order, on a one-time basis, for the specified term, with a maximum distribution equal to the number that you have ordered. Any links or other content accompanying the Material are not the subject of this license.

1. You agree to include the following copyright and permission notice with the reproduction of the Material:"Reprinted with permission from [FULL CITATION]. Copyright [PUBLICATION YEAR], AIP Publishing LLC." For an article, the copyright and permission notice must be printed on the first page of the article or book chapter. For photographs, covers, or tables, the copyright and permission notice may appear with the Material, in a footnote, or in the reference list.
2. If you have licensed reuse of a figure, photograph, cover, or table, it is your responsibility to ensure that the material is original to AIPP and does not contain the copyright of another entity, and that the copyright notice of the figure, photograph, cover, or table does not indicate that it was reprinted by AIPP, with permission, from another source. Under no circumstances does AIPP, purport or intend to grant permission to reuse material to which it does not hold copyright.
3. You may not alter or modify the Material in any manner. You may translate the Material into another language only if you have licensed translation rights. You may not use the

List of Publications

1. R. Bhaskaran and M. Sarma, Accepted in Phys. Chem. Chem. Phys. (2015).

2. R. Bhaskaran and M. Sarma, J. Chem. Phys **141**, 104309 (2014).

3. R. Bhaskaran and M. Sarma, J. Chem. Phys **139**, 045103 (2013).

4. S. Bhowmick, Renjith B, M. K. Mishra, and M. Sarma, J. Chem. Phys **137**, 064310 (2012).

5. Renjith B, S. Bhowmick, M. K. Mishra, and M. Sarma, J. Phys. Chem. A **115**, 13753 (2011).

6. R. Bhaskaran and M. Sarma, in preparation.